Systems Immunology Approaches for Precision Medicine

Andrew James Leber

Dissertation submitted to the faculty of the Virginia Polytechnic Institute and State University in partial fulfillment of the requirements for the degree of

Doctor of Philosophy
In
Genetics, Bioinformatics, and Computational Biology

Josep Bassaganya-Riera, chair
Raquel Hontecillas
David R. Bevan
Vida Abedi

March 29, 2017
Blacksburg, Virginia

Keywords: *Clostridium difficile*, inflammatory bowel disease, influenza, computational modeling, immunology

Systems Immunology Approaches for Precision Medicine

Andrew James Leber

ABSTRACT

The mucosal immune system encompasses a wide array of interactions that work in concert to protect an individual from harmful agents while retaining tolerance to molecules, microbes, and self-antigens that present no danger. The upheaval in the regulation-response balance is a critical aspect in both infectious and immune-mediated disease. To understand this balance and methods of its restoration, iterative and integrative modeling cycles on the pathogenesis of disease are necessary. In this thesis, I present three studies highlighting phases of a systems immunology cycle. Firstly, the thesis provides a description of the construction of a computational ordinary differential equation based model on the host-pathogen-microbiota interactions during *Clostridium difficile* infection and the use of this model for the development of the hypothesis that host-antimicrobial peptide production may correlate with increased disease severity and promote increased recurrence. Secondly, it provides insight into the necessity of trans-disciplinary analysis for the understanding of novel molecular targets in disease through the immunometabolic regulation of CD4+ T cell by NLRX1 in inflammatory bowel disease. Third, it provides the assessment of novel therapeutics in disease through the evaluation of LANCL2 activation in influenza virus infection. In total, the computational and experimental strategies used in this dissertation are critical foundational pieces in the framework of precision medicine initiatives that can assist in the diagnosis, understanding, and treatment of disease.

Systems Immunology Approaches for Precision Medicine

Andrew James Leber

GENERAL AUDIENCE ABSTRACT

Many diseases are a result of altered patterns of interaction between the body, bacteria, viruses or nutrients. When these patterns are altered, inflammation occurs. If not controlled, the inflammation can cause pain, damage to the affected area, and other specific symptoms depending on the type of disease. This dissertation details the use of alternative methods of treating disease and analyzing disease in the context of *Clostridium difficile* infection, inflammatory bowel disease and influenza infection. It provides insight into the development of computational models with equations to capture the response patterns. It assesses the connections between immunology and metabolism that can lead to inflammation. And, it identifies a new therapeutic target for influenza infection. Together, these three phases are important pieces toward a future with improved understanding of disease and treatments that can be specific and customized for every individual.

Acknowledgements

This dissertation and accomplishments over the past few years would not have been possible without the guidance, support and contributions from so many others. Foremost, are my committee members who have fostered my intellectual growth and shaped my research. Thank you: Dr. Josep Bassaganya-Riera, for his strength and conviction in the mission of NIMML that made it easy to believe in the worth of projects day in and day out while still affording me the freedom to expand and pursue my own ideas and hypotheses; Dr. Raquel Hontecillas, for her precision and detailed knowledge that have refined numerous projects and plans to the point of minimal errors; Dr. Vida Abedi, for the care and motivation she provided in addition to never lacking an alternative for what could be next should a method fail; Dr. David Bevan, for his consistent reminders to stay confident and enthusiastic in the work that I was doing.

I also owe thanks to all of my colleagues at NIMML. To all of the students preceding me, thank you for helping to build the environment of which I was a part. Specifically, to Monica, Cassy and Pinyi, thank you for your patience in getting me up to speed on arrival and providing exemplary models of success. To Noah, thank you for the peak laboratory organization and the in-depth training on tasks, without which I would have been lost. To Nuria, thank you for being the one person to count on for help in the laboratory and for all of the random conversations when we were stuck in a hood, in the colony or waiting on an assay to finish for hours on end. To Meghna, thank you for being a willing teammate in learning ENISI and the days we spent trying to figure it out. And, to all of the undergraduates, whether lasting one semester or nearly the entire time I spent in NIMML or a period in between, your contributions, big or small, were valuable and it was a joy to work with you and assist you in your research experience. Good luck to all those I am leaving behind and I will gladly pay back these debts with any future requests I can help with.

Research is made possible not only by those performing the experiments but also everyone behind the scenes: from Amy and Steve to Shelana and Betty to Ben and all of the LS1 animal care technicians to Dennie to the multitude of others. Thank you for all you do on a daily basis, smoothly integrating orders, supplies, facility management and degree requirements, to ensure that students like me can maximize their focus on research.

Finally, I would not have made it this far without my family and friends. I can easily state that I would not be who I am without the devotion of my parents and the sacrifices they made along the way. Thank you to my sister, Amanda, for being a companion whenever I needed her and for making the transition to Blacksburg incredibly simple. And to all of my friends who have made too many unique contributions to my life to list by name.

To everyone, may we find even greater success should our paths cross again.

Attributions

The presented work has resulted from the collective effort of multiple team members. Those who have contributed significantly to these projects are outlined below:

Chapter 1
Josep Bassaganya-Riera (Virginia Tech, Nutritional Immunology and Molecular Medicine Laboratory) and Raquel Hontecillas (Virginia Tech, Nutritional Immunology and Molecular Medicine Laboratory) contributed to the editing and revision of the chapter.

Chapter 2
Josep Bassaganya-Riera and Raquel Hontecillas aided in the preparation of the manuscript and study design. Vida Abedi (Virginia Tech, Nutritional Immunology and Molecular Medicine Laboratory) and Stefan Hoops (Virginia Tech, Nutritional Immunology and Molecular Medicine Laboratory) contributed to the analysis of data and construction of computational models. Monica Viladomiu (Virginia Tech, Nutritional Immunology and Molecular Medicine Laboratory), Casandra Philipson (Virginia Tech, Nutritional Immunology and Molecular Medicine Laboratory), and Brad Howard (Virginia Tech, Nutritional Immunology and Molecular Medicine Laboratory) helped in the generation of data.

Chapter 3
Josep Bassaganya-Riera and Raquel Hontecillas aided in the preparation of the manuscript and study design. Nuria Tubau Juni (Virginia Tech, Nutritional Immunology and Molecular Medicine Laboratory), Victoria Zoccoli-Rodriguez (Virginia Tech, Nutritional Immunology and Molecular Medicine Laboratory) and Kristin Eden (Virginia Tech, Nutritional Immunology and Molecular Medicine Laboratory) contributed to the generation of in vivo animal data. Matthew Hulver (Virginia Tech, Metabolic Phenotyping Core) and Ryan McMillan (Virginia Tech, Metabolic Phenotyping Core) contributed to the generation and analysis of metabolic data. Irving Coy Allen (Virginia Tech, Biomedical Sciences and Pathobiology) aided in the analysis of data and preparation of the manuscript.

Chapter 4
Josep Bassaganya-Riera and Raquel Hontecillas aided in the preparation of the manuscript and study design. Nuria Tubau Juni and Victoria Zoccoli-Rodriguez contributed to the generation of in vivo animal data. Pinyi Lu (Virginia Tech, Nutritional Immunology and Molecular Medicine Laboratory) and Victoria Godfrey (Virginia Tech, Nutritional Immunology and Molecular Medicine Laboratory) contributed to the expression of LANCL2 protein. Shiv Kale (Virginia Tech, Nutritional Immunology and Molecular Medicine Laboratory) aided in the analysis of surface plasmon resonance data.

Chapter 5
Josep Bassaganya-Riera and Raquel Hontecillas contributed to the editing and revision of the text.

Table of Contents

Chapter 4

Lanthionine Synthetase C-like 2 Modulates Immune Responses to Influenza Virus Infection

Chapter 5

List of figures

Chapter 1

Introduction: Systems Approaches for the Design of Novel Treatments in Infectious and Immune-Mediated Diseases

Andrew Leber, Raquel Hontecillas, Josep Bassaganya-Riera

1.1 Summary

Traditional immunology offers the potential for the in-depth characterization of specific pathways and response elements in disease. However, the immune system possesses many layers of complex interactions that are incompatible with a reductionist approach to experimentation. By taking a systems level view to immunology, through the use of computational modeling, analytics, and transcriptomics and similar datasets in combination with traditional experimentation, the ability to identify, characterize and validate hypotheses is amplified and accelerated. Further, the availability of rich, diverse datasets in pre-clinical and clinical settings has opened the possibility for the intelligent design of novel therapeutics and the prediction of treatment response from pre-treatment markers. The integration of computational and experimental work spanning traditional scientific disciplines, such as immunology, microbiology, and metabolism, is needed to accomplish this goal. The three studies presented within this dissertation highlight these aspects through the computational modeling of host-pathogen-microbiome interactions in *Clostridium difficile* infection (CDI), the identification of a molecular target, NLRX1, at the interface of immunity and metabolism in inflammatory bowel disease (IBD), and the evaluation of a novel immunoregulatory pathway, LANCL2, for the development of anti-viral alternatives in influenza infection. While at differing stages of experimentation, the motivation and methods of each project highlight the potential of systems immunology in the creation of non-intuitive hypothesis, generation of mechanistic knowledge and the development of novel therapeutic pathways.

1.2 *Clostridium difficile* infection

C. difficile is a spore-forming, anaerobic, Gram-positive bacterium identified as the causative agent of human pseudomembranous colitis and the most common cause of nosocomial antibiotic-associated diarrhea. CDI affects over 500,000 people and causes over 25,000 deaths yearly in the United States, according to recent estimates [1]. *C. difficile*

is present in approximately 5% of the population without the presentation of any symptoms. However, the prevalence increases to nearly 40% in hospitalized individuals [2]. Following broad-spectrum antibiotic usage, *C. difficile* is able to expand with the gastrointestinal tract, produce toxins, and perturb the integrity of the epithelial barrier leading to diarrhea and intestinal inflammation. Despite this association, the primary treatment remains antibiotics, leading to high rates of recurrent infections.

Currently, the estimated rate of relapse averages between 20 and 25% across multiple estimates[3-5]. The current rate has more than doubled the estimated recurrence rates from 15 to 20 years ago of less than 10% [5]. While differences in diagnostic practices of each era may contribute to the size of the discrepancy, it is clear that slight changes in dosing and treatment strategies have not been effective in reducing these rates despite increased awareness of recurrence dating back to the 1980s [6, 7]. Further, the recurrence of *C. difficile* is not limited to a single episode either, with subsequent episodes occurring in 40-60% of patients who experience a first recurrence [8]. Recurrence could occur through re-infection via a second exposure or re-growth of persistent spores, though evidence based on the timing of recurrent episodes suggests that a re-growth scenario is more likely [3]. Continued disruptions of the colonic microflora and a lack of a serum anti-toxin antibody response are two of the major factors contributing to an increased risk of recurrence, though age and co-morbidities can also contribute [9-11]. In particular, a summation of contributing factors has helped to develop a prediction rule for the identification of patients at high risk for recurrence [9]. The altered microbiome and immune status during recurrence can disrupt treatment of other co-occurring disease states [12, 13]. The development of novel treatments and precision medicine advances can help to decrease recurrence rates and lower the healthcare burden of CDI.

1.3 Inflammatory bowel disease

Within the last 50 years, the incidence of IBD has greatly accelerated reaching an estimated total of 1.6 million Americans in the most recent Crohn's and Colitis Foundation release, corresponding to changes in lifestyle in developed countries. Due to the relatively stable genetic susceptibility in this timeframe, it is clear that environmental factors largely contribute the pathogenesis of disease [14]. Factors ranging from diet and exercise, hygiene and microbiota, and sleep and stress patterns are highly significant in the severity of disease and onset of disease flares, resulting in a high degree of variation from patient to patient [15].

The pathogenesis of IBD encompasses genetic predisposition, chronic and overzealous inflammation, and dysregulated host-microbiome interactions, although the mechanisms at the interface of these three-way interactions are incompletely understood [16, 17]. An inability to adequately sense microbial, dietary and metabolic components coupled with dysregulation of mucosal immune responses may result in IBD which leads to the characteristic relapsing periods of intestinal inflammation [18]. The alteration of epithelial barrier function increases the susceptibility to the translocation of antigen into intestinal layers, impairing the tolerance of the native commensal microflora [19]. This loss of immunoregulation generates the increased secretion of pro-inflammatory cytokines

creating a period of acute inflammation that is not resolved leading to chronic intestinal inflammation.

To suppress inflammation, IBD patients rely on life-long modestly successful treatment plans, many of which are accompanied by undesirable side effects [20]. Thus, identifying novel targets that modulate tolerance and immune-mediated intestinal inflammation whose expression can be modulated by exogenous ligands is significant for reaching an unmet clinical need for safer, more effective IBD therapies.

1.4 Influenza infection

Influenza virus A is an orthomyxovirus associated with 3 to 5 million severe infections worldwide on a yearly basis [21]. The exposure to and replication of the virus within the lungs leads to the development of fever, cough, and other respiratory symptoms lasting two weeks and 250,000 to 500,000 deaths per year [22]. The fast mutation rate of the virus leads to the need to develop new vaccines for prevalent strains on a yearly basis and create the potential for reduction in anti-viral efficacy.

Influenza virus possesses 8 RNA segments, encoding 11 proteins [23]. These genes are mainly responsible for the integrity of viral particle, the adhesion and entry of the virus into the cell and the replication of the virus. Influenza enters and replicates within epithelial cells, which can lead to their necrosis and thinning throughout lung airways [24]. This damage to the epithelium can lead to infiltration of neutrophils and other leukocytes and the filling of air spaces with edema and fibrin. As active replication of virus is typically stopped nearly 5 days post-exposure, the majority of the symptomatic period is rather the recovery from infection [24]. Therefore, unless treated immediately at the onset of symptoms, the activation of recovery mechanisms may be more efficacious in disease progression and the prevention of mortality than traditional anti-viral therapies.

1.5 Precision medicine advances

In both infectious and immune-mediated disease, there is a high level of variability between patients in the development, severity and complications to disease. Despite this, the majority of infections and chronic diseases have a singular treatment or small group of treatments with poorly characterized patient groupings. For example, the currently prescribed treatment for mild, severe, and recurrent CDI is antibiotic therapy [25, 26]. However, the clinical outcomes and associated pathologies of CDI correlate more with markers of intestinal inflammation rather than with the eradication of *C. difficile*, suggesting that the majority of patients could benefit from alternative modes of treatment [27]. Recent advances have led to the development of certain alternative strategies target the replenishment of the commensal microbiome, such as fecal microbiome transplantation or the administration of non-toxigenic *C. difficile* [28, 29].

In silico methods have recently been developed for the assessment of novel treatments and categorization of patients in tuberculosis, type 1 diabetes and traumatic injury [30-32]. While these *in silico* clinical trials have slight differences in design, the framework remains

consistent throughout in a computational model of simulation method, the generation of synthetic avatars that vary similar to an authentic population, and the calibration with known clinical data [33]. With further development, these methods can help to accelerate the progression of therapeutic candidates through the approval process and promote confidence in emerging treatments in pre-clinical settings [34].

Beyond the testing of novel treatment methods, computational approaches and advanced analytics have fostered the development of tools that provide precision medicine advice from the incorporation of high resolution, individual level response data. Notable studies utilizing these strategies have assessed personalization in nutrition, coronary artery disease, Lyme disease, and respiratory virus infections [35-38]. By measuring variable factors such as general anthropometrics, surveys, blood draws, host transcriptomics and molecular metabolites, these studies have shown the capability to accelerate the diagnosis of disease with sensitivities and specificities exceeding 95%, identify high risk patients that can benefit from prophylactic treatment, and predict postprandial glycemic responses with high accuracy to aid in glucose control. The harmonization of obtainable omics data with clinical observations can lead to the development of similar biosignatures of disease that can optimize response to treatment and reduce the likelihood of adverse effects.

1.6 Conclusions

The study of host immune responses to infectious disease and in immune-mediated disease enables the discovery and analysis potent immunoregulatory targets that are capable of producing beneficial effects across a spectrum of diseases. The synergism of classical experimentation with computational modeling and data analytics can greatly accelerate the discovery of these targets. Further, these new approaches can also be used in the design of systems that inform optimal treatment strategies given inputs on immune, metabolic and microbial markers on an individual patient basis.

Chapter 2

Systems modeling of interactions between mucosal immunity and the gut microbiome during Clostridium difficile infection

Andrew Leber, Monica Viladomiu, Raquel Hontecillas, Vida Abedi, Casandra Philipson, Stefan Hoops, Brad Howard, and Josep Bassaganya-Riera

Leber A, Viladomiu M, Hontecillas R, Abedi V, Philipson C, Hoops S, et al. (2015) Systems Modeling of Interactions between Mucosal Immunity and the Gut Microbiome during Clostridium difficile Infection. PLoS One 10: e0134849.

2.1 Summary

Clostridium difficile infections are associated with the use of broad-spectrum antibiotics and result in an exuberant inflammatory response, leading to nosocomial diarrhea, colitis and even death. To better understand the dynamics of mucosal immunity during *C. difficile* infection from initiation through expansion to resolution, we built a computational model of the mucosal immune response to the bacterium. The model was calibrated using data from a mouse model of *C. difficile* infection. The model demonstrates a crucial role of T helper 17 (Th17) effector responses in the colonic lamina propria and luminal commensal bacteria populations in the clearance of *C. difficile* and colonic pathology, whereas regulatory T (Treg) cells responses are associated with the recovery phase. In addition, the production of anti-microbial peptides by inflamed epithelial cells and activated neutrophils in response to *C. difficile* infection inhibit the re-growth of beneficial commensal bacterial species. Computational simulations suggest that the removal of neutrophil and epithelial cell derived anti-microbial inhibitions, separately and together, on commensal bacterial regrowth promote recovery and minimize colonic inflammatory pathology. Simulation results predict a decrease in colonic inflammatory markers, such as neutrophilic influx and Th17 cells in the colonic lamina propria, and length of infection with accelerated commensal bacteria re-growth through altered anti-microbial inhibition. Computational modeling provides novel insights on the therapeutic value of repopulating the colonic microbiome and inducing regulatory mucosal immune responses during *C. difficile* infection. Thus, modeling mucosal immunity-gut microbiota interactions has the potential to guide the development of targeted fecal transplantation therapies in the context of precision medicine interventions.

2.2 Introduction

Clostridium difficile, a Gram-positive spore-forming, anaerobic bacterium, often colonizes the human gastrointestinal tract after disruption of the normal intestinal flora. *C. difficile* infection (CDI) is a leading cause of diarrhea and pseudomembranous colitis in hospital acquired infection due to prolonged doses of antibiotics [39]. Based on a study published in 2015, the occurrence rate of *C. difficile* in the United States is 147 cases per 100,000 people. Additionally, *C. difficile* is estimated to be responsible for 29,000 deaths per year, a 50% increase from the 2007 estimate of 14,000 [40, 41]. The rate of *C. difficile*-associated infections and deaths may be rising due to the emergence of the hyper virulent strains that exhibit resistance to traditional fluoroquinolone antibiotics [42]. Paradoxically, standard treatment of *C. difficile* associated disease (CDAD), an illness linked to antimicrobial usage, includes administration of more antibiotics such as metronidazole or vancomycin. Indeed, this therapeutic approach may contribute to the considerable rates of recurrence, estimated to be between 5 to 30% [43]. Recently, alternative strategies have been devised to decrease rates of recurrence through use of toxin neutralizing antibodies or gut microbiome reconstitution through fecal transplantation [44, 45]. Beyond the implications in CDI, the gut microbiome has also been implicated as a predictor of autoimmune and inflammatory diseases such as inflammatory bowel disease (IBD) as well as obesity [46]. The ability to functionally evaluate the impact of host-microbiota interactions on health outcomes could guide the use of reconstitution therapies for the treatment of a wide range of human diseases. Additionally, the *baiCD* gene, which encodes a bile acid processing enzyme, allows commensal microbes to utilize host-produced bile salts to synthesize metabolites, such as deoxycholate and lithocholate that provide resistance against *C. difficile* [47].

CDI is most often predicated by an alteration in commensal bacteria, usually as a result of prolonged administration of broad-spectrum antibiotics [48]. The decrease or removal of competitive species allows the vegetative *C. difficile* in the intestinal lumen to proliferate. In accordance with the increased population, there is enhanced production and release of the two toxins, TcdA and TcdB, thought to be the main virulent factors in CDI. TcdA is an enterotoxin which causes tissue damage and edema as a result of interaction with luminal epithelial cells [49]. The disruption of the epithelium by TcdA facilitates the migration of TcdB into the lamina propria layer where it triggers multiple immune response mechanisms. For instance, TcdB can directly interact with monocytes causing a shift in macrophage populations to an M1 phenotype and an increase in the concentration of pro-inflammatory cytokines [50]. The pro-inflammatory environment combines with the effects of TcdA to alter the state of epithelial cells leading to the activation and migration of neutrophils into the intestinal lumen [51]. Specifically, the inflamed epithelial cells have exhibited increased secretion of interleukin-8 (IL-8), an important cytokine in the creation of a gradient inducing neutrophil chemotaxis [52] and a biomarker of severity of disease. The migration of and subsequent release of cytotoxic granules from neutrophils reduces the pathogen number while also further damaging the epithelium. The presence of pathogenic *C. difficile* also increases accumulation of effector dendritic cells (DC) as a result of increased contact rates between the pathogen and immature DC sampling the

lumen, and the increased engulfment rate of the bacteria [53]. The prevalence of effector DC induces Th1 and Th17 effector responses [54]. These subsets of CD4+ T helper cells favor a pro-inflammatory environment in the colonic lamina propria (LP). To modulate the inflammatory microenvironment, immature DC are stimulated to become tolerogenic DC which induce the differentiation of naïve CD4+ T cells into induced regulatory T helper (Treg) cells. For instance, activation of PPARγ, also contributes to a production of Treg cells from fully differentiated Th17 cells, adding a second source pathway through mechanisms of plasticity [55]. Treg responses suppress mucosal inflammation through deactivation of effector dendritic cells, suppression of Th1 responses, and the shift of Th17 into Treg subsets [56]. Failure to mount this regulatory response may worsen symptoms and expected infection outcome. Our modeling approaches have examined how impaired regulatory responses may influence pathology and disease.

Computational modeling has shown promise in integrating theory, procedural knowledge, and data for capturing the experimental observations in synthetic information processing systems and predicting emerging behaviors. Recently, models have been developed in the context of bacterial or viral infection and inflammatory diseases [57-59]. Additionally, the involvement of various cell types across varying dynamic patterns in mucosal immune responses requires improved methodology to understand complex and massively interacting host-microbiota networks. Through the creation of a computational host-microbiome network, the merging of computational and in vivo experimental immunology approaches offers the ability to analyze the microbiome-driven changes in the gut immune cell composition that have been shown to extend to a systemic alteration of the immune environment in the context of multiple diseases [60]. Once calibrated and validated, these models become valuable tools to generate novel hypotheses and guide the design of innovative non-intuitive experiments *in vivo*. In addition, the validated models could contribute to the development of microbiome-based therapeutics for the prevention and amelioration of disease.

It has been shown that a shift towards a pro-inflammatory phenotype, specifically a Th17-driven response with a decreased Treg cell population occurs due to a lack of PPARγ in CD4 T cells, leading to increased disease symptoms and colonic pathology during CDI [61]. To further understand these cellular dynamics and the overall host response to the bacterium, we have generated a tissue-level computational model of *C. difficile* infection using ordinary differential equations (ODEs) to describe the experimentally observed dynamics from individual cells to the gut mucosal immune system. In addition to the immune response, the model incorporates the interactions between host, pathogen and commensal bacteria and can be customized to model other bacteria and associated conditions. Modeling results illustrate the relative impacts of regulatory and effector components of the mucosal immune response in the clearance of *C. difficile* and damage to the colonic mucosa. Model predictions highlight the role of the host microbiome re-growth in controlling the immune response and CDI dynamics at the colonic mucosa.

2.3 Modeling mucosal immune responses to *Clostridium difficile* infection

The model topology is shown in Fig. 1. The network represents the immune response to CDI in the colonic mucosa. The *C. difficile* immune response model incorporates three reactions for the *C. difficile* species (*Cdiff*), which are activated or inhibited by seven host or gut microbiota modifiers. The *Cdiff* species may proliferate. The proliferation reaction is activated by the infection-exacerbating commensal species, *CommH*, and inhibited by the protective commensal species, *CommB*. The *Cdiff* species may also die, in which the *Cdiff* population is reduced. The latter is triggered by the activated macrophage species, *M*, as well as the activated neutrophil species, N_{Lum}. *Cdiff* death is also inhibited by the *CommH* species. Furthermore, *Cdiff* may interact with a dendritic cell, iDC_{Ep}, to produce an activated dendritic cell, with the effector and tolerogenic balance regulated by the comparative population of *CommB* to the dead commensal species, *CommD*. In addition, the *Cdiff* species acts as a modifier of five reactions: the inflammation of colonic epithelial cells, the activation and migration of neutrophils, the activation of macrophages, the death of Treg cells, and the plasticity between Treg and Th17 CD4+ T cell subsets. The computational model is comprised of four compartments (lumen, epithelium, lamina propria and mesenteric lymph nodes) and 23 species whose interactions are described by 30 reactions. The resulting ordinary differential equations (ODE) utilize 49 parameters to describe the dynamics of the system. Parameter values were determined using data generated through a murine model of CDI.

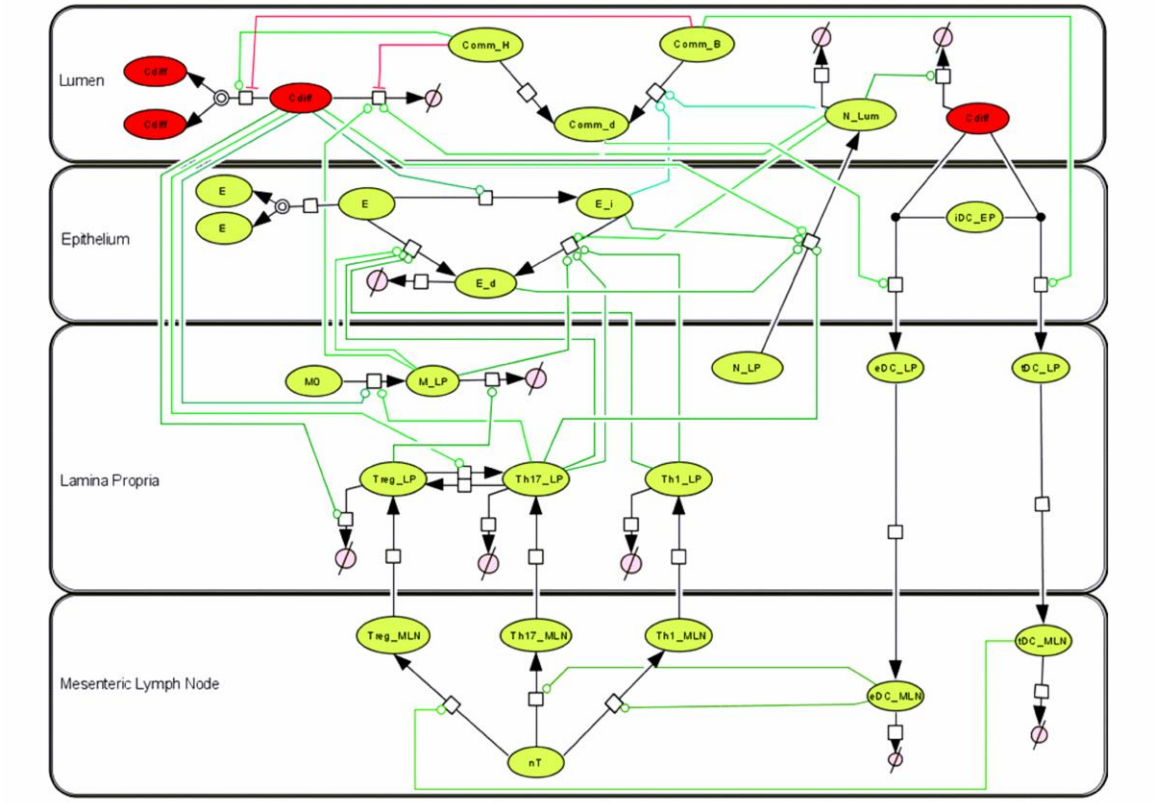

Figure 2.1. Network topology of model illustrating mucosal immune responses to *Clostridium difficile*. Systems biology markup language (SBML) compliant network of interactions between *C. difficile* and cellular immune components created in CellDesigner. Reaction modifiers connect cell nodes to reaction arrows with green as indication of activation and red of inhibition. Species consist

of *C. difficile* (*Cdiff*), infection-exacerbating commensal bacteria (*CommH*), protective commensal bacteria (*CommB*), dead commensal bacteria (*CommD*), epithelial cells (*E*), inflamed epithelial cells (E_i), neutrophils (*N*), macrophages (*M*), dendritic cells (*tDC* and *eDC*), T cells (*nT*, *Treg*, *Th17*, *Th1*) existing in multiple compartments lumen (*Lum*), epithelium (*EP*), lamina propria (*LP*), and mesenteric lymph node (*MLN*).

2.4 Kinetics of *Clostridium difficile*-induced CD4 T cell responses in mice

A time course study was performed to evaluate changes in immune cell composition following CDI. On days 1, 3, 4, 5, 7, 8, and 10 post-infection, colons and MLN were collected, processed and assayed to determine alterations in immune cell subsets by flow cytometry conducted in two sets. In addition, colonic contents were collected and plated to measure the *C. difficile* population size. The response to infection was observed to be Th17 dominant with a large neutrophilic influx in the colonic mucosa. Chronologically, the pro-inflammatory response, marked by an increase in the Th17 effector cell subset, was initiated between days 3 and 4 post-infection (Fig. 2b). The Th17 response peaked on day five post-infection and corresponds with the largest increase in macrophage accumulation. In contrast a regulatory response, characterized by the accumulation of CD4+CD25+Foxp3+ Treg cells was detected between days 8 and 10, and preceded by a slight suppression between days 4 and 7 post-infection (Fig. 2a). Bacterial re-isolation from colonic contents displayed that the peak of the *C. difficile* population occurred on day 4 post-infection and the bacterium was largely cleared by day 8 (Fig. 2c). The data displays that CD4+ T cells may crucially contribute to the response to CDI. For this reason, these populations were foundational elements of the computational model. Combined, this data displays that while the peak of the *C. difficile* population occurs on day 4 post-infection, important events continue to occur through day 10 post-infection. The results established key time points during infection for the evaluation of simulation results such as the peak of *C. difficile* population between days 3 and 4, of the inflammatory response between days 4 and 5, and of the regulatory response between days 8 and 10. Additional data from Buffie, *et al.* was used to calibrate the commensal populations with 16S analysis of the host microbiome regrowth following antibiotic ablation [47]. Data from Blake, *et al.* was used in combination with generated data to calibrate neutrophil populations [62]. Epithelial cells were calibrated with a combination of previously reported data [63, 64]. The data from two time courses of infection was compiled into separate calibration and validation datasets. The calibration dataset includes data gathered during the first experiment on days 1, 4, 7 and 10 post-infection as well as further sourced data from intermediate days. The validation dataset includes data generated on days 3, 5 and 8 post-infection. Parameters for the computational model were estimated using Particle Swarm and Genetic algorithms as implemented in COPASI [65]. The calibrated ODE model is able to replicate the dynamics observed in the time course of infection shown in Fig. 3.

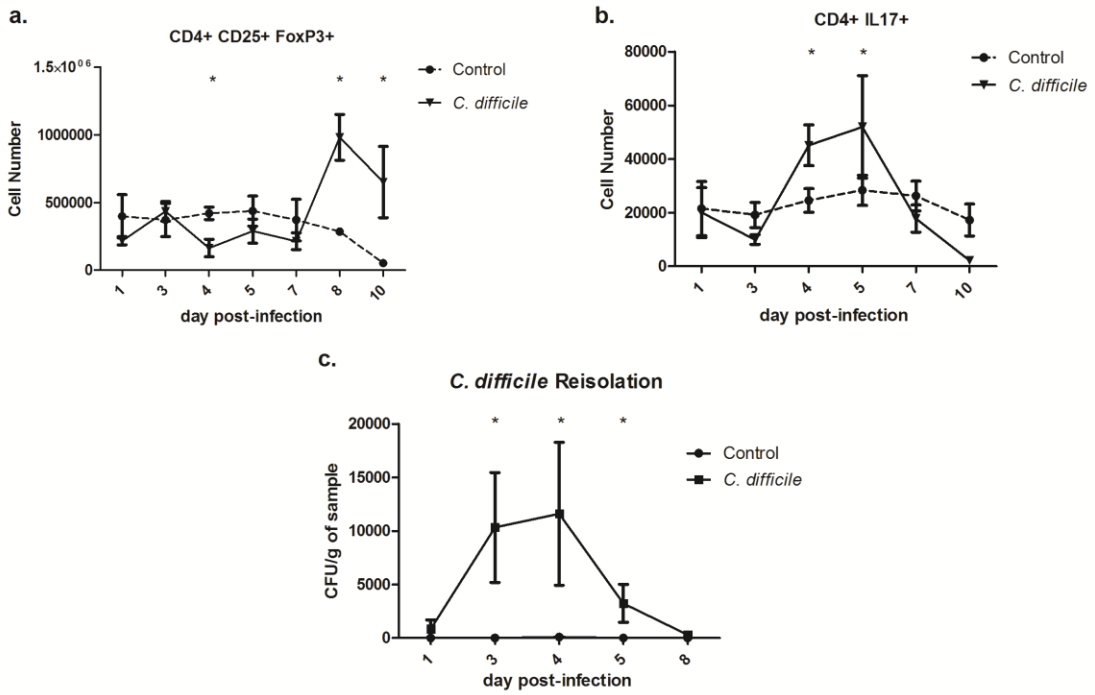

Figure 2.2. Time course of *Clostridium difficile* infection in mice. (a and b) Flow cytometry analysis of colonic lamina propria lymphocytes from days 1 to 10 post-infection showing the differences in CD4+ CD25+ FoxP3+ regulatory T (Treg) and CD4+ IL17+ T helper 17 (Th17) cells, respectively, between control and *C. difficile* challenged wild type mice. (c) Re-isolation data of *C. difficile* from colonic contents from day 1 to day 8 post-infection. Data points and error bars represent mean ± standard error of the mean (SEM). Asterisks (*) mark significance ($P \leq 0.05$) in comparison between control and *C. difficile* infected mice (n=10).

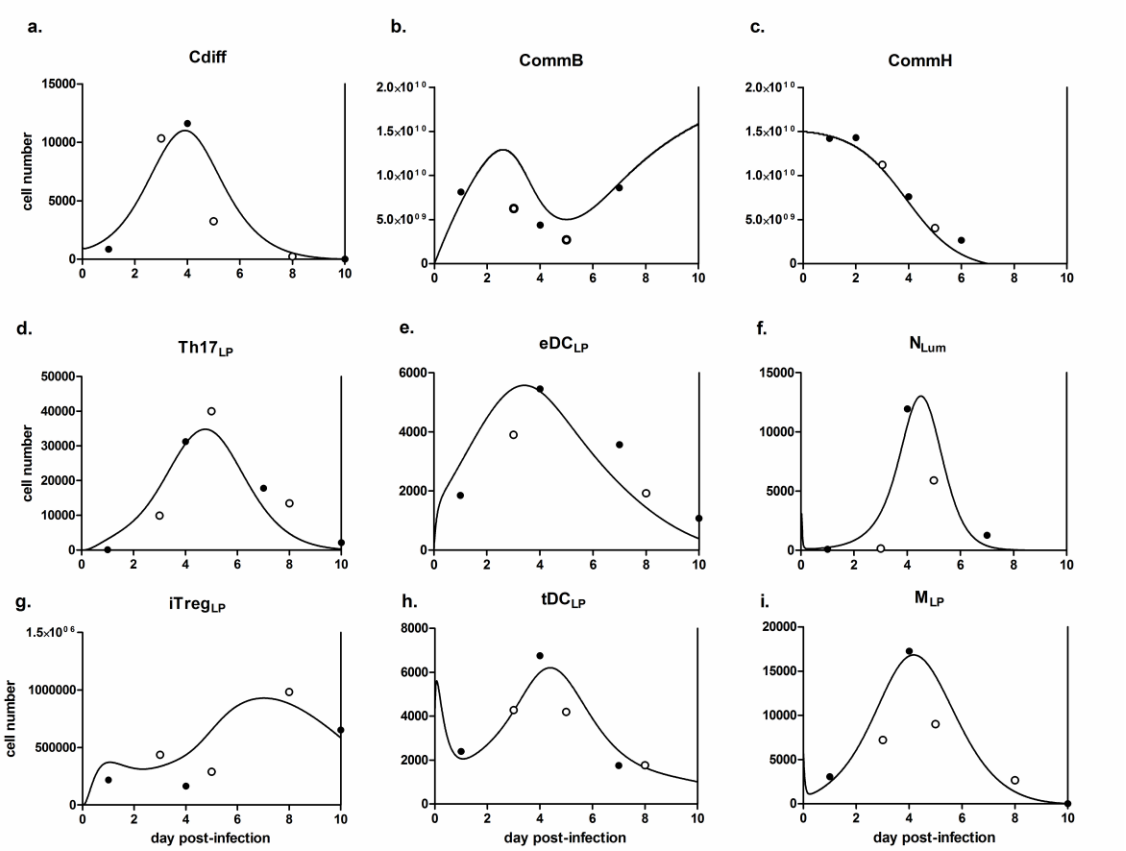

Figure 2.3. Simulated dynamics of mucosal immune response to *Clostridium difficile*. Modeling results following calibration and validation of the host response model in populations of (a) *C. difficile*, (b) protective commensal bacteria, (c) infection-exacerbating commensal bacteria, (d) lamina propria T helper 17 cells, (e) effector dendritic cells, (f) infiltrating neutrophils, (g) regulatory T cells, (h) tolerogenic dendritic cells and (i) activated macrophages. Lines represent simulation results, filled points represent experimental calibration data and unfilled points represent experimental validation data.

2.5 Sensitivity analysis helps identify determinants of C. difficile population control and epithelial damage

The clearance of *C. difficile* and colonic epithelial damage are two interconnected end effects that contribute to the overall infection severity. Sensitivity analysis on the computational model was used to determine which parameters in the network had the greatest influence on these factors. Each quantity has a distribution of parameter impacts with a large number of low impact parameters centered around zero, and smaller amounts with both positive and negative effects at larger magnitudes (Figs. 4a and b). In each case the very large impact parameters are, by majority, directly involved with the population being analyzed. Because of this direct relation, little can be gained beyond what is naturally intuitive from delving into these parameters further. As a result, these parameters were not evaluated further. Parameter 5 through 8 in Fig. 4c were associated with an increase in the *C. difficile* population in the lumen and included the degradation and death rates of effector

immune cells, macrophages, neutrophils and Th17 cells, as well as the death rate of commensal species. In contrast, the production of effector DC, parameter 1, greatly contributed to a decrease in the *C. difficile* population. The impact of balancing regulatory and effector arms of the mucosal immune response is also displayed through effects on epithelial cell death (Fig. 4d). The induction of the Treg cell response through the production of tolerogenic DC (P1), plasticity with Th17 cells (P2) and a regrowth of commensal bacterial species (P3) possess strong decreasing effects on the amount of epithelial cell death.

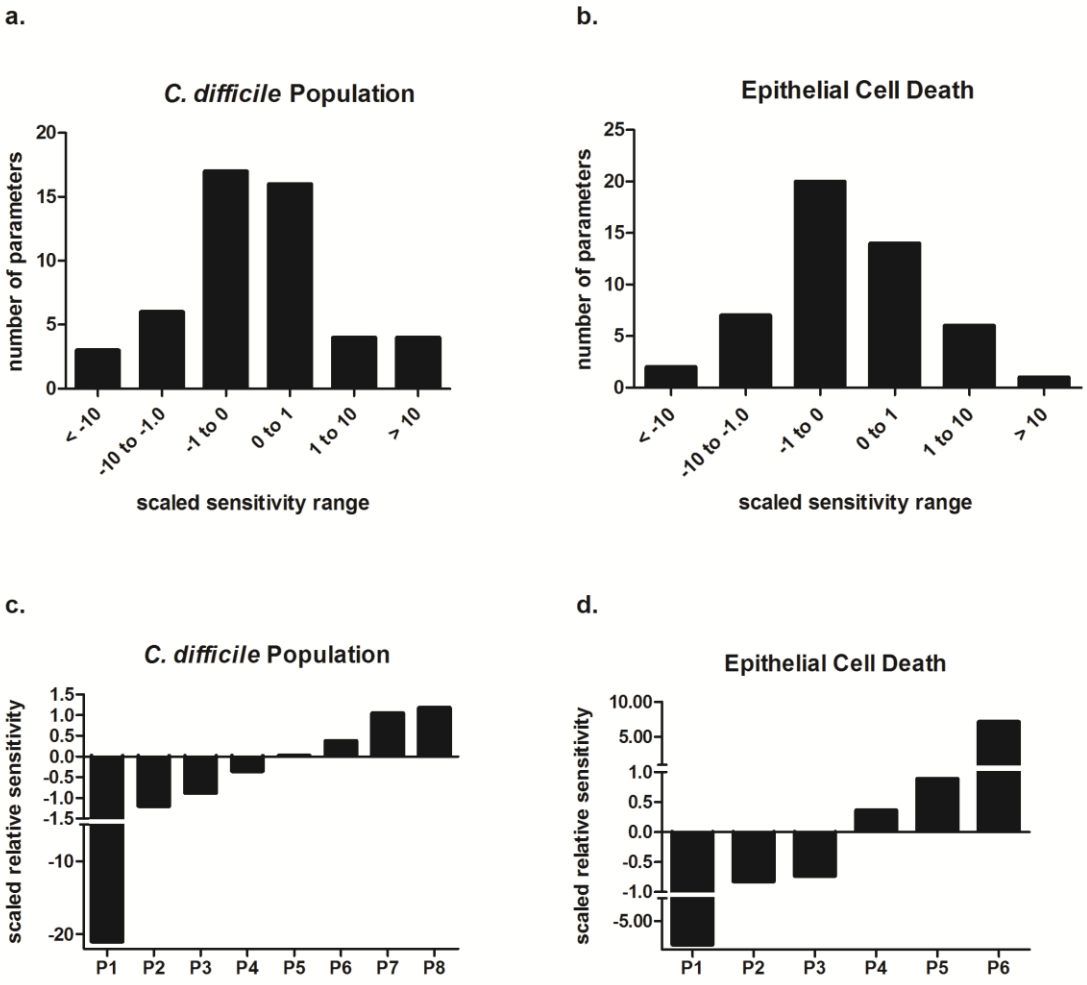

Figure 2.4. Relative effects of parameters on *Clostridium difficile* population and epithelial cell death. (a and b) Histograms showing the distribution of parameter impact on *C. difficile* population and epithelial cell death, respectively. Measurements are based on sensitivity analysis of the calibrated model. (c and d) Highest impact parameters for each quantity in which positive amounts indicate an increasing effect on the quantity and negative amounts indicate a decreasing effect. For the *C. difficile* population results, P1 contributes to effector dendritic cell production, P2 to neutrophil activation and migration, P3 to protective commensal bacteria regrowth, P4 to macrophage activation, P5 to commensal bacteria death, P6 to macrophage death, P7 to Th17 cell death, and P8 to neutrophil death. For epithelial cell death, P1 contributes to tolerogenic dendritic

cell production, P2 to Th17 to Treg cell plasticity, P3 to commensal bacteria death, P4 to Treg to Th17 cell plasticity, P5 to macrophage activation and P6 to *C. difficile* growth.

2.6 Increased production of anti-microbial peptides by epithelial cells exerts an inhibitory effect on beneficial commensal microbiota species

Quantitative RT-PCR analyses conducted on colonic contents demonstrated a difference in commensal species regrowth between *C. difficile* challenged and control mice (Fig. 5a). After intraperitoneal injection of clindamycin, amount of the *baiCD* gene is reduced 1.5 orders of magnitude on day zero compared to the initial amount on day 5 pre-infection, showing a dramatic reduction of protective commensal species after administration of antibiotics. Additionally, prior to challenge, there is no significant difference between the two experimental groups. The control mice quickly recover nearly one-third of *baiCD* containing microbiota levels as early as day one with slight fluctuations around that point for the remainder of the time course. After *C. difficile* challenge, the *baiCD* containing microbiota levels continue to decrease through day 5 post-infection. The level begins to rebound to pre-challenge amount by day seven. The difference between the *C. difficile* challenged and control levels of *baiCD* content suggest that a *C. difficile*- or immune-mediated effect is present during CDI that prevents the regrowth of protective commensal species. The colonic expression of anti-microbial peptides, DefB1 and S100A8, was assayed by using qRT-PCR. The expression of DefB1 is significantly upregulated on days 2 and 4 post-infection in colonic contents of *C. difficile* infected mice before returning to control level on day 6 (Fig. 5b). Concurrently, the expression of S100A8 in the *C. difficile* challenged mice followed that of the uninfected controls with the exception of a significantly upregulated peak on day 4 post-infection (Fig. 5c).

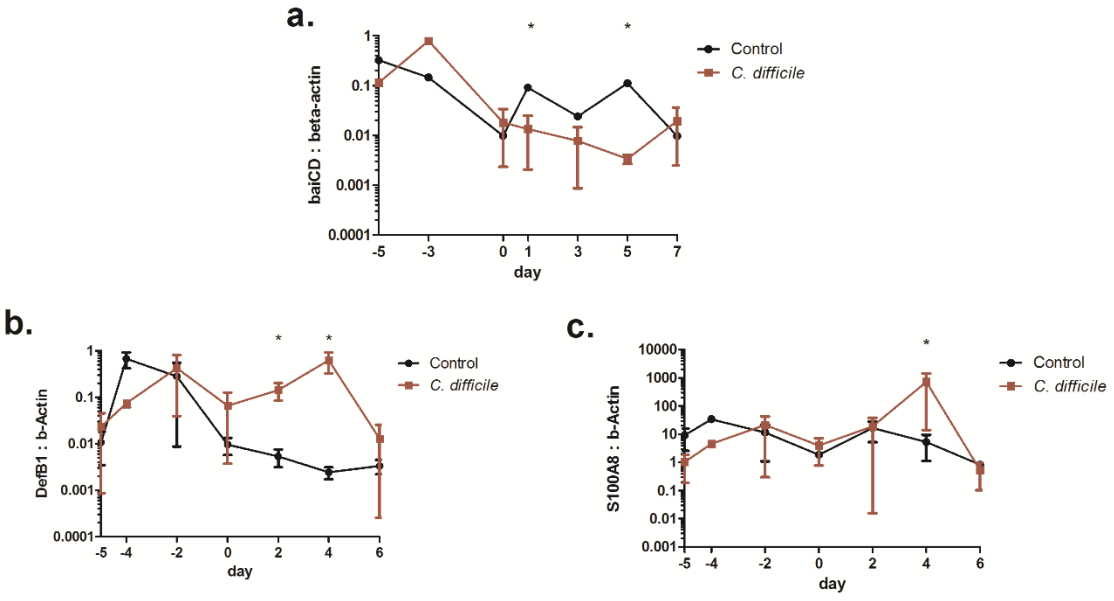

Figure 2.5. Commensal bacteria regrowth inhibited with *Clostridium difficile* infection. (a) The *baiCD* content is decreased by antibiotic treatment in both control and *C. difficile* challenged

mice and further decreased post-infection in the *C. difficile* challenged mice compared to the controls. (b and c) The expression of anti-microbial peptides DefB1 and S100A8 are upregulated with infection. Data points and error bars represent mean ± standard error of the mean (SEM). Asterisks (*) mark significance ($p \leq 0.05$) in comparison between control and *C. difficile* infected mice (n=10).

2.7 Removal of commensal bacteria regrowth inhibition alters host response to infection

To display the effect of neutrophil and epithelial cell-derived anti-microbial peptides on the regrowth of commensal species, four scenarios were considered. A simulation exists for the combined inhibition by neutrophils and inflamed epithelial cells (*NE*), by only neutrophils (*N*), by only inflamed epithelial cells (*E*) and by neither. In both the *NE* and *E* simulations, the initial regrowth of beneficial commensal species, within the first two days post-infection, is slowed compared to the uninhibited case (Fig. 6a). In comparison, the *N* simulation follows a similar pattern to the uninhibited case over the same time period. The *NE* simulation displays a reduction in beneficial commensal species following the initial stage and continuing through day 5 post infection. This reduction and deviation from regrowth of *baiCD* content on day 5 is representative of the *in vivo* data displayed in Fig. 5a. The *NE* simulation further mimics the *in vivo* situation with a clear commitment to regrowth from day 5 to day 7. The *N* simulation has a similar trend to a smaller degree while the uninhibited and *E* simulations show continuation of their respective initial trends. In the final stage of the simulation, the *N* and *NE* cases return to increasing trends. The regrowth begins to slow in the uninhibited case and has an even greater deceleration in the *E* simulation. The *E* simulation showed little change in the *C. difficile* population at the peak of infection and a delayed clearance (Fig. 6b) compared to the *NE* simulation. Both the *N* and uninhibited simulations displayed small reductions of *C. difficile* at the peak of infection relative to the *NE* case; however, only the uninhibited case cleared the *Cdiff* species by an earlier time point. The three altered simulations had reductions in peak neutrophil activation and influx compared to the *NE* case as well as occurring at slightly earlier times (Fig. 6c). Each simulation possessed a larger iTreg peak in comparison to the *NE* case prior to converging to a similar resolution (Fig. 6d). Only the uninhibited simulation greatly altered the timing of the peak in the iTreg response with an advance of approximately one half of a day.

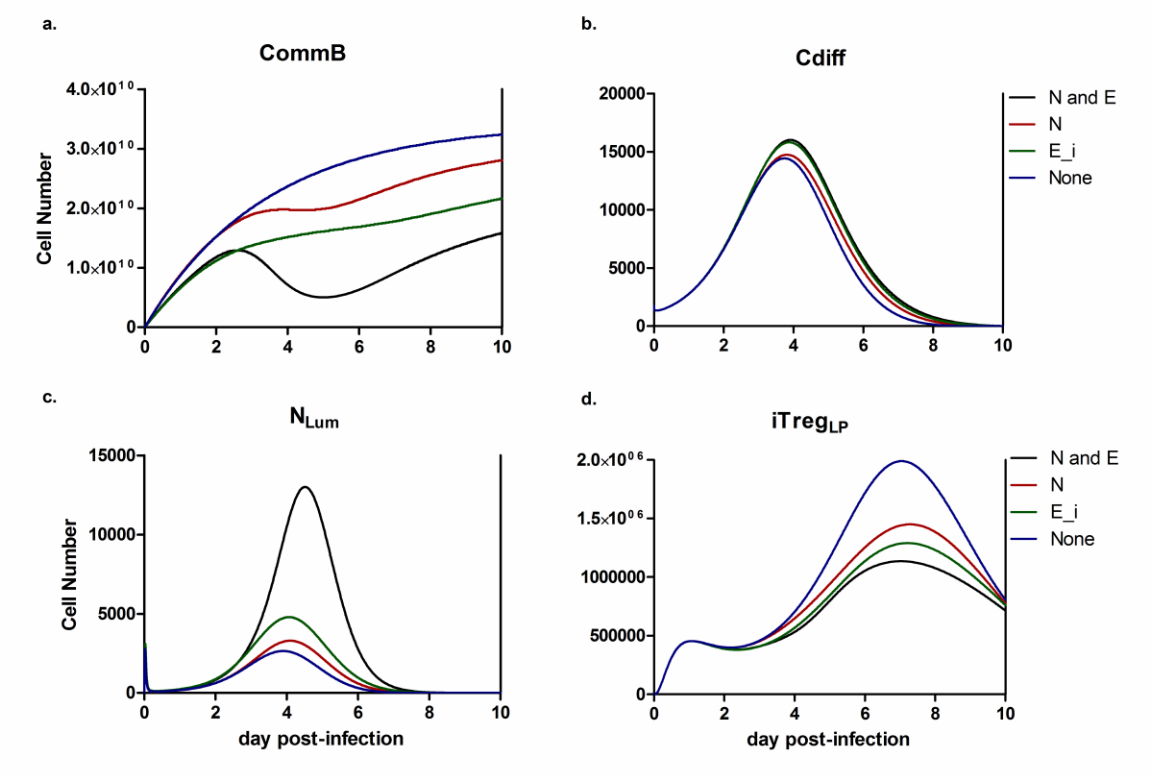

Figure 2.6. *In silico* simulation of altered commensal bacteria regrowth during *Clostridium difficile* infection. Four cases were tested with variations to the inhibition of the commensal bacteria growth: inhibited by both neutrophils and inflamed epithelial cells (N and E_i), by only neutrophils (N), by only inflamed epithelial cells (E_i), and by neither (none). Resulting changes in species populations for each case are shown: (a) *baiCD*-containing commensal species, (b) *C. difficile*, (c) activated neutrophils, and (d) iTreg cells in the lamina propria.

2.8 Discussion and Conclusions

CDI is a rising problem in the health care system. The standard treatment of infection is the discontinuation of any previous antibiotics and the administration of a new antibiotic regime. While the treatment is effective in certain cases, it can also result in significant rates of re-occurrence of CDI starting from a baseline of 25% [66]. Currently, numerous methods of alleviation of these treatment methods are under investigation, including the development of vaccines, toxin-based antibodies and microbiome reconstitution [45, 67, 68]. In this study, we used computational modeling in combination with immunology experimentation *in vivo* in an iterative systems biology cycle to better understand the dynamics of infection and the mechanisms of immunoregulation underlying mucosal immune responses to *C. difficile*.

The computational model described captures the roles and dynamics of multiple immune and epithelial cell types at the colonic mucosa during the course of CDI (Fig. 3). The validated model enables the initial testing of interventions or modulation hypotheses aimed at the improvement of the understanding or treating the CDI. This model could also be used as a tool in determining crucial time points for data collection to maximize the utility of

specific pre-clinical and clinical studies. The combined effect of initial testing and targeted time points may greatly improve the cost-efficiency of wetlab experimentation. The model replicates other previously reported experimental results. For instance, treatment with anti-Gr-1 reduces both neutrophil and monocyte levels in the context of a mouse model of *C. difficile* infection [69]. However, the reduction does not result in a large change in either the *C. difficile* population or disease severity, which also can be shown through varying parameter values and the resulting neutrophil and monocyte levels *in silico*. The association between antibiotic use and recurrence of CDI has been described clinically [66]. Following a simulated reduction of all bacterial species after the initiation of the time course study, the clearance of *C. difficile* is incomplete and results in the occurrence of a second peak at a time beyond when complete resolution would occur without intervention. Together with our own generated data, these published experiments serve to verify and validate the ability of the computational model to replicate an *in vivo* infection and produce reliable predictions.

The presence of a robust pro-inflammatory mucosal immune response following CDI at the colonic mucosa is a crucial determinant of the resulting severity of infection. Sensitivity analyses demonstrate that the induction of a regulatory response decreases damage to the epithelium following CDI (Fig. 4). Specifically, parameters controlling the production of tolerogenic DC and the plasticity of Th17 cells to become Treg cells are highly associated with decreased epithelial damage. However, the induction of regulatory responses can also slow *C. difficile* clearance and increase the overall length of infection, as the removal of pro-inflammatory cell types is largely associated with a larger *C. difficile* population. In sensitivity analyses, parameters relating to the production of activated dendritic cells show a large effect in comparison to other parameters. While this may be partially due to the sequential nature of the dendritic cell section of the model network, further investigation of this behavior could be very insightful and immunologically relevant. In many cases, *C. difficile* acts as a non-invasive pathogen and the resultant damage is toxin-mediated [70]. However, the epithelium, after damage by the toxins, is still breached, often by bacterial species present in the healthy microbiome that do not normally exhibit pathogenic behavior [71, 72]. Toxin-mediated activation of immune cells occurs, but dendritic cells could potentially exert control over the reactivity to non-*C. difficile* infiltrating bacteria. From the high sensitivities in model analysis, the relative ability or inability of dendritic cells or mononuclear phagocytes to maintain tolerogenic responses to commensal bacteria may contribute to the variation in disease severity between patients. Specifically, dendritic cells appear to act as the main drivers of establishing the Th17 response during the peak of infection that controls the pathogenic bacterial population, while also acting as a crucial element in the switch to an iTreg-dominated state during resolution. Similar impact of dendritic cells could be seen in other infections that cause broad damage to the epithelium or are a result of a non-invasive pathogen. Indeed, CX_3CR1+ mononuclear phagocytes, a population with similar functions to macrophages and conventional dendritic cells, has been shown to prevent reactions to commensal bacteria via driving the differentiation of innate lymphoid cells into subclasses that promote maintenance of barrier integrity and intestinal homeostasis. Recently, these populations have been implicated in the prevention of disease in the context of inflammatory bowel disease and *H. pylori* [73]. The use of computational modeling in precision medicine may allow for the determination of a proper

balance between pro-inflammatory and regulatory arms of the mucosal immune response in the context of new therapeutic interventions.

CDI is associated with the use of broad-spectrum antibiotics, and microbiome reconstitution through fecal transplantation or probiotic treatment has gained some traction with varying degrees of success [74, 75]. The unspecific nature of these treatments results in the proliferation of a spectrum of *Bifidobacterium* that promotes tolerance to commensal species. However, the *C. difficile* population dynamics may be unchanged or poorly altered as a result. Among other methods of inhibition, the growth of *C. difficile* has been shown to be slowed by the presence of secondary bile acids [76, 77]. Recently, specific commensal species, that convert primary bile acid to secondary bile acids, have displayed a protective ability against *C. difficile* infection [47, 78]. However, the presence of *C. difficile* indirectly inhibits the regrowth of these commensal species. Anti-microbial peptides DefB1 and S100A8 are upregulated in colons of *C. difficile*-infected mice at distinct time points during infection (Fig. 5). DefB1, the gene responsible for beta-defensin-1 produced largely by epithelial cells, is upregulated early and for an extended period in the time course between days 2 and 4 post-infection [79]. While beta-defensin-1 has broad membrane lysis ability, it has its largest effect on gram-negative bacteria [80]. Notably, *C. scindens*, a highly prevalent member of bile acid inducible operon containing microbiome, is gram-negative. The combination of elevated beta defensin-1 and the susceptibility of a major constituent of the beneficial microbiome to this anti-microbial peptide suggest a strong probability that the host response to *C. difficile* is also inhibitory to the regrowth of beneficial commensal strains. In contrast, expression of S100A8, a component of calprotectin sourced mainly from neutrophils and monocytes, is elevated with a distinct peak on day 4 corresponding with the peak of neutrophil activation [81]. The combined anti-microbial activity may contribute to decreased efficiency in the regrowth of the native microbiome during CDI suggested by computational experimentation (Fig. 6). The simulated removal of epithelial cell-related inhibition of commensal bacterial regrowth in the model allows for an increased amount of beneficial commensal species early in the infection, resulting in slightly decreased *C. difficile* levels through direct competitive effects on the population itself and indirectly through down-regulation of neutrophil and Th17 cell-mediated effector responses. The alterations within the *C. difficile* population during this simulation would be unlikely to significantly affect the initial establishment of a clinical cure through clearance of *C. difficile* [82]. However, the lack of effect is still an important result as it suggests that the simulated changes do not result in an inhibition of *C. difficile* clearance or a worsening of the hypothetical prognosis. Additionally, the increased and quicker re-growth of commensal bacteria would likely exhibit greater direct effects on the *C. difficile* population through the prevention of relapse. The lack of microbial diversity is a major predictor of relapse susceptibility [83]. The return of this diversity would greatly reduce the capacity for the persisting *C. difficile* population to expand back to pathogenic levels. During the course of the initial infection, the effect of continued commensal re-growth is largely immunomodulatory rather than displaying a large effect on the *C. difficile* population. Continued commensal re-growth throughout the time course displays an ability to shorten the length of CDI and decrease the overall magnitude of the inflammatory host response at the colonic mucosa and resultant collateral damage. This suggests a need for a microbiome reconstitution intervention to restore beneficial effects in terms of the *C.*

difficile growth inhibition and regulation of a pro-inflammatory environment. The ability to further increase the specificity and success of microbiome reconstitution therapies can be aided by computational modeling.

Neutrophilic influx is a major cause of symptom severity as indicated by sensitivity analysis of our model (Fig. 4) and previously reported connections [84, 85]. Subsequently, the chemokine, IL-8, has been studied as a potential marker for severity and prognosis in the diagnosis of *C. difficile* infection [86]. In addition to IL-8, other promising biomarkers of *C. difficile* associated disease severity include the antimicrobial peptide calprotectin, hepatocyte growth factor, and procalcitonin [87-89]. A future direction in the analysis and application of multiscale models of CDI could be the determination of a non-intuitive vital node in the network; the latter may allow for the extrapolation of easily measurable biomarkers of disease in the context of data-driven models and multiscale models of mucosal immune responses [90]. Consequently, the discovered marker could indicate the stage of infection or the need for or extension of treatment. Methods have been described based on the correlational evaluation of model quantities in virtual populations and global sensitivities in the analysis and discovery of potential biomarkers in the context of lipoprotein metabolism and acute inflammation, respectively [91, 92]. The sensitivity analysis allows for the determination model parameters that are most impactful on immune response and infection outcome. Both methods illustrate the difficulty in the determination of biomarkers without the aid of computational modeling due to the inherent variation of expression levels between individuals. As we have demonstrated the potential changes in mucosal immune response following modifications to the microbiome composition, measurement of beneficial commensal bacterial metabolites, such as deoxycholate and lithocholate, in combination with the computational modeling simulations could help predict the effectiveness of fecal microbiota transplantation and other therapeutic or prophylactic interventions on a patient-to-patient basis or prove to be an effective predictor of untreated outcome. The generation of a synthetic population through a random sampling of parameter values within a normal distribution of the calibrated values would allow for these predictions to be extended into *in silico* clinical trials of CDI.

The model developed and analyzed in this article was specific for the host response to *C. difficile*; however, many of the strategies used for this purpose can be extended to better the understanding the responses to other enteric pathogens and inflammatory conditions. Specifically, while fecal transplantation and microbiome reconstitution may be more greatly established in the context of CDI, the concept of promoting the growth of beneficial bacteria could have wide reaching implications in the understanding of mucosal immunity. Currently, there is an increasing prevalence of auto-immune and auto-inflammatory diseases, especially within developed countries [93]. One hypothesis is that improved hygiene and the resultant reduction in microbial exposure have led to decreased regulation of the immune system and an over-exuberant response when an exposure does occur [94]. Additionally, the ability of the host to generate an accommodating environment for commensal species, such as through the secretion of polysaccharides, has been shown to affect the susceptibility to disease [95, 96]. Through the creation of a computational model describing the interactions of bacterial families with the epithelium and elements of the mucosal immune system, an enhanced understanding of which species contribute to the

susceptibility and severity of the response could be generated. Furthermore, this increase in knowledge could contribute to the development of targeted pro-biotic and reconstitution therapies to combat the rising rates of auto-immune and auto-inflammatory disease and altered microbiomes resulting from genetic and environmental differences.

In conclusion, we have examined the time course of the immune response to *C. difficile* infection through a combination of experimental and computational approaches using an iterative systems biology cycle. We described the importance of maintaining a balance between effector and regulatory arms of the mucosal immune response in the clearance of pathogen and severity of infection. Specifically, the production of anti-microbial peptides may exacerbate disease and pathology, and prolong the CDI due to non-specific inhibition of commensal bacterial regrowth. Computational simulations supported the role of this inhibition on the disease severity with a virtual removal of neutrophil and epithelial cell derived anti-microbial inhibitions, separately and together, on commensal bacterial regrowth. The simulated shifts in host response behavior provide novel insights underlying the mechanisms of interaction between the mucosal immune system and the gut microbiota during CDI.

2.9 Materials and methods

Ethics Statement

All experimental procedures were approved by the Institutional Animal Care and Use Committee (IACUC) of Virginia Tech and met or exceeded requirements of the Public Health Service/National Institutes of Health and the Animal Welfare Act. The IACUC approval ID for the study was 12-173-VBI. C57BL/6J wild type mice were bred and maintained in experimental facilities at Virginia Polytechnic Institute and State University. Mice were housed two to five per cage on a ventilated rack in a room with a standard 12 hours on, 12 hours off light cycle. The animals were given ad libitum access to standard rodent chow and water. After infection, mice were monitored daily for signs of disease severity and weighed. Four hour checks were triggered when an animal reached a score of three. Mice were euthanized prior to scheduled end point if severe signs of illness, such as a large weight loss, piloerection or a loss of mobility, were present. All mice were euthanized with carbon dioxide narcosis and a secondary cervical dislocation.

C. difficile Animal Model

This study followed a previously reported model of *Clostridium difficile* infection [97]. Prior to bacterial challenge, mice were treated with a mixture of antibiotics in drinking water. The mixture consisted of colistin 850 U/mL (4.2 mg/kg), gentamycin 0.035 mg/mL (3.5 mg/kg), metronidazole 0.215 mg/mL (21.5 mg/kg), and vancomycin 0.045 mg/mL (4.5 mg/kg). Mice were kept on the antibiotic water for a three day period corresponding to days 5 to 3 prior to challenge. The mice were returned to standard autoclaved water two days before challenge. The mice were given an intraperitoneal injection of clindamycin, 32 mg/kg, one day prior to infection. The control group received the same antibiotic pretreatment. The infected group was challenged through intragastric gavage with *Clostridium difficile* strain VPI 10463 (ATCC 43255) 10^7 cfu in 200 uL/mouse of Brucella broth. Mice were weighed and scored daily to assess the presence of disease symptoms

(diarrhea, piloerection, hunchback position, etc.). Mice were sacrificed through CO_2 narcosis and secondary cervical dislocation at different time points (days 1, 3, 4, 5, 7, 8, 10) post infection.

Sample Processing

Mesenteric lymph nodes and colons were collected. Mesenteric lymph nodes (MLN) were crushed using the frosted ends of microscope slides. Samples were centrifuged and washed with phosphate buffered saline (PBS) containing 5% fetal bovine serum (FBS) and Golgi stop. Cells were centrifuged and re-suspended in FACS buffer and counted using BD Coulter cell counter. Colon samples were washed in BD Cell Recovery Media to remove epithelial cells. Remaining tissue was degraded in RPMI containing collagenase and DNase at 37°C while stirring. Samples were filtered using and centrifuged. Remaining cells were re-suspended and purified in a Percoll gradient. Cells at the Percoll interface were collected and counted.

Flow cytometry

MLN and colonic lamina propria lymphocytes were plated in 96 well plates ($6x10^5$ cells/well). Cells were incubated with fluorochrome conjugated antibodies to extracellular markers, anti-CD45 APC-Cy7, anti-CD3 PE-Cy5, anti-CD4 PE-Cy7, anti-CD25 biotin, anti-CD64 PE, anti-CD11b AlexaFluor700, anti-F4/80 PE-Cy5, anti-CD11c FITC, anti-Gr1 PE-Cy7, anti-Ly6c PerCP-Cy5.5, and anti-MHC-II biotin. Samples needing a secondary staining were incubated with Streptavidin-Texas Red. The samples were then fixed and permeabilized. Cells were incubated with antibodies to intracellular markers, anti-FoxP3 FITC, anti-IL-10 APC, anti-RORγT PE, and anti-IL-17 APC. Data was acquired with a BD LSRII flow cytometer and analyzed using FACS Diva software (BD Pharmingen).

Bacterial re-isolation

Colonic contents were collected from excised colons. Samples were homogenized in Brucella broth and incubated at 68°C for one hour. Samples were centrifuged at 10,000 rpm for 30 seconds and the supernatant was collected. The supernatant was serially diluted (1:10, 1:100, 1:1000) and plated on Oxoid *Clostridium difficile* agar plates containing *Clostridium difficile* selective supplement. Plates were incubated in anaerobic conditions using a BD EZ anaerobic container system kit for 2 days at 37°C. Colonies were counted and compared to sample weight for normalization.

Gene expression

Total RNA was isolated from mouse colonic contents using a Qiagen RNA isolation mini kit. Complementary DNA (cDNA) was generated from each sample using the iScript cDNA synthesis kit. Standards were produced through a polymerase chain reaction on the cDNA with Taq DNA polymerase from Invitrogen. The amplicon was purified using the Mini-Elute PCR purification kit from Qiagen. Expression levels were obtained through quantitative real-time PCR on a Bio-Rad CFX 96 Thermal Cycler using the Bio-Rad SYBR Green Supermix. For analysis, the starting amount of anti-microbial peptide cDNA was compared to that of beta-actin, as a control. Primer sequences are provided in supplemental information (S3 Table).

Computational modeling

The generation of a computational model was used in combination with experimental methods to improve our understanding of gathered data, to create a more systematic experimental process and to generate new knowledge. The model generation was a multi-step process, including the creation of a model network, calibration and validation of the model equations, analysis of the model, and execution of *in silico* simulations. The structure of the computational model, which includes the species and their interactions, was constructed in CellDesigner, a Systems Biology Markup Language (SBML) compliant software. The network was generated based on a combination of generated time course data and a thorough literature review and depicts the cellular host involving interactions between dendritic cells, T helper cells, macrophages, neutrophils, epithelial cells and commensal bacteria. The model was imported into Complex Pathway Simulator (COPASI) software[65]. In COPASI, the interactions and transitions were assigned ordinary differential equations representing multiple kinetics including mass action, simple activation and Hill-type activation and inhibition, available in supplemental information (S1 File). The resulting parameters were estimated using Particle Swarm and Genetic algorithms with time course data generated through the mouse model of infection on days 1, 4, 7 and 10 in addition to extra days post-infection included in sourced data. The parameter search algorithms seek to minimize the sum of squares for the calibration dataset. To further train the model, a separate dataset set containing data from days 3, 5, and 8 post-infection was used as a validation dataset. In the parameter estimation process, the sum of squares for the validation dataset is monitored but not minimized. Rather an increase in the sum of squares for the validation dataset is used as a stop criterion for the search algorithm which serves as a preventative measure against over-fitting. Parameters values and further information on the parameter fitting process are available in supplemental information (S1 Table and S2 File). Time course simulations were conducted using an LSODA deterministic method. The model displays the ability to represent activation, differentiation and death of the cell types involved and allows for distinctions to be made in patterns and sequences of events. Local sensitivities were calculated through numerical differentiation using a finite difference method with delta factor 0.001 and delta minimum $1x10^{-12}$. The sensitivity analysis was used to elucidate the combination of direct and indirect effects. Furthermore, all model quantities had on specific outcome events which allows for the identification of potential target nodes with which a desired change can be induced. *In silico* simulations on the effects of anti-microbial inhibition of commensal regrowth were conducted through modification of the CommB to CommD transition. The resulting changes were observed in a time course simulation.

Model assumptions

Initial particle numbers are assumed to be representative of a post-antibiotic ablation state in which commensal species are greatly reduced. The model requires an initial amount of the *Cdiff* species to be present for the response to be initiated. Reactions may represent direct cell-to-cell contact (sensing of *C. difficile* by dendritic cells), cytokine- or toxin-mediated effects (the differentiation and activation of CD4+ T cell populations), or cellular movement (migration of T cells from the mesenteric lymph nodes to the lamina propria). Cross-compartmental reactions are possible through the environmental changes induced by the effector cell in the reaction. The model assumes that protective commensal species

follow a regrowth pattern similar to a summation of *Clostridiaceae*, *Ruminococceae*, *Verrucomicrobiaceae*, *Porphyromonadaceae*, *Turicibacteraceae*, and *Eubacteriaceae* bacterial families, while the infection-exacerbating population is assumed to follow that of *Enterobacteriaceae*, *Streptococcaceae*, and *Enterococcaceae* families. Reactions in the model may be simplifications of multi-step processes. Non-informative parameters were eliminated from the model through simple deletion of the reaction or fusion with a related neighboring reaction. Parameters were deemed non-informative through local sensitivity analysis within COPASI using numerical differentiation through finite differences. For instance, the initial model contained separate steps for the activation and migration of neutrophils. Because the sensitivity to the migration parameter was five orders of magnitude less than the sensitivity to the activation parameter, the reaction corresponding to the migration was combined into the activation reaction.

Statistical analysis

A one way analysis of variance (ANOVA) was performed to determine significance in the data using a SAS (SAS Institute) general linear model procedure. Differences of $p \leq 0.05$ were considered significant. Data was comprised of multiple experiments. The number of samples per for each group at each time point varied between five and eight. Data is displayed as mean values with error bars representing standard error of the mean and asterisks to mark significance.

Chapter 3

Systems modeling of interactions between mucosal immunity and the gut microbiome during Clostridium difficile infection

Andrew Leber, Raquel Hontecillas, Nuria Tubau-Juni, Victoria Zoccoli-Rodriguez, Matthew Hulver, Ryan McMillan, Kristin Eden, Irving C. Allen, and Josep Bassaganya-Riera

Leber A, Hontecillas R, Tubau-Juni N, Zoccoli-Rodriguez V, Hulver M, et al. (2017) NLRX1 Regulates Effector and Metabolic Functions of CD4+ T Cells. J Immunol 198: 2260-2268. (http://www.jimmunol.org/)

3.1 Summary

Nucleotide oligomerization domain (NOD) like receptor X1 (NLRX1) has been implicated in viral response, cancer progression and inflammatory disorders; however, its role as a dual modulator of CD4+ T cell function and metabolism has not yet been defined. The loss of NLRX1 results in increased disease severity, populations of T helper 1 and T helper 17, and inflammatory markers (IFNγ, TNFα, and IL-17) in mice with DSS colitis. To further characterize this phenotype, we employed *in vitro* CD4+ T cell differentiation assays and show that NLRX1 deficient T cells have a greater ability to differentiate into inflammatory phenotype and greater proliferation rates. Further, NLRX1-/- cells have a decreased responsiveness to immune checkpoint pathways and greater rates of lactate dehydrogenase activity. When metabolic effects of the knockout are impaired, NLRX1 deficient cells do not display significant differences in differentiation or proliferation. To confirm the role of NLRX1 specifically in T cells, we used an adoptive transfer model of colitis. Rag2-/- recipient mice of NLRX1-/- naïve or effector T cells experienced increased disease activity and effector T cell populations, while no differences were observed between groups receiving wild-type or NLRX1-/- regulatory T cells. Metabolic effects of NLRX1 deficiency are observed in a CD4-specific knockout of NLRX1 within a *C. rodentium* model of colitis. The aerobic glycolytic preference in NLRX1-/- is combined with a decreased sensitivity to immunosuppressive checkpoint pathways to provide greater

proliferative capabilities and an inflammatory phenotype bias leading to increased disease severity.

3.2 Introduction

Nucleotide oligomerization domain (NOD) like receptor X1, NLRX1, is a pattern recognition receptor and a member of the negative regulatory subclass of NLRs [1-3]. Previously, NLRX1 has been linked to the viral response, innate immunity and downstream effects on NF-κB signaling [4-7]. Located on the outer mitochondrial membrane, NLRX1 has been shown to influence reactive oxygen species production and the proliferation of epithelial cells in the context of colorectal cancer disease models [8-10]. As such, NLRX1 is a potential immunoregulatory molecule that integrates immune and metabolic function. However, its role in the adaptive mucosal immune response, specifically CD4+ T cells has not been described.

The differentiation of T cells is an important determinant in the progression of immune-mediated disease and response to infectious disease contributing to exacerbated and sustained inflammatory responses [11-14]. As amplifiers or controllers of the immune response, CD4+ T cells are highly sensitive and responsive to their environment with activation occurring through multiple mechanisms including dendritic cell (DC) contact or the cytokine microenvironment [15-17]. The activation is paired with a phenotype commitment, albeit a plastic commitment, with distinct effector (Th1, Th2, Th9, Th17, Th22, Tfh) and regulatory (nTreg, iTreg, Tr1, Tfr) behavior[12, 18]. Recently, the effect of metabolic pathways on the differentiation and proliferation of T cells has arisen as a potential factor in these cell phenotype decisions [19-21]. In particular, a divide exists in the preferred metabolic activity of effector and regulatory T cells [22]. Effector T cells display a preference for glycolysis, even in the presence of sufficient oxygen, similar to the Warburg effect described within cancer cells [21]. In contrast, regulatory T cells have a lower metabolic rate as well as an oxidative means of energy production [22].

Also contributing to the homeostasis of T cells is signaling derived from immune checkpoint pathways. PD-1 and CTLA-4 signaling are the most prominent and the earliest described of these pathways; although, more recently discovered pathways, such as LAG3, TIM3 and TIGIT, have displayed similar functionality in terms of suppressive effects on the proliferation, metabolism and levels of cytokine production [23-25]. While the blockade of the immune checkpoint pathways is an emerging cancer therapy, impaired immune checkpoint responses have been implicated in many inflammatory and immune-mediated diseases [26-28]. PD-1 and PD-L1 polymorphisms have been associated with SLE, arthritis, multiple sclerosis and Crohn's disease [24]. Both Crohn's disease and ulcerative colitis, the two main clinical manifestations of inflammatory bowel disease (IBD), have been mechanistically linked to overly exuberant T cell responses within the gastrointestinal (GI) mucosa [29].

Herein, we describe the integrative effects of NLRX1 on immunity and metabolism through the greater proliferation, inflammatory bias, and decreased sensitivity to immune

checkpoint pathways of CD4+ T cells. We employ in vitro and in vivo findings to illustrate the implications of NLRX1 deficiency in T cells by using three mouse models of IBD.

3.3 Loss of NLRX1 increases disease severity and inflammatory T cell subsets in a DSS model of colitis

Wild-type and NLRX1-/- mice were administered DSS within drinking water over a seven day period. Significant increases in disease activity index were observed within NLRX1-/- as soon as day 3 of DSS challenge and continuing through the remainder of the administration period (Fig. 3.1A). The increased disease severity was paired with increased Th1 and Th17 populations both within the colonic lamina propria (Fig. 3.1B-C) and spleen (Fig. 3.1E-F) at days 3 and 7 of DSS challenge. No differences were observed in splenic or LPL Treg cells through the experimental period (Fig. 3.1D, G). A significant increase in TNF-producing CD4+ T cells was also observed, but no differences in IL-22-producing or IL-4-producing CD4+ T cells were observed between genotypes. Broad increases in the expression of inflammatory cytokines, IL-17, IFNγ, and TNFα, were observed in whole colon RNA (Fig. 3.1H-J).

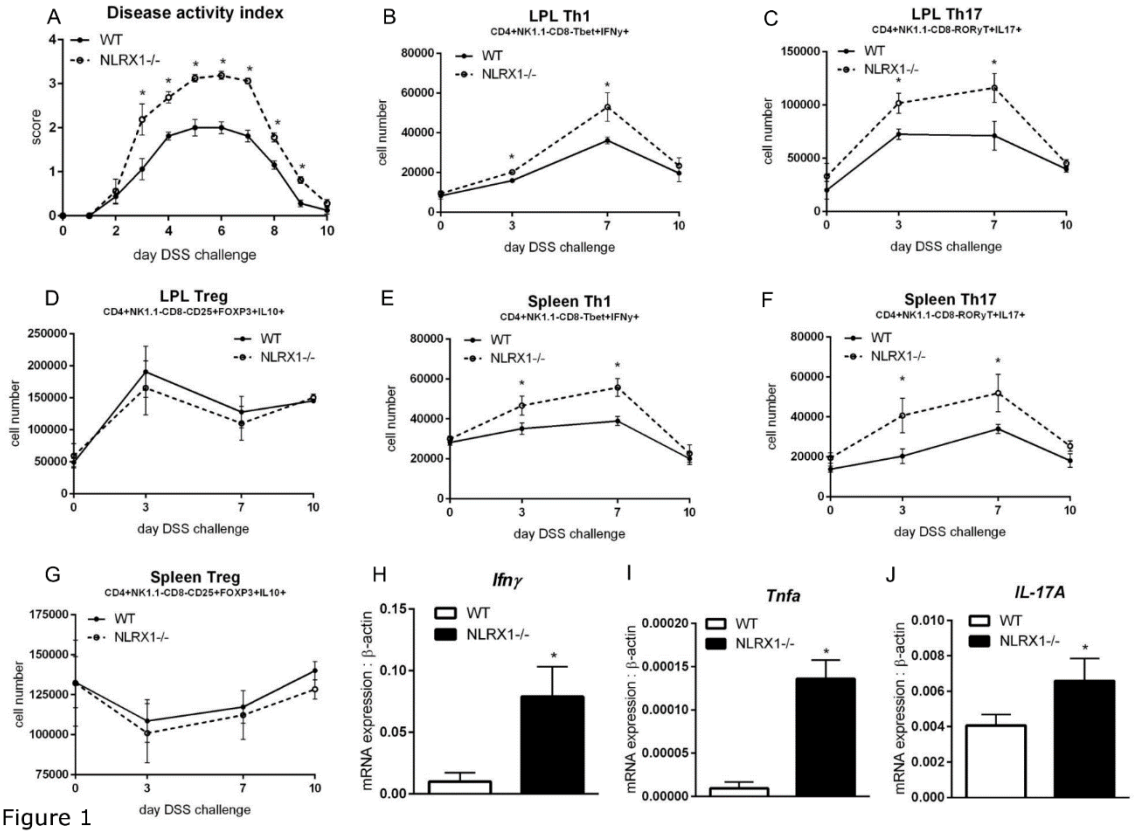

Figure 1

Figure 3.1. DSS colitis induces greater inflammatory T cell populations in NLRX1-/-. Disease activity index of wild type and NLRX1-/- on DSS for 7 days followed by three days of water (A). Colonic lamina propria (B) and spleen (E) cell numbers of Th1 (CD4+NK1.1-CD8-Tbet+IFNγ+). Colonic lamina propria (C) and spleen (F) cell numbers of Th17 (CD4+NK1.1-CD8-RORγT+IL17+). Colonic lamina propria (D) and spleen (G) cell numbers of Treg (CD4+NK1.1-

CD8-CD25+FOXP3+IL10+). mRNA expression of Ifny (H), Tnfa (I) and IL17A (J) in colons of mice on day 7 of DSS challenge. Asterisks mark significance (P<0.05, n=12).

Using the cre-lox recombination system, NLRX1fl/fl;CD4Cre+ (NLRX1$^{\Delta T}$) were generated and challenged with DSS to validate whether NLRX1 has an intrinsic role within T cells during colitis. In a similar manner to the NLRX1-/-, NLRX1ΔT displayed worsened disease activity (Fig. 3.2A) throughout the time course culminating in increased colonic LPL (Fig. 3.2B-C) and splenic (Fig. 3.2E-F) Th17 and Th1 at day 7 of DSS challenge. However, no differences in regulatory T cells were observed at the colonic (Fig. 3.2D) or splenic (Fig. 3.2G) level.

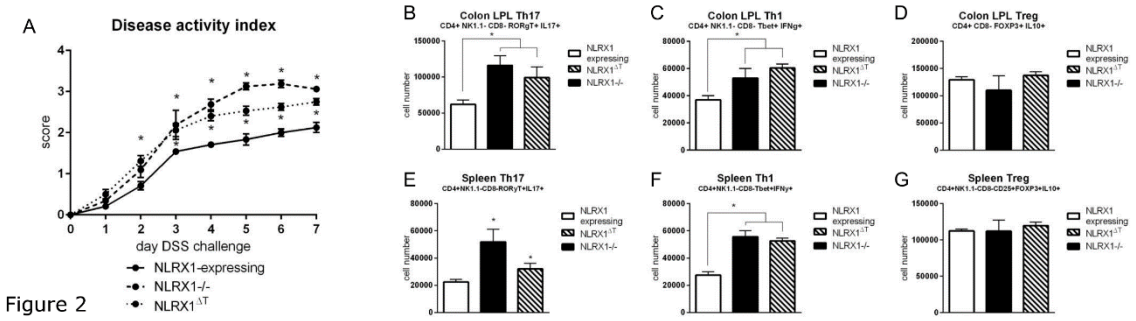

Figure 2

Figure 3.2. DSS colitis induces greater inflammatory T cell populations with T cell specific deletion of NLRX1. Disease activity index of wild type and NLRX1fl/fl;CD4cre+ on DSS for 7 days (A). Colonic lamina propria (B) and spleen (E) cell numbers of Th17 (CD4+NK1.1-CD8-RORγT+IL17+). Colonic lamina propria (C) and spleen (F) cell numbers of Th1 (CD4+NK1.1-CD8-Tbet+IFNγ+). Colonic lamina propria (D) and spleen (G) cell numbers of Treg (CD4+NK1.1-CD8-CD25+FOXP3+IL10+). Asterisks mark significance (P<0.05, n=12).

3.4 NLRX1 deficiency leads to increased Th17 differentiation and proliferation.

To determine the direct effect of the loss of NLRX1 on the differentiation of CD4+ T cells, we sorted naïve CD4+ T cells from the spleens of wild-type and NLRX1-/- mice. When exposed to a Th17 promoting cytokine environment (IL-6, TGF-β, IL-23, α-IL-4, α-IFNγ), NLRX1-/- T cells possessed a higher rate of differentiation into Th17 cells than wild-type T cells (Fig. 3.3A). In contrast, when exposed to an iTreg promoting cytokine environment (TGF-β, IL-10, α-IL-4, α-IFNγ), NLRX1-/- T cells did not behave significantly differently than wild type cells in regards to iTreg differentiation rate (Fig. 3.3B). However, the rate of iTreg differentiation within Th17-promoting media was significantly lower for NLRX1-/- T cells (Fig. 3.3C). The difference was exacerbated by the addition of PD-L1 to the culture media, which significantly increased the population in wild type samples but induced no change in NLRX1-/- samples (Fig. 3.3C). The proliferation of the CD4+ T cells was measured in vitro by CFSE staining. NLRX1-/- Th17 differentiated cells displayed a greater proliferative index than wild-type Th17 cells (Fig. 3.3D). The administration of PD-L1 decreased the proliferative index at a greater magnitude in wild-type cells (Fig. 3.3D). Increased PD-L1 expression was observed within both WT and NLRX1-/- mice on day 7 of DSS challenge compared to non-DSS controls.

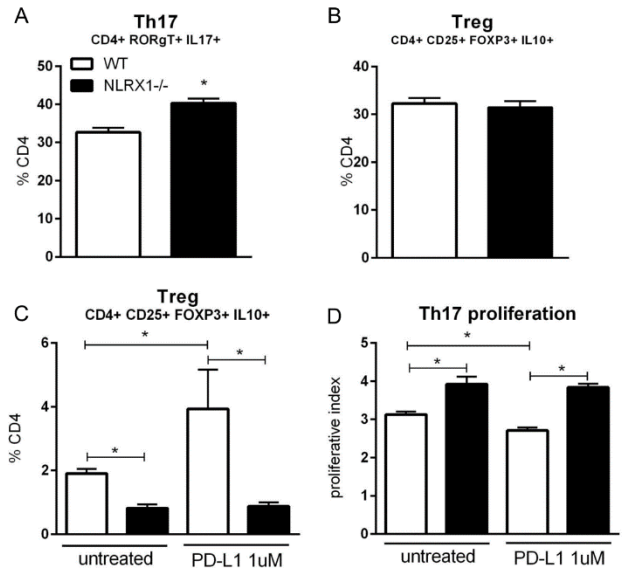

Figure 3.3. NLRX1-/- CD4+ T cells have greater inflammatory and proliferation potential. Proportion of Th17 differentiated cells in vitro in Th17 differentiating media (A). Proportion of Treg differentiated cells in vitro in Treg differentiating media (B). Proportion of Treg differentiated cells in vitro in Th17 differentiating media with and without addition of PD-L1 (C). Th17 proliferation index by CFSE staining with and without addition of PD-L1 (D). Data is a result of three experiments with triplicate samples ($p<0.05$, $n=9$).

3.5 NLRX1 contributes to the switch from oxidative to anaerobic metabolic pathways.

Based on the *in vitro* proliferation results and the *in vivo* RNA-seq metabolic differences at the colonic level, we sought to determine the effect of NLRX1 on the metabolic processes of T cells. NLRX1 deficiency results in increased expression of Cpt1a, Fabp4 and Glut1 genes responsible for the uptake and utilization of glucose and fatty acids (Fig. 3.4A-C). Similarly, the loss of NLRX1 increases the activity of lactate dehydrogenase and the rate of incomplete fatty acid oxidation, a measure of acid soluble metabolites following the oxidation of labeled palmitate as opposed to complete oxidation to carbon dioxide (Fig. 3.4D-E). Administration of PD-L1 decreased the activity of lactate dehydrogenase and increased total fatty acid oxidation in wild-type Th17 cells but provided no significant changes in NLRX1-/- (Fig. 3.4D). Additionally, the rate of total fatty acid oxidation failed to increase following PD-L1 stimulation within NLRX1-/- cells (Fig. 3.4F). The increased glycolytic flux in NLRX1-/- Th17 cells was further confirmed by an increased extracellular acidification rate (Fig. 3.4G). No consistent differences existed in oxygen consumption rate in Th17 cells between genotypes (Fig. 4H). Similar differences were observed in CD4+ T cells isolated from the colons of mice on day 3 of DSS challenge. However, no differences were observed in either extracellular acidification or oxygen consumption rates within differentiated regulatory T cells. NLRX1-/- differentiated Th17 cells also displayed increased glycolytic flux, compared to WT, by measure of carbon dioxide production from the metabolism of radiolabeled glucose (Fig. 3.4I). Direct inhibition of lactate dehydrogenase activity, through treatment with sodium oxamate, normalized NLRX1-/- Th17 differentiation rates and proliferative index to wild-type levels (Fig. 3.4J-K). The

administration of sodium oxamate *in vivo* provided similar decreases in NLRX1-/- Th17 cell numbers in addition to Th1 cell numbers during DSS colitis. Additionally, treatment with metformin, an activator of 5' adenosine monophosphate-activated protein kinase (AMPK), rescued the responsiveness to PD-L1 signaling and decreased lactate dehydrogenase activity (Fig. 3.4L-M). Notably, culture within microaerophilic conditions further increased the differences between NLRX1-/- and wild-type in measures of Th17 differentiation rate and lactate dehydrogenase activity (Fig. 3.4N-O). The lack of NLRX1 increased the expression of hypoxia inducible factor 1α, Hif1a, both in normoxic and microaerophilic conditions (Fig. 3.4P).

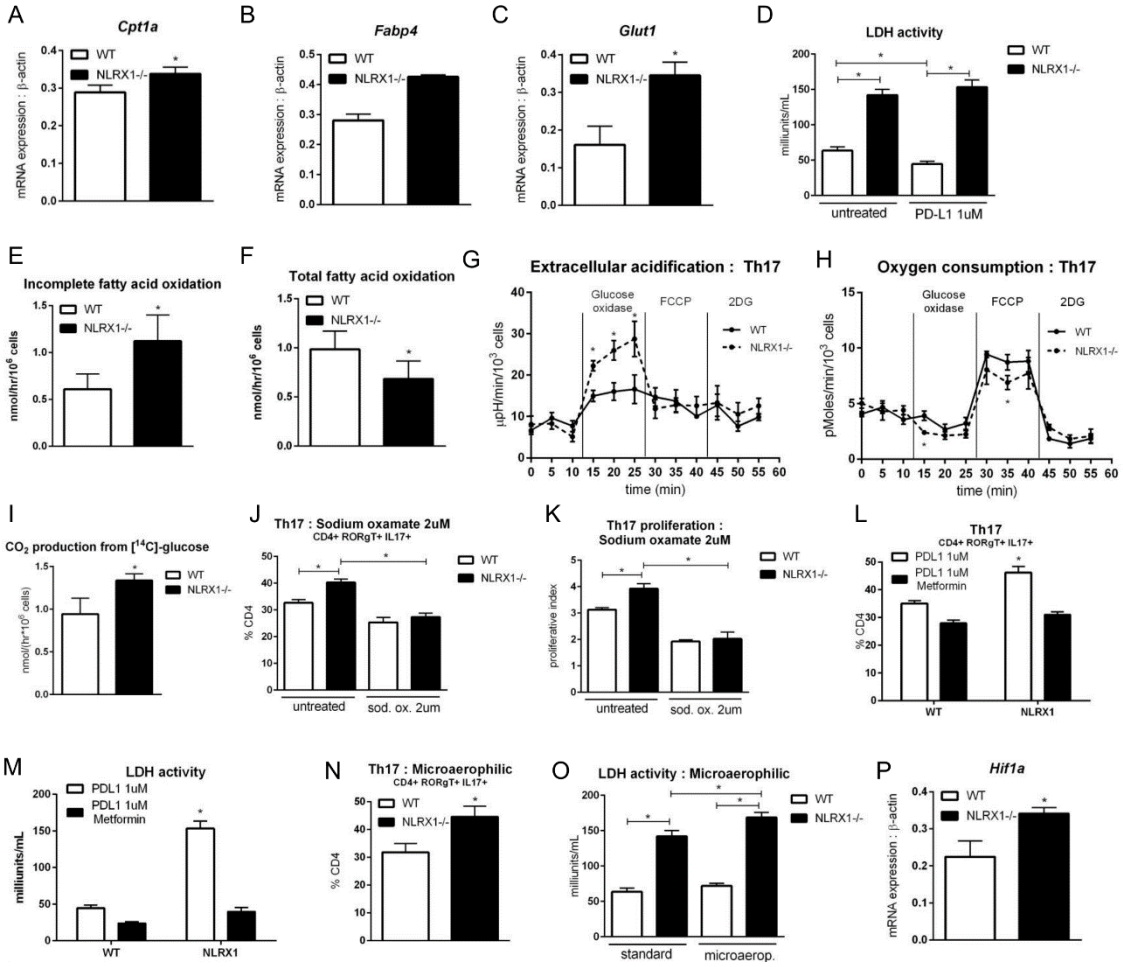

Figure 3.4. NLRX1-/- CD4+ T cells have altered metabolic behavior. mRNA expression of Cpt1a (A), Fabp4 (B), and Glut1 (C). Activity of lactate dehydrogenase with and without addition of PD-L1 (D). Incomplete fatty acid oxidation as a measure of acid soluble metabolite production (E). Total fatty acid oxidation with addition of PD-L1 (F). Extracellular acidification (G), and oxygen consumption rates (H) from differentiated CD4+ Th17 cells. Cells were measured over a time course and exposed to glucose oxidase, carbonyl cyanide-4-phenylhydrazone (FCCP), and 2-deoxy-D-glucose (2DG) at the indicated time periods. Carbon dioxide production from radiolabeled [14C]-glucose in WT and NLRX1-/- differentiated Th17 cells (I) Differentiation (J) and proliferation (K) of Th17 cells in presence of sodium oxamate. Differentiation (L) and LDH activity (M) of Th17 cells in presence of PDL1 and metformin. Differentiation (N) and LDH

activity (O) of Th17 cells in microaerophilic conditions. mRNA expression of Hif1a (P). Data is a result of three experiments with triplicate samples ($P<0.05$, n=9).

3.6 Adoptive transfer of NLRX1-/- CD4+ T cells results in increased pathology, local and systemic inflammation.

To determine the impact of effector and regulatory CD4+ T cells on experimental IBD, Rag2-/- mice were administered wild-type or NLRX1-/- sorted naïve CD4+ T cells via intraperitoneal injection (Fig. 3.5A). Post-administration, increased leukocytic infiltration and epithelial erosion were observed in mice given NLRX1-/- cells (Fig. 3.5D, G-I). Spleen and colonic lamina propria samples contained greater percentages and absolute numbers of Th1 and Th17 cells in mice administered NLRX1-/- cells (Fig. 3.5B-C, E-F). To determine if the effect of NLRX1 was through effects on effector or regulatory cells, effector and regulatory T cell subsets were sorted from wild-type and NLRX1-/- spleens.

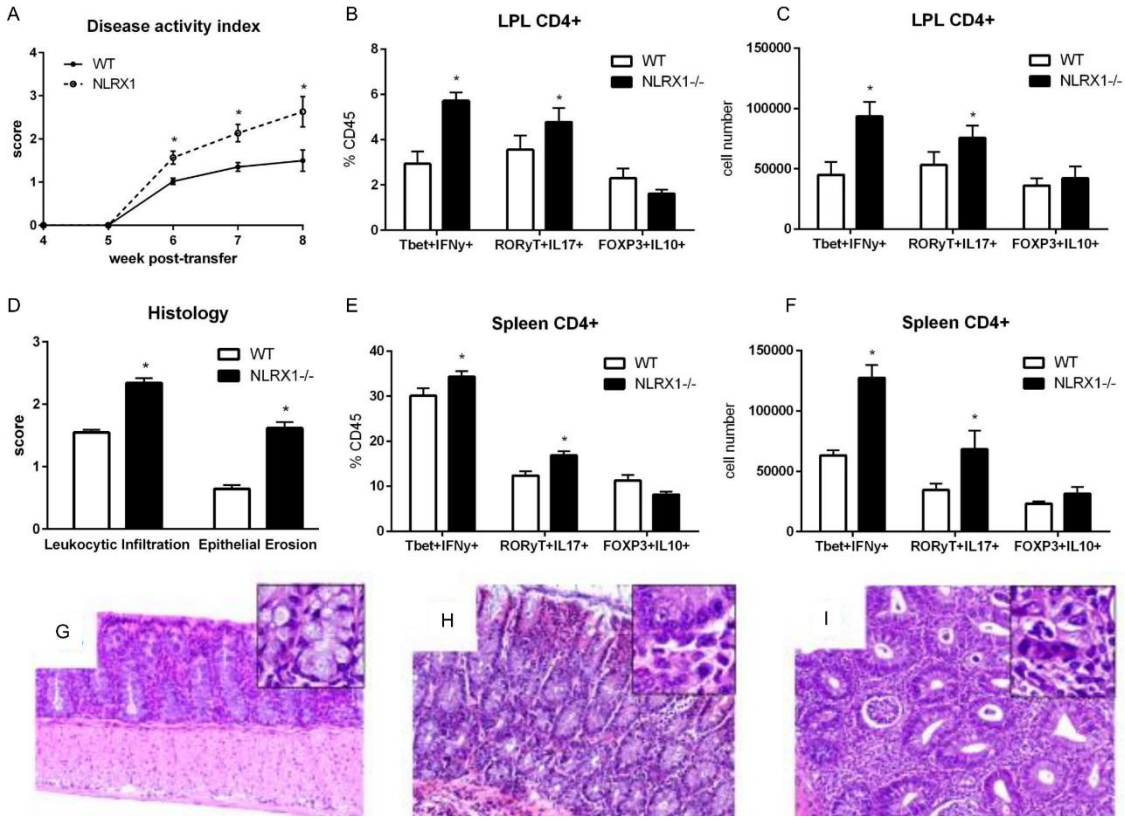

Figure 3.5. Adoptive transfer of naïve NLRX1-/- T cells results in increased disease severity. Disease activity index of Rag2-/- transferred wild type and NLRX1-/- naïve CD4+ T cells (A). Percentage (B) and absolute number (C) of CD4+ T cell populations in colonic lamina propria eight weeks after transfer. Summarized histology scores in leukocytic infiltration and epithelial erosion (D). Percentage (E) and absolute number (F) of CD4+ T cell populations in spleen eight weeks after transfer. Representative photomicrographs of control (G), wild-type transferred (H), and NLRX1-/- transferred (I) Rag2-/- colons eight weeks post-transfer. Asterisks mark significance ($P<0.05$, n=10).

Rag2-/- mice were then administered either only wild-type effectors, wild-type effectors and regulatory cells, wild-type effectors and NLRX1-/- regulatory cells, NLRX1-/- effectors, NLRX1-/- effectors and regulatory cells, or NLRX1-/- effectors and wild-type regulatory cells. Transfers and sorting of WT and NLRX1-/- occurred concurrently. The administration of NLRX1-/- effectors accelerated disease onset on overall severity (Fig. 3.6A). Groups given NLRX1-/- effector T cells possessed increased numbers of Th1 and Th17 subsets than respective groups given wild-type effector T cells, suggesting an effector-intrinsic role of NLRX1 (Fig. 3.6C-H). Groups given NLRX1-/- regulatory T cells displayed no significant differences in Th1 and Th17 populations compared to corresponding groups given wild-type regulatory T cells (Fig. 3.6C-H).

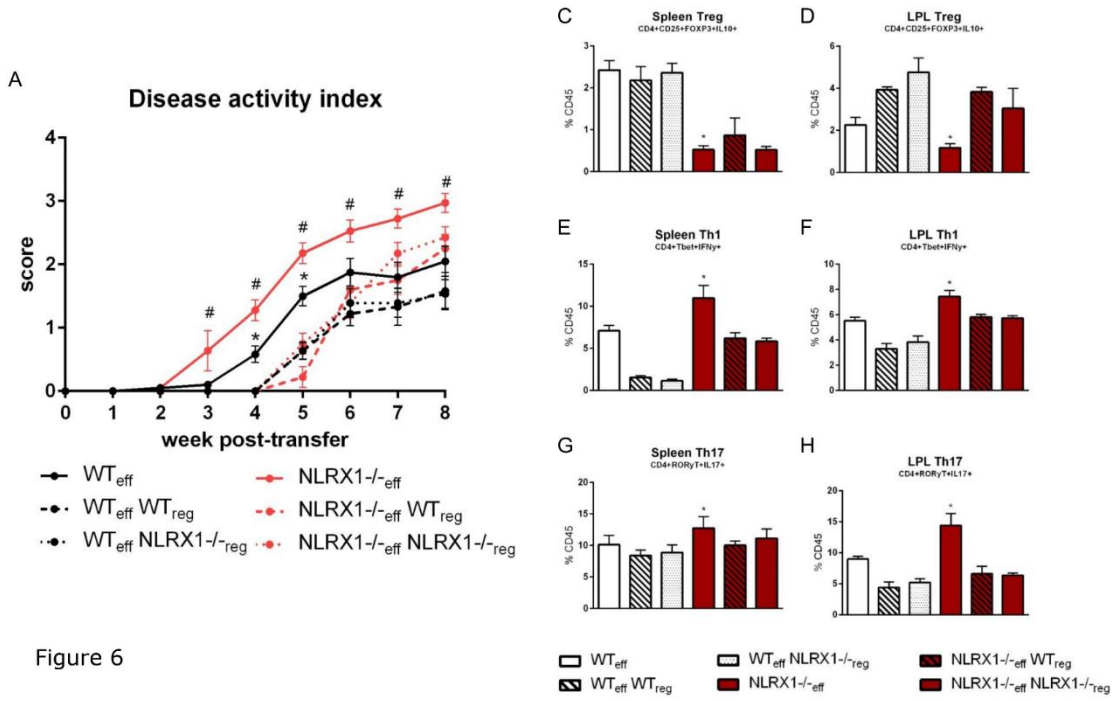

Figure 3.6. Adoptive transfer of NLRX1-/- effector T cells increases disease severity. Disease activity index of Rag2-/- transferred wild type and NLRX1-/- (A) effector and regulatory CD4+ T cells. Spleen (C) and colonic lamina propria (D) cell numbers of Treg (CD4+NK1.1-CD8-CD25+FOXP3+IL10+). Spleen (E) and colonic lamina propria (F) cell numbers of Th1 (CD4+NK1.1-CD8-Tbet+IFNy+). Spleen (G) and colonic lamina propria (H) cell numbers of Th17 (CD4+NK1.1-CD8-RORγT+IL17+). Asterisks mark significance between effector and regulatory groups and number signs mark significance between genotypes ($p<0.05$, n=10).

3.7 T cell specific deletion of NLRX1 increases inflammation in *Citrobacter rodentium* model of colitis.

To confirm the findings within an infectious model of colitis, NLRX1$^{\Delta T}$ were challenged with *C. rodentium*. At peak inflammatory response, NLRX1$^{\Delta T}$ had greater numbers of Th1 and T follicular helper (Tfh) cells in the colonic lamina propria and spleen (Fig. 3.7A-D). A significant increase in Th17 cell number was observed in the colonic lamina propria (Fig

3.7E). In addition, NLRX1$^{\Delta T}$ had lower levels of IL10-producing cells in the colonic lamina propria, including iTreg and Tr1 populations (Fig. 3.7G-H). From sorted colonic T cells at peak inflammation, NLRX1$^{\Delta T}$ samples possessed higher lactate dehydrogenase activity than wild-type samples (Fig. 3.7I). The expression of Glut 1 was also increased in NLRX1$^{\Delta T}$ mice (Fig. 3.7J). As a result of increased inflammation, NLRX1$^{\Delta T}$ had lower *C. rodentium* burdens at day 12 post-infection as measured by re-isolation from fecal samples (Fig. 3.7K). Meanwhile, the NLRX1$^{\Delta T}$ scored higher in histological assessment of leukocytic infiltration and mucosal thickness (Fig. 3.7L).

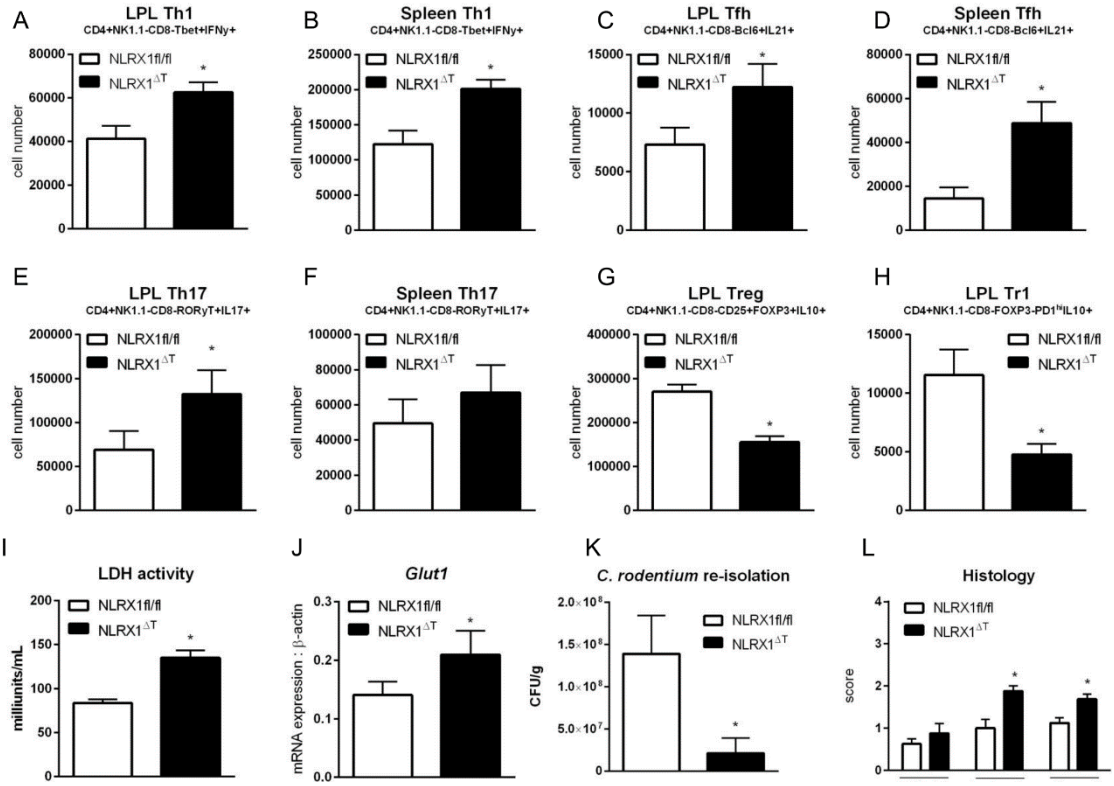

Figure 3.7. Citrobacter rodentium challenge of T cell specific knockouts of NLRX1 results in greater inflammation. Colonic lamina propria (A) and spleen (B) cell numbers of Th1 (CD4+NK1.1-CD8-Tbet+IFNy+). Colonic lamina propria (C) and spleen (D) cell numbers of Tfh (CD4+NK1.1-CD8-Bcl6+IL21+). Colonic lamina propria (E) and spleen (F) cell numbers of Th17 (CD4+NK1.1-CD8-RORγT+IL17+). Colonic lamina propria cell numbers of Treg (CD4+NK1.1-CD8-CD25+FOXP3+IL10+) (G) and Tr1 (H) cells. LDH activity (I) and mRNA expression of Glut1 (J) of sorted CD4+ T cells from colons of mice 12 days post infection. Re-isolation of C. rodentium from fecal samples at 12 days post-infection (K). Histological scores of epithelial erosion, leukocytic infiltration and mucosal thickness of colonic sections at 12 days post-infection (L). Asterisks mark significance ($P<0.05$, n=10).

3.8 Discussion and Conclusions

NLRX1 is important in controlling the proliferation and differentiation of CD4+ T cells, suggesting that it is implicated in T cell-mediated diseases. We present evidence that NLRX1 in T cells may provide protection from IBD as demonstrated in three disease

models spanning chemical, infectious and cellular induced disease. The loss of NLRX1 leads to the expansion of inflammatory T cell subsets including Th1, Th17 and Tfh both locally in the colonic lamina propria and systemically within the spleen. Our in vivo and in vitro observations suggest that NLRX1-/- T cells have biasing towards inflammatory phenotypes, increased proliferation and decreased sensitivity to immune checkpoint pathways.

Notably, the increased proliferation and Th17 differentiation in vitro is paired with an increase in aerobic glycolysis and expression of glucose transporters. The receptor, PD-1, has been previously described to promote immunosuppressive effects through multiple pathways including switching the metabolic pathways of a cell from a glycolysis-dominated state to a fatty acid utilization state [31, 32]. In colonic biopsies from IBD patients, the expression of PD-L1 on intestinal epithelial cells was upregulated to suppress inflammation [33]. Meanwhile, the presence of PD-1+ T cells has been negatively correlated with disease severity [34] and initial testing of PD-L1 treatment has shown efficacy in suppressing disease [35]. However, the stimulation of PD-1 by PD-L1 does not activate this switch nor attenuate the inflammatory phenotype within NLRX1-/- cells. The activation of AMPK is among the pathways affected by PD-1 signaling and is a well-described factor in the control of cellular metabolic flexibility [32, 36, 37]. When AMPK is directly stimulated by metformin, both the metabolic and immunologic differences between wild-type and NLRX1-/- T cells are abrogated suggesting that NLRX1 may be a critical element in the linkage between PD-1 and AMPK signaling. In addition to metabolic contributions, PD-1 and other immune checkpoint signaling contribute to the development of regulatory and memory cell types [38-40]. While the deficiency of NLRX1 in regulatory T cell does not impair their function or abundance, the impaired responsiveness to PD-L1 treatment does lead to lower levels of iTreg in Th17 differentiating media. We propose that PD-1 signaling may be important in the known plasticity between Th17 and iTreg cells and the lack of NLRX1 could contribute to the flexibility of cell phenotype as well as metabolism. The effect of NLRX1 on memory T cell development was unexplored but could contribute to the increased reactivity to native commensal bacteria, a known factor in the progression of IBD.

The loss of NLRX1 selectively influences the differentiation and behavior of effector CD4+ T cells. When transferred, NLRX1-/- regulatory T cells retained equal regulatory effects on disease severity, histopathological markers and expansion of effector populations as their wild-type counterparts. Importantly, the regulation of metabolism differs in thymus-derived, or natural, Treg cells (nTreg) and peripheral, or induced, Treg cells (iTreg) [22]. iTregs are dependent on a switch to lipid metabolism while nTregs are balanced in their substrate utilization. Due to a decreased need for metabolic reprogramming, the development of nTregs may be unaffected metabolically by the loss of NLRX1. However, the metabolic switch dependent iTregs are more likely affected by the loss of NLRX1, particularly in regards to plasticity between the Th17 phenotype. In the mixed adoptive transfer, the sorting of already committed Treg cells may negate some of the assumed differences in dynamic and flexible Treg commitment resulting from the NLRX1-/-. Similarly, in vitro the differences between WT and NLRX1-/- Tregs do not

exist from a de novo differentiation but rather in the persistence and greater abundance of the Treg phenotype in inflammatory and PD-1 induced conditions.

As opposed to Treg cells, effector CD4+ T cells have an established preference for energy production through the lactate dehydrogenase pathway [21]. Therefore, the increase of LDH activity in in vitro differentiated T cells and colonic isolated T cells during peak disease in the absence of NLRX1 is notable. Importantly, the inhibition of LDH abrogates the increased proliferation and Th17 differentiation differences in NLRX1-/- cells implying that the activation of LDH activity may not only be a characteristic of effector CD4+ T cells but also a contributing factor in their differentiation. Additionally, NLRX1-/- T cells had a higher rate of incomplete fatty acid oxidation. Rather than being an indicator of oxidative phosphorylation as complete fatty acid oxidation would be, higher rates of incomplete fatty acid oxidation have been linked to mitochondrial overload [41]and dysregulated metabolic pathways [42]. While the effect of NLRX1 on LDH may be through multiple mechanisms, a potential contributor is the effect of NLRX1 on reactive oxygen species production. Previously, NLRX1 has been shown to be crucial in the production of ROS [9, 43]. The loss of NLRX1 may not allow a cell to correctly sense the oxygen environment or the ROS concentration within the cell, promoting the utilization of both oxidative and anaerobic metabolic pathways in all conditions. The inability to switch metabolic pathways to influence ROS levels may also affect the ability of a cell to respond to canonical death pathways, such as TNF-mediated death, for which NLRX1 has previously been shown to contribute [43].

With the suggestion that an alteration in oxygen sensing may be involved, HIF1α may be implicated downstream of NLRX1 signaling [44]. Not only has the activation of HIF1α been linked to an increase in LDH activity but also an increase in Th17 differentiation through the activation of IL23R and RORγT and the inhibition of FOXP3 [45-47]. Combined, HIF1α is an important transcription factor controlling effector CD4+ T cell differentiation and cytokine production. The loss of NLRX1 leads to increased HIF1α expression and the culture of NLRX1-/- CD4+ T cells in microaerophilic conditions further increases the magnitude of difference between wild-type and NLRX1-/- Th17 differentiation. HIF1α is activated by MITF while sumoylation by RanBP2 decreases its transcription activity [48, 49]. Regulated by ROS production, RanBP2 is also important for the entry of virus into the nucleus, potentially an additional mechanism by which NLRX1 contributes to viral susceptibility [5, 50].

NLRX1 has been linked to viral susceptibility and other disease models such as EAE and cancer [1, 10, 51]. While these previous studies have focused largely on the role of NLRX1 in innate immune cells, neurons, and tumor cells, we provide evidence that NLRX1 is important in the metabolic and proliferative control of effector CD4+ T cells. The involvement of effector CD4+ T cells in IBD has been well characterized from the increased number, the resistance to apoptosis and spontaneous reaction to the commensal microflora [52-54]. The provided evidence in multiple models of IBD suggests that NLRX1 joins multiple other members of the NLR family in the pathogenesis of IBD. Further, the contribution of NLRX1 to effector T cell differentiation merits study in other T cell immune-mediated diseases.

In conclusion, the loss of NLRX1 in T cell promotes increased metabolic activity and a preference for LDH activity. The metabolic preferences are combined with a decreased sensitivity to immunosuppressive checkpoint pathways to provide greater proliferative capabilities and an inflammatory phenotype bias. The immunometabolic dysregulation caused by the loss of NLRX1 may exacerbate disease severity and gut pathology in DSS, adoptive transfer and C. rodentium models of IBD. The contribution of NLRX1 deficiency to worsened disease suggest further work on mechanisms of NLRX1 activation may provide useful therapeutic advances in IBD and other T cell immune-mediated diseases.

3.9 Materials and methods

DSS-induced colitis

C57BL/6 wild-type (WT) and NLRX1-/- mice ranging from 8-10 weeks of age were administered DSS in drinking water for seven days. Control mice received standard drinking water. All mice were weighed and scored daily. Disease activity index was scored holistically by physical appearance, fecal consistency, rectal bleeding and weight loss. Mice were euthanized by carbon dioxide narcosis for sample collection on days 3, 7, and 10 post-DSS initiation. All experimental procedures were approved by the Institutional Animal Care and Use Committee.

Adoptive Transfer

CD4+ T cells were enriched by I-Mag cell separation system from WT and NLRX1-/- donor spleens. For FACS sorting, cells were labeled with CD45RB, CD4, and CD25 and separated into CD4+CD45RBhiCD62L+CD25− cells (naive T cells), CD4+CD45RBhiCD25- (effector T cells), and CD4+CD45RBloCD25+ (regulatory T cells) in a FACSAria cell sorter. Rag2-/- mice were transferred with 4 × 105 sorted naive CD4+ cells from WT or NLRX1-/- mice for initial studies or 4 x 105 effector T cells and 1 x 105 sorted regulatory T cells for secondary studies. Mice were weighed and scored on a weekly basis until the development of clinical signs. After development of clinical signs, mice were weighed and scored daily until necropsy. Mice were euthanized for sample collection 8 weeks post-transfer.

Citrobacter rodentium challenge

C. rodentium (strain DBS100) was grown aerobically, at 37˚C and 200 rpm shaking, in LB broth within a capped Erlenmeyer flask overnight. An aliquot of bacterial suspension was added to fresh LB broth five hours prior to challenge to provide bacteria in log-phase growth. Bacterial concentration was adjusted to 5x1010 cfu/mL by spectrophotometer. Mice were given 1x109 cfu/mouse in LB broth by orogastric gavage. Control mice were given equal volume sterile LB broth. Mice were weighed and scored daily post-challenge. Colonization was monitored by feces collection every other day. Mice were euthanized for sample collection at day 12 and week 4 post-challenge.

In vitro CD4+ T cell differentiation

Naïve CD4+ T cells were obtained by magnetic sorting of WT and NLRX1-/- splenocytes. 12-well plates were prepared through incubation with anti-CD3 and anti-CD28 antibodies for 1 hour at 37˚C. Cells were prepared in complete IMDM media containing 10% FBS, 20mM HEPES, 55μM beta-mercaptoethanol, and penicillin/streptomycin. Cells were plated a 500,000 cells/well. Th17 cytokine differentiation mixture was composed of 2.5ng/mL TGFβ, 25ng/mL IL-6, 10μg/mL anti-IL4, 10μg/mL anti-IFNγ, and 50ng/mL IL-23. iTreg cytokine differentiation mixture was composed of 5ng/mL TGFβ, 5ng/mL IL-10, 10μg/mL anti-IL4, and 10μg/mL anti-IFNγ. Cells were collected for assay after 60hrs culture. Five hours prior to collection cells were stimulated with PMA/ionomycin and incubated with GolgiStop. Cell proliferation was measured by CFSE staining. A lactate dehydrogenase activity kit was utilized to measure LDH activity. Briefly, cells were homogenized and the homogenate was assayed using colorimetric detection of the reduction of NAD to NADH. Fatty acid oxidation from measures of 14CO2 production and acid soluble metabolites from the oxidation of [1-14C]-palmitic acid, as previously described [30].

Flow cytometry

Mesenteric lymph nodes (MLN) and spleen were excised, single cell suspensions prepared and re-suspended in PBS with 5% BSA and GolgiStop. Colon sections were incubated in RPMI/FBS buffer (87.5% RPMI, 10% FBS, 2.5% HEPES) containing collagenase at 300U/mL and DNAase at 50U/mL for one hour with stirring at 37°C. From the cell suspension, immune cells were purified by Percoll gradient. Cells were labeled with extracellular and intracellular antibodies within 96 well plates. A BD LSRII flow cytometer, in combination with FACSDiva software, was used to acquire and analyze flow cytometry data.

Histopathology

Colonic samples were fixed in 10% buffered formalin, embedded in paraffin, processed routinely and sectioned at 5 μm. Sections were stained with hematoxylin and eosin (H&E) and then examined and graded by a board-certified veterinary pathologist using an Olympus microscope and ImagePro software. Sections were graded for leukocyte infiltration, epithelial erosion and mucosal thickness on a scale from 0 to 3.

Gene Expression

Total RNA was isolated from mouse colons using a Qiagen RNA Isolation Mini kit and used to generate cDNA via the iScript cDNA Synthesis Kit. Standards were produced through a polymerase chain reaction on the cDNA with Taq DNA polymerase from Invitrogen. The amplicon was purified using the Mini-Elute PCR purification kit from Qiagen. Expression levels were obtained through quantitative real-time PCR on a Bio-Rad CFX 96 Thermal Cycler using the Bio-Rad SYBR Green Supermix. For analysis, the starting amount of target gene cDNA was compared to that of beta-actin, as a control.

Western Blot

Nuclear and cytoplasmic protein extracts were quantified with the Pierce BCA protein assay. Standardized samples were run on 10% gels, transferred to nitrocellulose membranes, and incubated with target or control antibodies overnight at 4C. Secondary antibodies were anti-rabbit-HRP and anti-mouse HRP for one hour at room temperature upon which the membrane was visualized using ImageLab software.

Statistics

Data are expressed as mean and standard error of the mean. Parametric data were analyzed by using the analysis of variance followed by Scheffe's multiple comparisons test as previously described. Analysis of variance (ANOVA) was performed by using the general linear model procedure of SAS (SAS Institute Inc., Cary, NC). A 2x2 factorial arrangement comparing genotype and treatment was employed. Statistical significant was determined at $p \leq 0.05$.

Chapter 4

Lanthionine Synthetase C-like 2 Modulates Immune Responses to Influenza Virus Infection

Andrew Leber, Josep Bassaganya-Riera, Nuria Tubau-Juni, Victoria Zoccoli-Rodriguez, Victoria Godfrey, and Raquel Hontecillas

Leber A, Bassaganya-Riera J, Tubau-Juni N, Zoccoli-Rodriguez V, Lu P, et al. (2017) Lanthionine Synthetase C-Like 2 Modulates Immune Responses to Influenza Virus Infection. Front Immunol. doi: 10.3389/fimmu.2017.00178

4.1 Summary

Broad-based, host-targeted therapeutics have the potential to ameliorate viral infections without inducing antiviral resistance. We identified lanthionine synthetase C-like 2 (LANCL2) as a potential new therapeutic target for immunoinflammatory diseases. To examine the therapeutic efficacy of oral NSC61610 administration on influenza, we infected C57BL/6 mice with influenza A H1N1pdm virus and evaluated influenza-related mortality, lung inflammatory profiles, and pulmonary histopathology. Oral treatment with NSC61610 ameliorates influenza virus infection by down-modulating pulmonary inflammation through the downregulation of TNF-α and MCP-1 and reduction in the infiltration of neutrophils. NSC61610 treatment increases IL10-producing CD8+ T cells and macrophages in the lungs during the resolution phase of disease. The loss of LANCL2 or neutralization of IL-10 in mice infected with influenza virus abrogates the ability of NSC61610 to accelerate recovery and induce IL-10-mediated regulatory responses. These studies validate that oral treatment with NSC61610 ameliorates morbidity, mortality and accelerates recovery during influenza virus infection through a mechanism mediated by activation of LANCL2 and subsequent induction of IL-10 responses by CD8+ T cells and macrophages in the lungs.

4.2 Introduction

Seasonal influenza causes an estimated 200,000 hospitalizations and 25,000 to 35,000 deaths annually in the United States, afflicting mainly people older than 65 years of age [98]. Aside from the seasonal flu, pandemic influenza originating from emerging strains

can significantly change the disease dynamics. Influenza pandemics cause considerable disease, with associated mortality ranging from approximately 50 million deaths during the 1918 pandemic to 1 to 4 million deaths in 1957 and approximately 1 million deaths in 1968. In 2009, a novel H1N1 virus emerged and spread rapidly in humans, causing severe disease in susceptible populations, and high numbers of respiratory and cardiovascular-related deaths [99]. Overall, seasonal flu is one of the most relevant infectious disease-related public health problems since it causes important economic losses ranging from 71 to 166 billion dollars during one influenza pandemic [100].

Current approaches for the prevention and treatment of influenza infections include vaccination and early administration of antiviral drugs [101]. Typically, a minimum of 6 months are needed to develop a new vaccine, creating a lag period between the identification of a new strain and the administration of the first vaccine doses, in which the population is unprotected against the virus [102]. The use of anti-viral drugs is associated with the emergence of resistance. A promising therapeutic avenue is the modulation the host response to the virus by targeting the immune system in the pulmonary mucosa and systemically to minimize viral pneumonia and improve survival rates [103]. The excessive release of pro-inflammatory cytokines in the lungs often leads to a cytokine storm, which is a key contributor to lung immunopathology and disease severity. For example, mortality induced by the highly pathogenic H5N1 strain correlates with high levels of circulating cytokines and chemokines [104]. Hence, the use of drugs that target the host response instead of directly targeting the virus or its cytopathic effects is receiving attention for the treatment of infections [105, 106]. In contrast to vaccines, immune modulators and inflammation blockers provide efficacy independently of changes in viral antigenicity; are faster acting, and relatively inexpensive [107] although they have not been approved as host-targeted therapeutics. Moreover, in contrast to anti-virals, immune modulators do not cause resistance.

We have recently investigated the potential role of abscisic acid (ABA), as a ligand of lanthionine synthetase C-like 2 (LANCL2) leading to elevation of intracellular cAMP and activation of protein kinase A (PKA) [108]. We used molecular modeling approaches to predict the binding of ABA to LANCL2 [109]. *In vitro* studies have confirmed direct binding of ABA to LANCL2 [110]. Moreover, oral administration of ABA as a pre- and post-exposure therapeutic upregulates LANCL2 expression in the lungs of influenza infected mice, reduces influenza virus-related immunopathology and accelerates recovery in infected mice [111]. LANCL2 is widely expressed in specialized organs of the immune system, including blood, spleen, lymph node, and thymus. LANCL2 is expressed by T cells, macrophages, endothelial and epithelial cells, and dendritic cells suggesting its potential as a target for immunoregulation [112]. Other members of the LANCL family of proteins include LANCL2 which has been shown to contribute to cellular homeostasis and nervous system disorders [113, 114].

In this study, we examined the feasibility of using LANCL2 ligands to induce immunoregulatory responses and ameliorate morbidity and mortality associated with influenza virus infection. PubChem compound 247228, a 3.3’-bis(benzimidazolyl) terephthalanilide (BTT), also known as NSC61610 was selected from the National Cancer

Institute Diversity Set II by LANCL2 structure-based virtual screening and previously shown to induce immunomodulatory effects in mouse models of colitis [115, 116]. Additionally, the safety efficacy profiles of BT-11, a newly developed LANCL2 ligand, is excellent based on single and 14-day repeated-dose toxicology studies in rats and mouse models of inflammatory bowel disease [117-119]. Given the demonstrated efficacy of ABA in accelerating recovery in mouse models of influenza infection, in this study we investigated the effects of NSC61610 in a mouse model of infection, elucidated its underlying immunoregulatory mechanisms, LANCL2 dependency and cell specificity in the lungs.

4.3 LANCL2 aids in resolution and recovery from influenza infection

To assess the role of LANCL2 in the response to influenza infection, wild-type C57BL6/J mice and LANCL2-/- mice were infected with 350 pfu/mouse of influenza A H1N1/California/04/09. Notably, LANCL2-/- mice had a decreased rate of survival and prolonged presence of symptoms (Figure 4.1A-B). Within the lungs of infected mice, LANCL2-/- possessed lower levels of IL-10 and higher levels of IL-6 at day 12 post-infection (Figure 4.1 I-J). In general, LANCL2-/- displayed lower numbers of IL-10 producing cells within the lungs during the same period and specifically within CX3CR1+ macrophage and CD8+ T cell populations (Figure 4.1 C-E). LANCL2-/- mice also showed lesser numbers of tissue repair and homeostasis cell types in alveolar macrophages and type 2 innate lymphoid cells at day 12 post-infection(Figure 4.1 G-H) while displaying greater number of neutrophils at day 7 post-infection (Figure 4.1F).

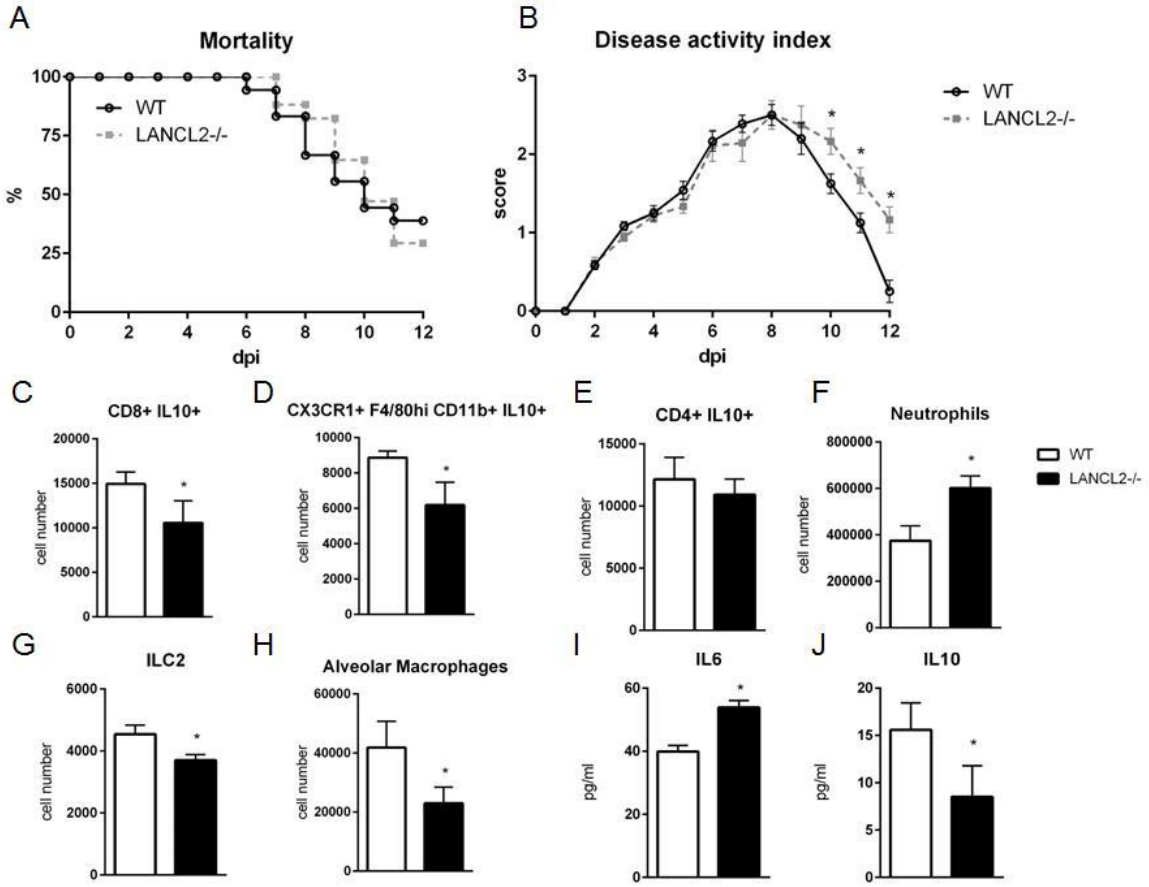

Figure 4.1. Loss of LANCL2 impairs resolution of influenza infection. Mortality (A) and disease activity (B) of WT and LANCL2-/- mice infected with influenza. Cell number of CD8+ IL10+ T cells (C), IL10 producing macrophages (D), CD4+ IL10+ T cells (E), neutrophils (F), type 2 innate lymphoid cells (G), and alveolar macrophages (H) at day 12 post-infection by flow cytometry. Concentration of IL-6 (I) and IL-10 (J) in lung homogenate at day 12 post-infection by cytokine bead array. Data points and error bars represent mean ± standard error of the mean (SEM). Asterisks (*) denote statistically significant ($p<0.05$) differences between the treatment group and control (n=12).

4.4 Myeloid LANCL2 is required for modulation of regulatory responses

Using a cre-recombinase system, myeloid (LANCL2fl/fl;LysCre+) and T cell (LANCL2fl/fl;CD4Cre+) specific knockouts of LANCL2 were generated. Myeloid cell knockouts recapitulated the LANCL2-/- phenotype in terms of mortality (Figure 4.2A). Both cell specific knockouts displayed decreased levels of IL-10 within the lungs at day 12 post-infection similar to the LANCL2-/- (Figure 4.2B). In addition, IL-10 producing macrophages and CD8+ T cells were similarly decreased in CD4Cre+ and LysCre+ compared to LANCL2-/- (Figure 4.2D and E). However, LANCL2fl/fl;CD4Cre+ mice had significantly increased numbers of alveolar macrophages compared to LANCL2-/- and LANCL2fl/fl;LysCre+ mice (Figure 4.2F). The number of alveolar macrophages in

LANCL2fl/fl;CD4Cre+ was similar to numbers in untreated wild-type mice. LANCL2fl/fl;CD4Cre+ mice also displayed lower concentrations of MCP-1 in lung homogenate than LANCL2-/- and LANCL2fl/fl;LysCre+ mice (Figure 4.2C). Together, this data suggests that a myeloid specific LANCL2 deficiency is capable of producing the same effects as the full body deletion of the protein.

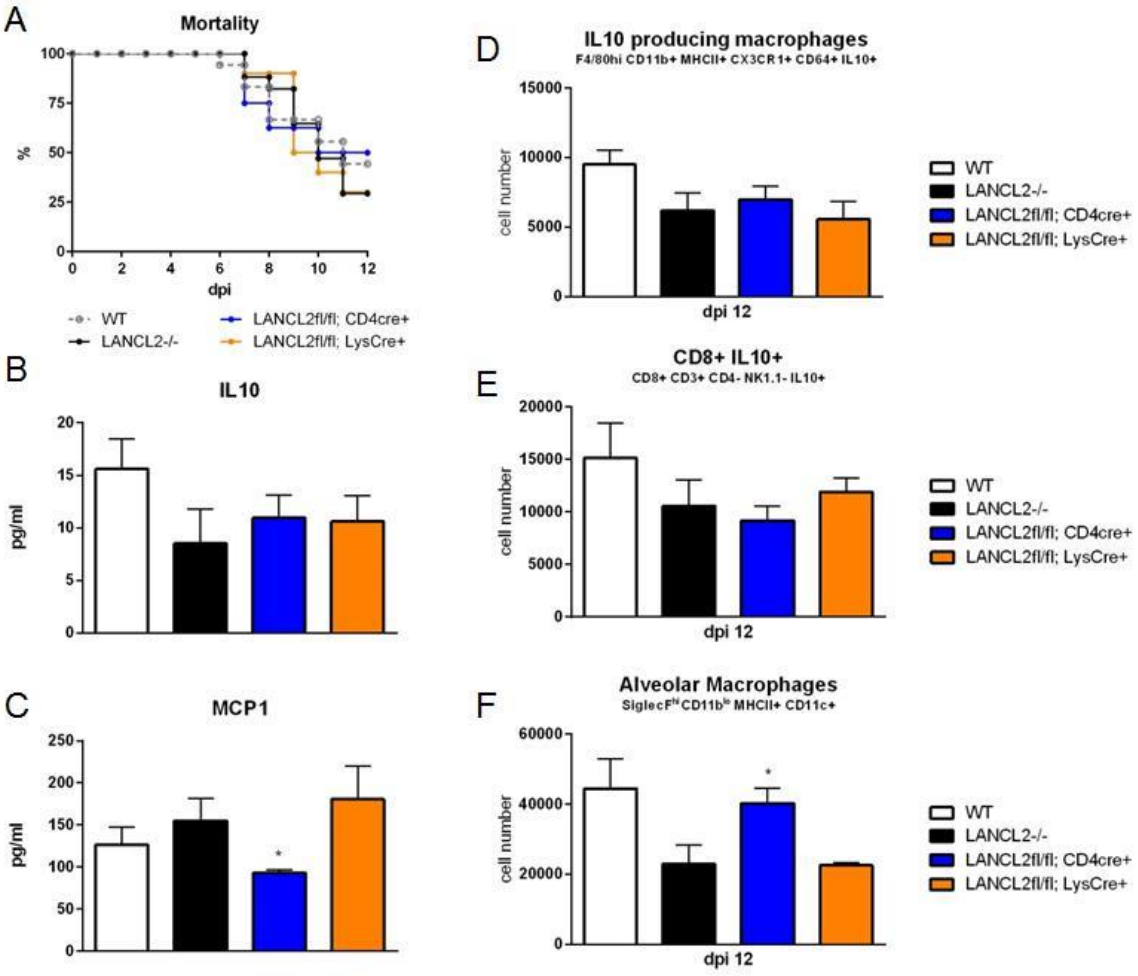

Figure 4.2. Myeloid LANCL2 is required for modulation of regulatory responses. Mortality (A) for LANCL2-/-, LANCL2fl/fl;CD4Cre+, and LANCL2fl/fl;LysCre+ mice infected with influenza H1N1. Concentration of IL-10 (B) and MCP1 (C) within lung homogenate by cytokine bead array. Cell number of CX3CR1+ IL-10+ macrophages (D), CD8+ IL-10+ T cells (E), and alveolar macrophages (F) in lungs by flow cytometry at 12 days post-infection. Data points and error bars represent mean ± standard error of the mean (SEM). Asterisks (*) denote statistically significant ($p<0.05$) differences between genotypes (n=8).

4.5 Oral NSC61610 treatment improves influenza virus-associated lung immunopathology and protects mice against lethal influenza virus infection

After observation of the importance of LANCL2 in the resolution phase of infection, we sought to identify if novel ligands of LANCL2 could aid in the response to influenza. Firstly, to validate *in silico* predictions that NSC61610 would bind to LANCL2, LANCL2 was expressed in *E. coli*. The binding of NSC61610 to the purified protein was analyzed via surface plasmon resonance and compared to the natural ligand of LANCL2, abscisic acid (Figure 4.3). Steady state equilibrium constants (K_D) were determined to be 2.252 μM for the ABA-LANC2 interaction, while the NSC61610-LANCL2 was 2.305 μM. Following the validation of binding, we performed an assessment of the ability of NSC61610 to improve influenza virus-induced morbidity and/or mortality. C57BL/6 wild-type mice were challenged with 350 pfu/mouse of influenza A H1N1/California/04/09. At 12 days post infection, the mortality rate was 60% in the control group versus 30% in the NSC61610-treated mice (Figure 4.4I). The onset of mortality differed by one day with the untreated wild type group beginning on day six compared to day 7 in the NSC61610-treated groups. Mice were also scored on a daily basis through observation of physical activity and appearance. NSC61610- treated mice were significantly more active and showed less signs of distress by this measure (Figure 4.4J). Our clinical data shows that oral NSC61610 treatment improves the resolution of infection and accelerates the recovery from disease. These findings are in line with the lower mortality rates recorded in the group that received oral NSC61610 treatment.

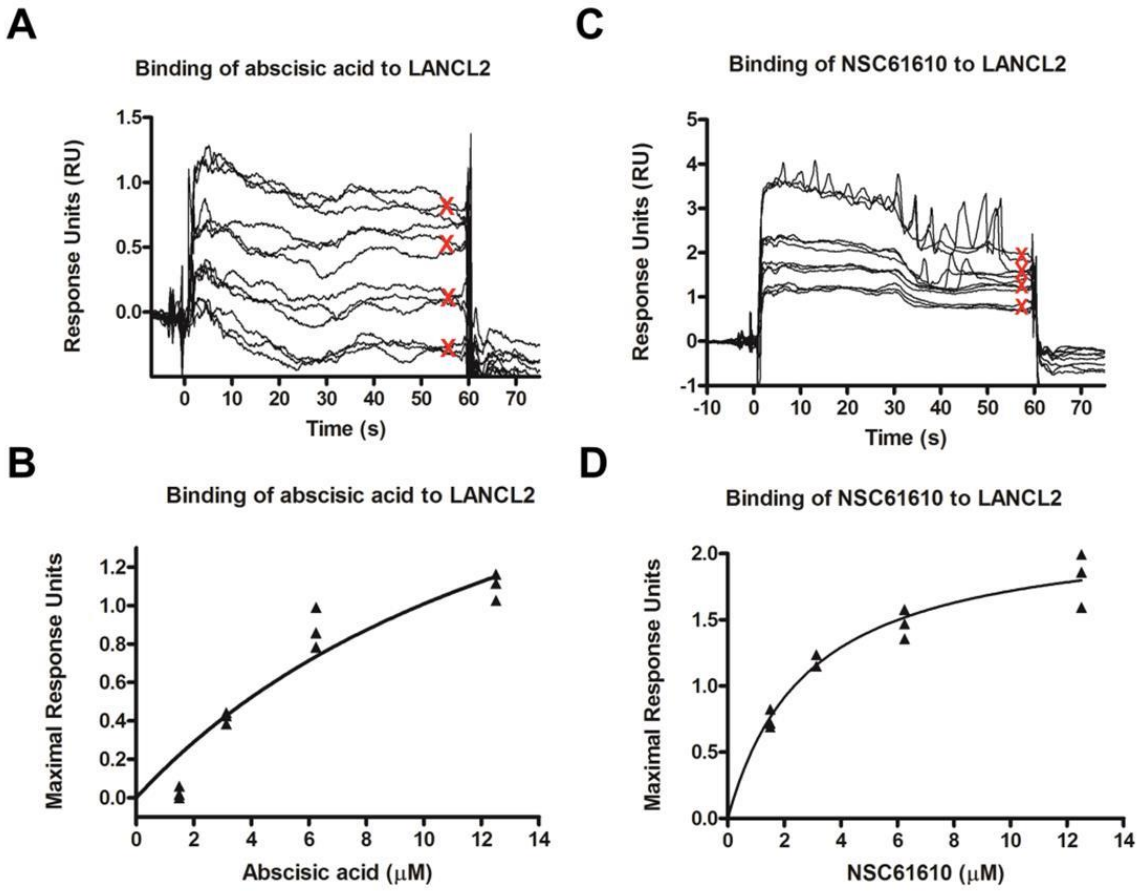

Figure 4.3. Binding kinetics of lanthionine synthetase C-like protein 2 (LANCL2) with abscisic acid (ABA) and NSC61610. Surface plasmon resonance (SPR) sensograms for the binding of varying concentrations of ABA (12.5 μM, 6.25 μM 3.13 μM and 1.57 μM) to immobilized LANCL2 (A). Plot of Maximal Resonance Unit versus concentration of ABA (B). Steady state Dissociation constant was calculated to be 2.252 μM utilizing a 1:1 binding model. SPR sensograms for the binding of varying concentrations of NSC61610 (12.5 μM, 6.25 μM 3.13 μM and 1.57 μM) to immobilized LANCL2 (C). Plot of Maximal Resonance Unit versus concentration of NSC61610 (D). Steady state Dissociation constant was calculated to be 2.305 μM utilizing a 1:1 binding model.

To determine whether the improved clinical symptoms observed in NSC61610-treated mice were accompanied by decreased lung pathology, we evaluated microscopic lung lesions at 3, 7 and 12 days post-infection. Examination of lung tissue was based on epithelial necrosis, including presence of debris in large and intermediate size airways, and leukocytic infiltration of the mucosa and submucosa of large airways. Chronologically, the first pulmonary lesion detected was epithelial cell necrosis, with presence of necrotic cells in the airway compartment at day 7 (Figure 4.4B and E) and marginated leukocytes in adjacent blood vessels and in some cases with perivascular edema. At later stages, the predominant findings were leukocytic infiltration of the mucosa and submucosa of large and medium size airways (Figure 4.4A, B, D and E). This was followed by the presence of inflammatory cells in the terminal airways (Figure 4.4C and F) on day 7 post-infection. To determine whether NSC61610 ameliorated lung immune-pathology associated with infection, we scored these lesions from 0 to 4 depending on extent and severity. The analysis shows that NSC61610 indeed exerted a significant impact in the extent of lung epithelial necrosis (Figure 4.4G) and leukocytic infiltration (Figure 4.4H). The decline in epithelial necrosis scores occurred 2 days earlier in NSC61610-treated mice when compared to untreated mice. Additionally, the severity of leukocytic infiltration was significantly lower in NSC61610-treated mice on day 7 post-challenge than in untreated mice. In untreated mice, the immune cell infiltration increased to reach a maximum score of 3 on day 7. In the NSC61610-treated mice the score was maintained under 2 throughout the experiment, suggesting lower inflammatory cells recruited to the lungs.

In NSC61610-treated wild type mice, oral treatment of NSC61610 increases expression of LANCL2 throughout the time course of influenza infection (Figure 4.4K). To confirm the decrease in inflammatory cell types during the peak of infection in NSC61610 treated mice, we measured the mRNA expression of inflammatory markers, IFNα, TNFα and MCP1, in the lungs of infected mice (Figure 4.4L-N). Notably, NSC61610 treatment reduced expression of TNFα, at day 7 post-infection, and MCP1 at days 3 and 7 post-infection. IFNα was not significantly altered at any of the observed time points.

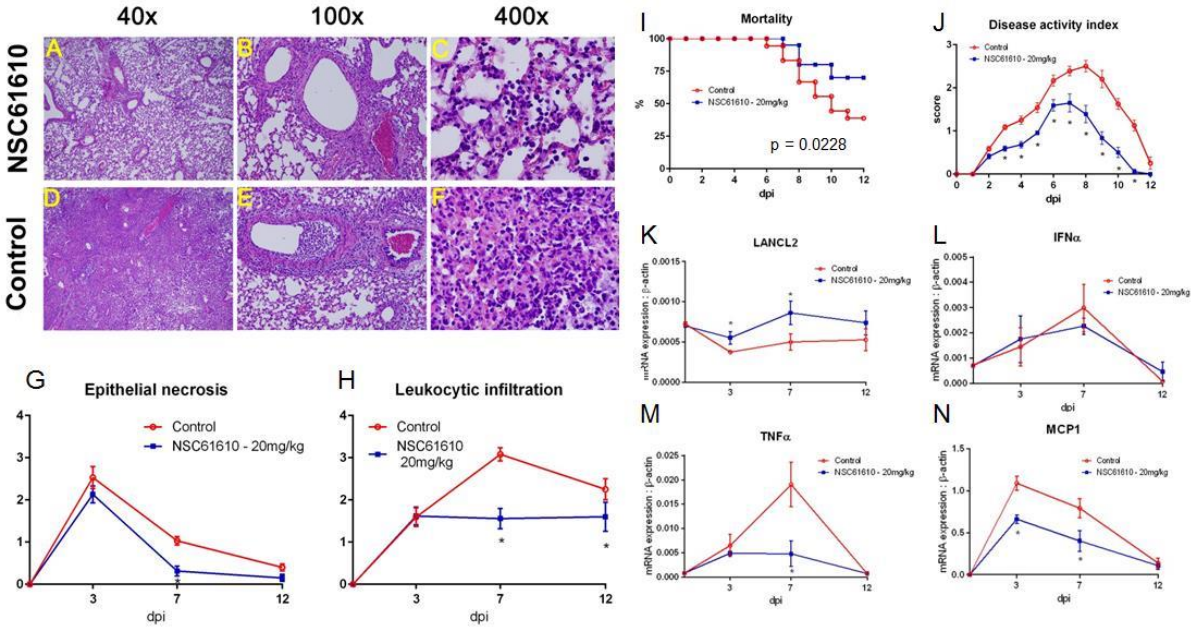

Figure 4.4. NSC61610 treatment decreases severity and improves recovery from influenza infection. Representative photomicrographs of H&E stained lung sections from NSC61610 (A-C) and control treated (D-F) mice following influenza infection. Summary of epithelial necrosis (G) and leukocytic infiltration (H) scores. Mortality (I) and disease activity (J) of WT mice infected with influenza with no treatment and NSC61610 treatment. mRNA expression of LANCL2 (K), IFNα (L), TNFα (M), and MCP1 (N) at days 0, 3, 7, and 12 post-infection in lung tissue during influenza infection of wild type mice administered PBS or NSC61610 (20mg/kg) by qRT-PCR. Data points and error bars represent mean ± standard error of the mean (SEM). Asterisks (*) denote statistically significant ($p<0.05$) differences between the treatment group and control (n=12).

4.6 NSC61610 promotes immunological mechanisms of regulation and repair in the lungs

Oral administration of NSC61610 increases the number of IL-10-producing macrophages and CD8+ T cells (Figure 4.5A and B). The number of IL-10-producing CD4+ T cells was not changed by treatment (Figure 4.5C). Numbers of alveolar macrophages and innate lymphoid cell type 2 were also significantly increased at day 12 post-infection (Figure 4.5D and E). Using a cytokine bead array, the concentration in lung homogenate of cytokines was measured at day 12 post-infection. The concentration of IL-10 was significantly increased by oral NSC61610 treatment (Figure 4.5G). Trends in IL-10 production were further confirmed by qRT-PCR with lung tissue (Figure 4.5I). No significant trends were observed in IL-6, MCP1 or IFNy at day 12 post-infection (Figure 4.5H, J and K). Expression of amphiregulin was also observed to be significantly increased by oral NSC61610 treatment (Figure 4.5L).

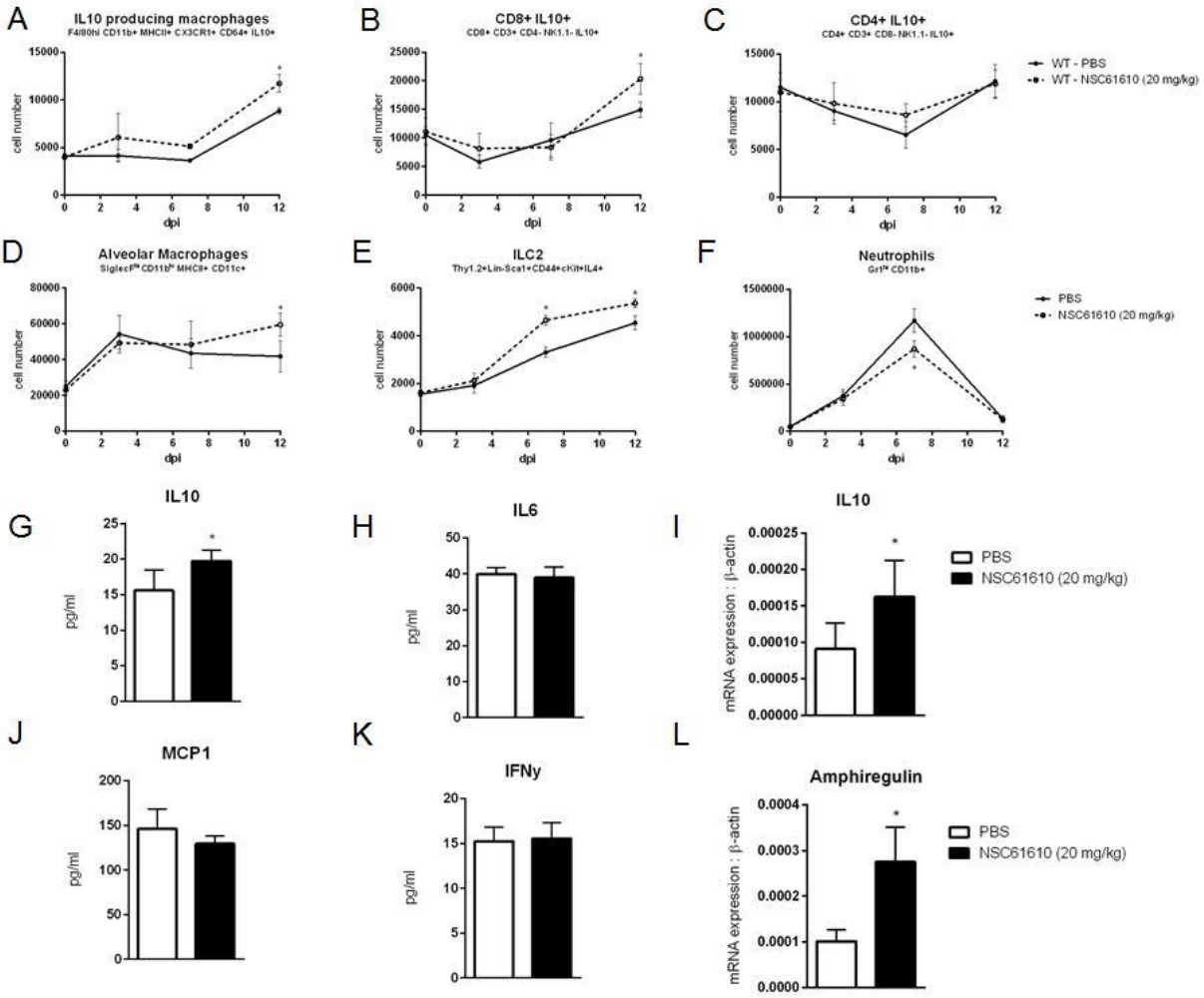

Figure 4.5. NSC61610 promotes regulatory responses during resolution phase of infection. Cell number of IL10 producing macrophages (A), CD8+ IL10+ T cells (B), CD4+ IL10+ T cells (C), alveolar macrophages (D), type 2 innate lymphoid cells (E), and neutrophils (F) through day 12 post-infection by flow cytometry. Concentration of IL-10 (G), IL-6 (H), MCP-1 (J), and IFNy (K) in lung homogenate at day 12 post-infection by cytokine bead array. mRNA expression of IL10 (I) and amphiregulin (L) in lung at day 12 post-infection by qRT-PCR. Data points and error bars represent mean ± standard error of the mean (SEM). Asterisks (*) denote statistically significant ($p<0.05$) differences between the treatment group and control (n=12).

4.7 LANCL2 is required for the beneficial effects of NSC61610

As NSC61610 is a predicted ligand of LANCL2, we sought to evaluate the specificity of the ligand's effects in LANCL2-/- mice. To determine if the efficacy of NSC61610 treatment is dependent on the presence of LANCL2, we administered PBS or NSC61610 to infected LANCL2-/- mice. No significant differences were apparent in mortality or disease activity scores (Figure 4.6A-B). Additionally, no differences were observable in cellular (Figure 4.6C-F) or molecular (Figure 4.6G-J) measures noted to be changed in wild type mice treated with NSC61610.

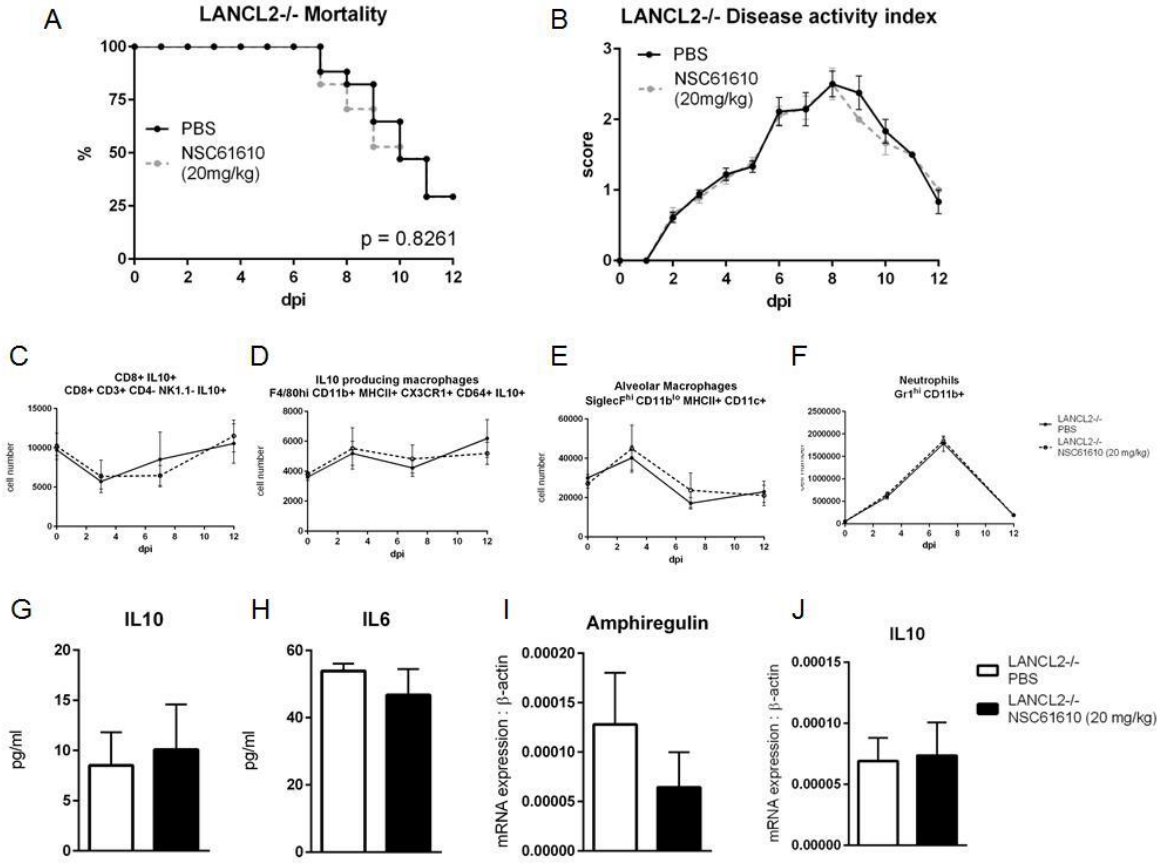

Figure 4.6. Loss of LANCL2 impairs recovery and diminishes clinical effects of NSC61610 treatment. Mortality (A) and disease activity (B) of LANCL2-/- mice infected with influenza with no treatment and NSC61610 treatment. Cell number of CD8+ IL10+ T cells (C), IL10 producing macrophages (D), alveolar macrophages (E), and neutrophils (F) through day 12 post-infection by flow cytometry. Concentration of IL-10 (G) and IL-6 (H) in lung homogenate at day 12 post-infection by cytokine bead array. mRNA expression of amphiregulin (I) and IL10 (J) in lung at day 12 post-infection by qRT-PCR. Data points and error bars represent mean ± standard error of the mean (SEM). Asterisks (*) denote statistically significant ($p<0.05$) differences between the treatment group and control (n=12).

4.8 Effects of NSC61610 are mediated by IL-10

Mice were infected with influenza virus as previously. After infection, mice were administered an IL-10 neutralizing antibody or isotype control. IL-10-neutralized mice treated with NSC61610 exhibited no differences from untreated IL-10-neutralized mice in clinical measures of disease activity index and mortality (Figure 4.7A-B). The isotype control antibody did not dampen the efficacy of NSC61610 against influenza. The IL-10 neutralization inhibited the increases in alveolar macrophages, CD103+ dendritic cells and ILC2 experienced with NSC61610 treatment (Figure 4.7C, D, and F). The neutralization of IL-10 also significantly increased the number of IFNγ producing CD4+ T cells (Figure 4.7E).

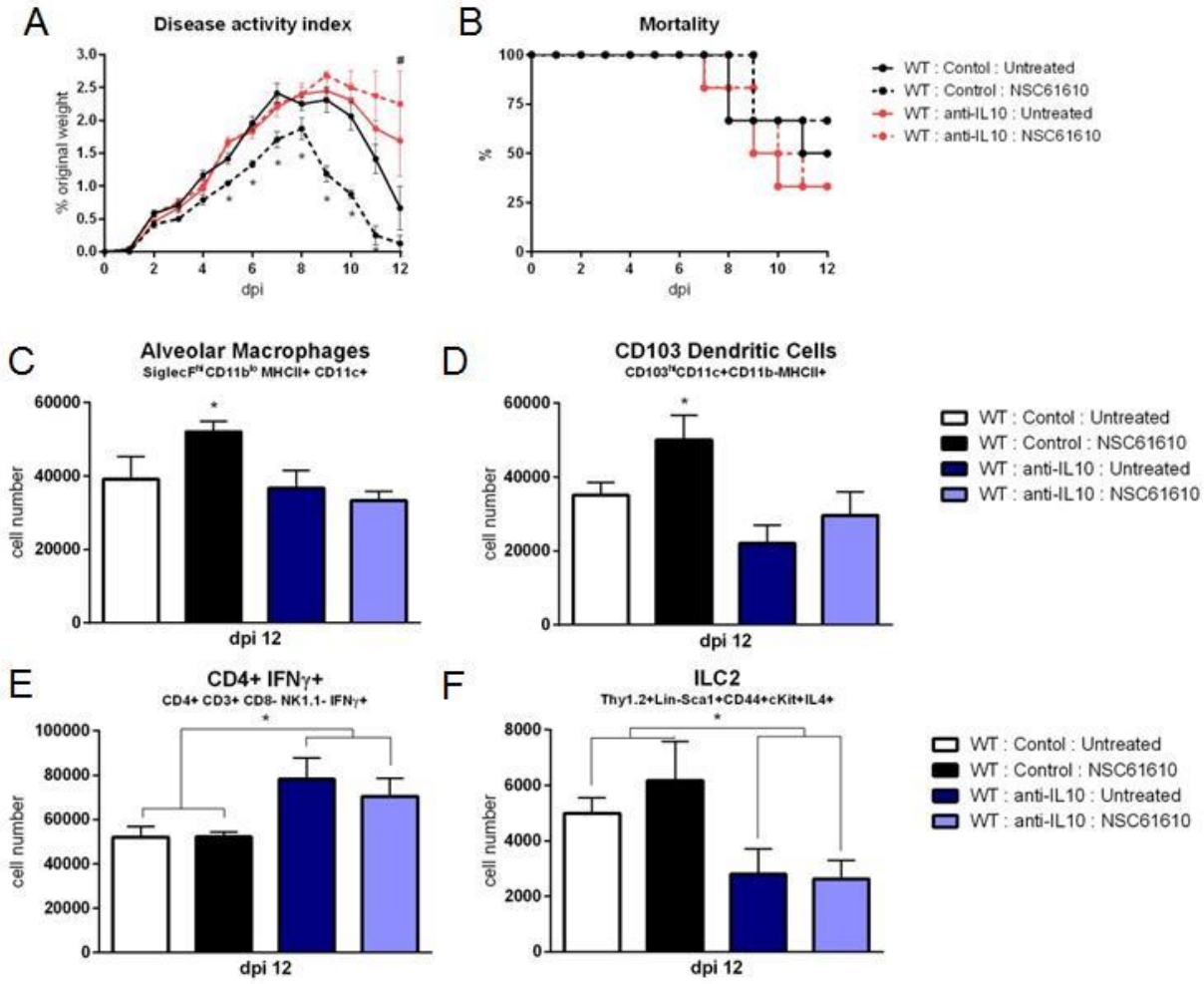

Figure 4.7. IL10 neutralization abrogates efficacy of NSC61610. Disease activity (A), and mortality (B) of wild type mice following IL10 neutralization during influenza infection. Cell number of alveolar macrophages (C), CD103+ dendritic cells (D), CD4+ IFNγ+ T cells (E), and type 2 innate lymphoid cells (F) within lungs at day 12 post-infection by flow cytometry. Data points and error bars represent mean ± standard error of the mean (SEM). Asterisks (*) denote statistically significant ($p<0.05$) differences between the NSC61610 treatment group and control (n=8). Number signs (#) denote statistically significant ($p<0.05$) differences between neutralization treatment group and control (n=8).

4.9 NSC61610 or combined therapy with NSC61610 and Tamiflu outperforms Tamiflu alone

To determine whether the treatment efficacy of NSC61610 could be further increased by combination with an anti-viral agent, we administered NSC61610 in combination with oseltamivir phosphate, an active ingredient of Tamiflu. NSC61610 and combination treatment improved the overall mortality and disease activity compared with treatment with oseltamivir alone (Figure 4.8A-B). Notably, treatment only with Tamiflu did not promote

cellular regulatory responses within the lungs while the combination therapy retained the regulatory benefits of NSC61610 treatment (Figure 4.8C-E). After the observation that treatment with NSC61610 induces regulatory and anti-inflammatory effects, we sought to determine if these effects impacted the viral burden within the lungs. The amount of virus was titrated by plaque assay of MDCK cells. Treatment with NSC61610 did not alter the amount of virus detected. Both Tamiflu and combination therapies significantly reduced the viral titer (Figure 4.8F).

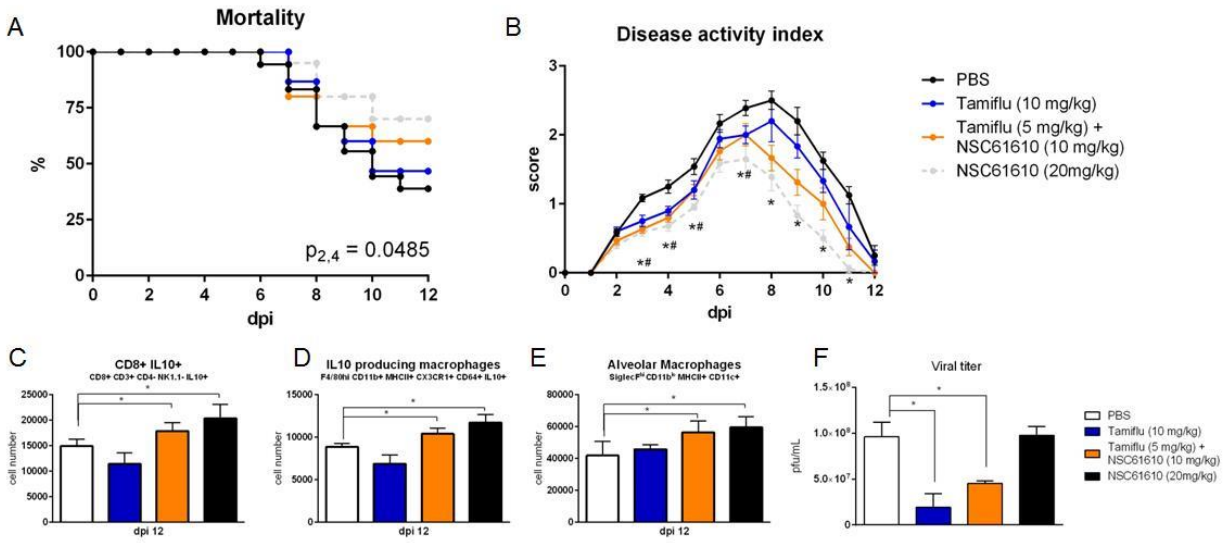

Figure 4.8. Combination of NSC61610 and Tamiflu promotes regulatory responses and suppresses viral replication. Mortality (A) and disease activity (B) of mice treated with PBS, Tamiflu (10mg/kg/day), Tamiflu and NSC61610 (5mg/kg/day and 10mg/kg/day respectively), or NSC61610 alone (20mg/kg/day). Cell number of CD8+IL10+ T cells (C), IL10 producing macrophages (D), and alveolar macrophages (E) at day 12 post-infection by flow cytometry. Viral titer (F) within the lungs on day 3 post-infection by MDCK cell plaque assay. Data points and error bars represent mean ± standard error of the mean (SEM). Asterisks (*) denote statistically significant ($p<0.05$) differences between the combination treatment group and control (n=12). Number signs (#) denote statistically significant ($p<0.05$) differences between Tamiflu treated and control groups (n=12). Ampersands (&) denote statistically significant ($p<0.05$) differences between combination and single treatment groups (n=12).

4.10 Discussion and Conclusions

The LANCL2 pathway has emerged as a therapeutic target for inflammatory, chronic and immune-mediated diseases [112]. By using pharmacologic activation of LANCL2 and loss-of-function approaches in knockout mice, we validate the LANCL2 pathway as a putative target for the treatment of influenza infection. ABA binds to LANCL2 [110] and causes elevation of intracellular cAMP and activation of PKA in macrophages [108]. In addition, ABA suppressed LPS-induced inflammation in mice [108], experimental colitis [120, 121], and accelerated recovery in influenza virus-driven lung immunopathology [111]. Previous work on ABA illustrates the similarities in host defense mechanisms between plants and animals, and the importance of understanding a common evolutionary

heritage. Based on the demonstrated efficacy of ABA as an immune modulatory compound and the discovery of the anti-inflammatory efficacy of the LANCL2 pathway, we screened chemical databases to identify new compounds that bind to LANCL2 and found that NSC61610 had the highest predicted binding affinity [116]. Previous studies demonstrated the efficacy of NSC61610 as an anti-inflammatory compound in mouse models of colitis [116]. Moreover, BT-11, a new LANCL2 ligands being developed for treating IBD, has an outstanding safety profile based on single and 14-day repeated-dose toxicology studies in rats, and it outperforms current IBD treatments in mice with dextran sodium sulfate colitis [117-119]. Recently, the binding of LANCL2 to ligand has been shown to affect the cellular localization of LANCL2 resulting in multiple methods of promoting downstream effects [122].

Our *in vivo* results demonstrate for the first time that oral treatment with NSC61610 and activation of the LANCL2 pathway ameliorates pulmonary immunopathology during influenza A virus infection by suppressing inflammation and enhancing IL-10-mediated immunoregulatory responses in the lungs. Specifically, oral treatment with NSC61610 lowered infiltration of the airway mucosa and submucosa and decreased epithelial necrosis in lungs of infected mice. NSC61610 exerted its anti-inflammatory effect by suppressing TNF-α and MCP-1 expression during early and peak phases. TNF-α is a pro-inflammatory cytokine implicated in priming epithelial cells for induced cytokine and chemokine production during influenza A virus infection, while MCP1 contributes to the recruitment of immune cells [123]. Anti-TNF-α humanized antibodies such as Remicade (Centocor, Malvern, PA) and Humira (Abbott Laboratories, Abbott Park, IL) are biologics that have been approved by the Food and Drug Administration (FDA) as therapeutics against immune-mediated diseases such as IBD [124]. The discovery of a small molecule with an oral route of administration that decreases these two inflammatory mediators expression through the selective and novel LANCL2 pathway holds similar promise in the treatment of autoimmune disorders and pathogen-initiated immunopathologies. At the cellular level, oral NSC61610 treatment significantly decreased the numbers of infiltrating neutrophils in the lungs of influenza virus-infected mice. Pulmonary neutrophil infiltration is a prominent feature of the early inflammatory response to influenza virus infection of humans, ferrets, and mice [125]. Neutrophils constitute a large proportion of the inflammatory leukocytes infiltrating the lung during influenza virus infection. Although their role in influenza virus clearance is not yet well defined, it has been suggested that excessive neutrophils and neutrophil extracellular traps contribute to acute lung injury of influenza pneumonitis [126].

While differences in inflammatory markers exist throughout the course of infection, the efficacy of oral treatment with NSC61610 is most apparent during the recovery phase, in which the increased activation of immunoregulatory pathways is most prevalent. Similar improvements in the recovery phase were reported by oral treatment of influenza virus-infected mice with ABA, the first LANCL2 ligand discovered [111]. Notably, the administration of ABA has been shown to activate PPARγ in a LANCL2-dependent manner suggesting that LANCL2 agonists may contribute to the activation of this regulatory pathway [108]. We provide molecular evidence *in vivo* that NSC61610 functions in a LANCL2-dependent manner during the recovery phase of infection, since

the beneficial effects of NSC61610 treatment observed in wild-type mice are abrogated in LANCL2 knockout mice. Indeed, the largest differences in clinical disease measures such as weight loss and mortality occur after the peak of infection as the NSC61610 treated wild type group experienced an earlier and more pronounced weight gain and decrease in mortality during this phase. Oral treatment with NSC61610 triggers a shift towards a regulatory tissue environment, evidenced by the increased LANCL2-dependent expression of IL-10 in the lungs.

As a crucial regulatory cytokine, IL-10 has previously been shown to suppress pulmonary inflammation and tissue damage [127, 128]. The cytokine exerts its regulatory control through a signaling cascade resulting in the down-regulation of inflammatory cytokines, such as MCP-1 or IFN-γ, the rampant production of which contribute to the damaging cytokine storm [129]. At the cellular level, oral treatment with NSC61610 induced increased levels of IL-10-producing CD8+ T cells and CD11b+F4/80hiCX3CR1+ macrophages in the lungs. CX3CR1+ macrophages are a myeloid cell type prominent in the promotion of a homeostatic tissue environment, predominately tied to the control of intestinal immune responses to bacteria [73]. Some inflammatory subsets of macrophages have been identified as susceptible to influenza infection and are crucial mediators of the well-categorized cytokine storm associated with the influenza virus [130]. The ability of LANCL2 activation to promote a regulatory, IL-10-producing, macrophage population suggests efficacy of this pathway to control the damaging effects of the influenza virus in the lungs throughout the course of infection. CD8+ T cell responses mediate resistance against intracellular infections through effector mechanisms with the potential to defend against infection [131]. For example, CD8+ T cells could eliminate influenza-virus-infected targets via the perforin/granzyme B, Fas/FasL or TRAIL pathways [132]. Meanwhile, CD8+ T cells have previously been identified as the main producer of IL-10 in the lungs during influenza infection [128]. While recent evidence suggests that the production of IL-10 from T cells may be crucial in switching from innate to adaptive immunity during infection and lesser production may be connected to enhanced morbidity in young populations [133]. Treatment with NSC61610 or similar LANCL2 ligands may help to boost this switch and prevent age-associated morbidities. The production of IL-10 from this subset, which can also be driven to secrete the effector cytokine IFNγ, is initiated in part through the presence of IL-4 within the environment [134].

IL-4 is a prototypical Th2-associated cytokine that is also produced by dendritic cells and innate lymphoid cells [135, 136]. In particular, the loss of the type 2 innate lymphoid cell population during influenza infection creates a loss of epithelial integrity and decreased lung function [137]. The increased expression of multiple ILC2-related genes upon treatment with NSC61610 indicates the involvement of LANCL2 in the generation and maintenance of this cellular phenotype. The dual roles of IL-4, as a chemoattractant stimulant of macrophages and eosinophils and an inhibitor of pro-inflammatory cytokines such as TNF-α and MIP-1, may suggest that its acute elevation can allow for ample recruitment of anti-viral cells while decreasing the likelihood of an excessive cytokine storm [138, 139]. In addition to the IL-10-related effects, a key mediator of the regulatory response is the growth factor, amphiregulin. A direct product of immune cells, amphiregulin has both traditional growth factor effects, in the maintenance and stimulation

of epithelial cell growth, as well as additional regulatory mechanisms, via the promotion of regulatory T cells [140, 141]. The increased expression of amphiregulin with LANCL2 activation may be a key component in the reduction of epithelial necrosis and lung damage during infection.

The spectrum of regulatory effects promoted by LANCL2 is dependent on signaling within myeloid cells and T cells. The promotion of IL-10 producing macrophages and CD8+ T cells is lost both in T cell and myeloid specific knockouts of LANCL2 suggesting that interplay between the cell types is necessary to induce these effects. In contrast, the suppression of inflammatory cytokine production and increased number of alveolar macrophages remained intact within T cell knockouts of LANCL2. Alveolar macrophages are responsible for initiating many of the virus clearing responses in addition to the promotion of tissue remodeling and prevention of secondary infections [142-144]. Therefore, the myeloid LANCL2- and IL10-dependent effects of NSC61610 administration are greatly beneficial to the alveolar macrophage mediated pathways of host defense.

A concern with immunoregulatory treatment of infectious disease is impaired clearance or increased burden of the infectious agent. However, no difference in viral load was observed at day 3 post-infection with NSC61610 treatment. When also treated with Tamiflu, the viral load at day 3 post-infection was decreased. Despite a lower viral load, mice treated only with Tamiflu did not exhibit the regulatory responses exhibited by NSC61610-treated mice, suggesting the regulatory benefits of NSC61610 are independent of changes in viral load. Indeed, the therapeutic efficacy of NSC61610 has been shown in non-infectious disease models [112]. Additionally, treatment with NSC61610 significantly increased survival rates compared to Tamiflu treated mice. While Tamiflu is directly effective against specific strains of influenza A, there is risk for adaptive strains to evade its inhibitory effects. Also, the treatment schedule of Tamiflu is very dependent on fast identification and treatment initiation with as little as a 24 hour delay nullifying the beneficial effects. In contrast, NSC61610 treatment was initiated at 24 post-infection in all studies and retained effects.

In summary, our data demonstrates for the first time that oral NSC61610 treatment ameliorates the morbidity and mortality associated with pandemic H1N1pdm influenza virus infection by suppressing the trafficking of inflammatory tissue-damaging cells (i.e., monocytes and neutrophils) and increasing IL-10-producing CD8+ T cells and regulatory macrophages in the lungs in a LANCL2-dependent manner, thereby validating the role of the LANCL2 pathway as a novel host-targeted therapeutic against influenza that modulates the balance of effector and regulatory host responses in the lungs and systemically. NSC61610 improves clinical measures of disease compared to a current standard of care, oseltamivir (Tamiflu). Given the risk of developing resistance to Tamiflu and other agents targeting directly the virus, future studies should explore utilizing LANCL2-based host-targeted therapeutics in combination with lower doses of licensed anti-viral drugs.

4.11 Materials and methods

Animal Procedures

Eight-to-ten week old wild type C57BL/6 mice and LANCL2 knockout mice on a C57BL/6 background were challenged intranasally with 350 pfu/mouse of Influenza A H1N1pdm strain. NSC61610 treated mice within this study received 20 mg/kg/day of NSC61610 orally by gavage. Formulations of NSC61610 treatment were prepared in PBS containing 25mg 2-hydroxypropyl-beta-cyclodextrin (HPBCD) per mg NSC61610. Untreated mice received equal volume of sterile PBS containing HPBCD. NSC61610 was given from day 0 to day 12, daily in 24-hour intervals. Mice treated with oseltamivir phosphate were given 10mg/kg/day in two doses separated by 12 hours. All mice were weighed daily. Mice were housed at the animal facilities at Virginia Tech. Mice (n=10-15 per group and time point) were sacrificed at 3, 7, or 12 days post-infection (dpi) and samples were collected for analysis of gene expression, immunophenotyping of infiltrating cells and histopathological examination. IL-10 neutralization was conducted by intraperitoneal injection of anti-IL10 antibody (R&D Systems #MAB417). 100 μg/mouse was injected on the same day as NSC61610 treatment initiation. The initial dosage was followed with a 50μg/mouse dose on days 6 and 9 post-infection.

All experimental procedures were approved by the Institutional Animal Care and Use Committee (IACUC) of Virginia Tech and met or exceeded requirements of the Public Health Service/National Institutes of Health and the Animal Welfare Act. The IACUC approval IDs for the study were 10-157-VBI and 14-007-VBI. Mice were monitored every 4 hours post-infection and humanely euthanized.

Histopathology

Lung samples were collected at 3, 7, or 12 days post-infection and fixed in 10% buffered formalin. Samples were stained with hematoxylin and eosin and lesions were graded 0 to 4 on the following categories: 1) epithelial necrosis, 2) perivascular cuffing, 3) leukocytic infiltration of the mucosa and submucosa of large airways and 4) terminal airway infiltration. Tissue slides were examined in an Olympus microscope (Olympus America Inc., Dulles, VA).

Quantitative Real Time RT-PCR

Total RNA was isolated from lungs. Quantitative PCR was performed on the cDNA using Taq DNA polymerase (Invitrogen, Carlsbad, CA) and using previously described conditions [145]. Purified amplicons were used to optimize quantitative real-time RT-PCR conditions and to generate standard curves. Primer concentrations and annealing temperatures were optimized for the iCycler iQ system (Bio-Rad) for each set of primers using the system's gradient protocol. cDNA concentrations for genes of interest were examined by RT-PCR using an iCycler IQ System and the iQ SYBR green supermix (Bio-Rad) [145]. A standard curve was generated for each gene using 10-fold dilutions of purified amplicons starting at 5 pg of cDNA. In order to determine the number of products synthesized during the real-time PCR, a melting curve analysis was performed on each product. RT-PCR was used to measure the starting amount of nucleic acid of each unknown

sample of cDNA on the same 96-well plate. Results are presented as starting quantity of target cDNA (picograms) per microgram of total RNA as previously described [145].

Immunophenotyping of Immune Cells Infiltrating the Lungs of Mice

The whole left lobe was collected in 15 mL of 1xRPMI supplemented with FBS, HEPES, and calcium chloride and chopped into small pieces to facilitate the digestion. Lung digestion was performed by adding 300 U/mL of Collagenase and 50 U/mL of DNAse and incubated for 60 to 90 minutes at 37°C under agitation. Cell yield was measured in a particle counter (Beckman Coulter) after digestion and subsequent filtration through 100μm strainers. Red blood cells were eliminated by hypotonic lysis and cells were finally resuspended in 1 mL of PBS containing 5% serum and 0.09% sodium azide (FACS buffer). Cells were incubated with combinations of up to 9 antibodies to markers (CD3, CD4, CD8, CD11b, CD11c, CD19, CD45, F4/80, Gr1, Ly6C, MHC-II, NK1.1, SiglecF, CX3CR1, CD64, PD-1, and IL-10). Thirty thousand events were computed in a LSRII flow cytometer (Becton Dickinson). Hematopoietic cell phenotype analysis was performed in FACS diva with the following gating discrimination: 1) live cells based of FS vs SS, 2) doublet exclusion based on FSC vs FSW, and 3) Selection of CD45+ events.

Plaque assay

MDCK cells were grown to confluency within 6 well plates. Cells were washed of serum containing media prior to exposure. Serial dilutions of virus sample were made in serum-free growth media containing fraction V BSA. Cells were incubated with 1mL of virus dilution for 1 hour at 37°C. Supernatant was removed and cells were washed. Cells were overlayed with a MEM-agar mixture and incubated for 72 hours. Overlay was removed and wells were stained with crystal violet. Lowest dilution with at least 50 plaques was counted.

Expression and purification of the recombinant LANCL2 proteins

Transformed BL21(DE3) *E. coli* cells were initially cultured in Luria–Bertani medium with 100 μg/ml ampicillin at 37°C 240 RPM until the culture reached an A_{600} of 0.3. GST-LANCL2 was expressed by adding 0.1 mM isopropyl-β-d-thiogalactopyranoside. Induced cells were incubated for 16 hours at 20°C 170 RPM. Cells were harvested by centrifugation 45 minutes 1,559 RCF and lysed by sonication in 50 mM Tris–HCl, pH 8.0, 150 mM NaCl with 0.3 mM Tris(2-carboxyethyl)phosphine (TCEP). Post membrane disruption, lysates were centrifuged at 17,211 RPM 20 minutes at 4 °C. GST-LANCL2 fusion protein was purified by affinity chromatography using Glutathione (GSH)-Sepharose-4B (GE Healthcare). GST-LANCL2 was eluted from GSH-Sepharose-4B by incubating the resin with 10 mM GSH in 50 mM Tris–HCl, pH 8.0, 150 mM NaCl with with 0.3 mM TCEP. GST-LANCL2 proteins were run through a gel filtration column. The fusion proteins were further purified by the AKTA Fast protein liquid chromatography (FPLC) purification systems (GE Healthcare). Protein concentrations were determined by bicinchoninic acid assay. Protein purity was assessed by SDS–PAGE (sodium dodecyl sulfate-

polyacrylamide gel electrophoresis); gels were stained with ProSieve Blue Protein Staining solution.

Sensor chip preparation

Direct binding experiments were performed via the Biacore T200 surface plasmon resonance (SPR) Technology (Georgetown University). The flow rates were 10 μL/min for all capture and initial testing studies and 100 μL/min for affinity studies. The GST-LANCL2 was immobilized to a CM4 chip by amine coupling method. Two adjacent surfaces were activated by injection of a 1:1 (v:v) mixture of 0.1 M N-Hydroxysuccinimide (NHS) and 0.4 M 1-Ethyl-3-(3-dimethyl-aminopropyl)-carbodiimide hydrochloride (EDC) for 720 seconds. Experimental flow cell was then injected with the GST-LANCL2 that was diluted in 10 mM pH 5.5 sodium acetate buffer to a final concentration of 25 μg/mL. Both experimental and the reference flow cells were inactivated by injection of 1M Ethanolamine-HCl pH 8.0 for 720 seconds.

Kinetic studies of ABA and NSC61610

A final GST-LANCL2 surface density (R_L) of 7500 RU equivalent to an R_{max} of 53 RU and 26 RU for NSC61610 and ABA was obtained, respectively. Following initial binding studies, it was determined that binding of small molecules to the LANCL2 was occurring with a fast off rate. Therefore, no regeneration step was required following small molecule injections. Binding affinity was calculated following injection of small molecules at 4 different concentrations (12.5 μM, 6.25 μM 3.13 μM and 1.57 μM) in triplicates. Injection time was 60 seconds and dissociation time was 300 seconds. Running buffer for binding studies was 25 mM MOPS (pH 6.5), 150 mM NaCl, 0.05% P-20, 5% DMSO. Data was analyzed by using the BiaEvaluation software v1 (GE Healthcare) with 1:1 binding model for steady state affinity. Raw data was exported and graphed using Prizm for Mac v5.0d.

Statistical Analysis

Data from the first mouse challenge study were analyzed as a series of factorial arrangement designs. To determine the statistical significance of the model, we performed analysis of variance (ANOVA) using the general linear model procedure of Statistical Analysis Software (SAS), and P value < 0.05 was considered to be significant. When the model was significant, ANOVA was followed by Fisher's Protected Least Significant Difference multiple comparison method.

Chapter 5

Concluding remarks

Andrew Leber, Raquel Hontecillas, Josep Bassaganya-Riera

The mucosal immune system is rich with complex behaviors from conditional interactions, patterns of feedback, and non-linear responses. Therefore the development of predictive mechanistic and data-driven models in concert with experimentation and observation can greatly aid in the completeness of scientific knowledge and the advancement of therapeutic and precision medicine modalities.

In Chapter 2, the dissertation describes a computational model of host pathogen interactions during *C. difficile* infection. The ordinary differential equation based model was calibrated to capture the dynamics of the immune system and microbiota observed within a mouse model of infection. From sensitivity analysis, the model identified that the balance between Th17 and Treg cells is critical to the balance *C. difficile* clearance with the prevention of epithelial cell damage. However, the strongest correlation with improved disease response was identified to be with the regrowth of commensal microbiota. Based on the simulation and analysis, the production of anti-microbial peptides was assessed experimentally and identified to be strongly correlated with commensal bacteria regrowth. Through computational simulation, inhibiting the production of anti-microbial peptides from epithelial cells and neutrophils decreased colonic inflammatory markers and accelerated regrowth of the commensal microbiome.

In Chapter 3, the immunometabolic role of NLRX1 in CD4+ T cells was described. With the loss of NLRX1, mice had altered disease response in DSS, adoptive transfer and C. rodentium models of colitis. These differences were highlighted by augmented responses in effector CD4+ T cells. With the aid of RNA-sequencing, a shift in metabolic behavior was observed with NLRX1-/- groups possessing higher expression of lactate associated genes and lower expression of tricarboxylic acid associated genes. Upon further examination *in vitro*, NLRX1-/- cells proliferated at greater rates and had higher glycolytic and lactate dehydrogenase activity. When these differences were inhibited, the differences in differentiation and proliferation were abrogated, suggested an immunometabolic role of NLRX1.

In Chapter 4, a novel ligand was used to identify the potential for activating the LANCL2 pathway for the treatment of influenza virus infection. Following the observation that the recovery of LANCL2-/- mice was impaired, the use of NSC61610 allowed for the determination that LANCL2 activation lessened disease severity, protected against mortality and accelerated recovery. Mechanistically, these effects were linked to the increased production of IL10 from CD8+ T cells and mononuclear phagocytes that activated tissue repair and recovery associated cell types and gene expression. When compared to the current influenza treatment, Tamiflu, LANCL2 activation displayed improved responses in severity and mortality.

The promise of systems immunology is illustrated by the three studies presented. Each represents a separate step on the path to precision medicine whether the establishment of robust *in silico* mechanistic models, the discovery of trans-disciplinary means of regulation or the development of alternative treatment strategies. In all the presented experiments, a common theme arises that the promotion of immunoregulatory pathways, in the promotion of commensal microbiota regrowth, the control of effector immune cell associated metabolism or the prevention of infection-associated tissue damage, is a promising avenue to pursue in both infectious and immune mediated disease.

References

1. Rupnik, M., M.H. Wilcox, and D.N. Gerding, *Clostridium difficile infection: new developments in epidemiology and pathogenesis.* Nat Rev Microbiol, 2009. **7**(7): p. 526-36.
2. Barbut, F., G. Jones, and C. Eckert, *Epidemiology and control of Clostridium difficile infections in healthcare settings: an update.* Curr Opin Infect Dis, 2011. **24**(4): p. 370-6.
3. Cornely, O.A., et al., *Treatment of first recurrence of Clostridium difficile infection: fidaxomicin versus vancomycin.* Clin Infect Dis, 2012. **55 Suppl 2**: p. S154-61.
4. Lessa, F.C., L.G. Winston, and L.C. McDonald, *Burden of Clostridium difficile infection in the United States.* N Engl J Med, 2015. **372**(24): p. 2369-70.
5. Pepin, J., et al., *Increasing risk of relapse after treatment of Clostridium difficile colitis in Quebec, Canada.* Clin Infect Dis, 2005. **40**(11): p. 1591-7.
6. Bartlett, J.G., *Clostridium difficile: clinical considerations.* Rev Infect Dis, 1990. **12 Suppl 2**: p. S243-51.
7. Walters, B.A., et al., *Relapse of antibiotic associated colitis: endogenous persistence of Clostridium difficile during vancomycin therapy.* Gut, 1983. **24**(3): p. 206-12.
8. Johnson, S., *Recurrent Clostridium difficile infection: a review of risk factors, treatments, and outcomes.* J Infect, 2009. **58**(6): p. 403-10.
9. Hu, M.Y., et al., *Prospective derivation and validation of a clinical prediction rule for recurrent Clostridium difficile infection.* Gastroenterology, 2009. **136**(4): p. 1206-14.
10. Kyne, L., et al., *Association between antibody response to toxin A and protection against recurrent Clostridium difficile diarrhoea.* Lancet, 2001. **357**(9251): p. 189-93.
11. Shields, K., et al., *Recurrent Clostridium difficile infection: From colonization to cure.* Anaerobe, 2015. **34**: p. 59-73.
12. Dubberke, E.R., et al., *Clostridium difficile-associated disease in allogeneic hematopoietic stem-cell transplant recipients: risk associations, protective associations, and outcomes.* Clin Transplant, 2010. **24**(2): p. 192-8.
13. Nguyen, G.C., et al., *A national survey of the prevalence and impact of Clostridium difficile infection among hospitalized inflammatory bowel disease patients.* Am J Gastroenterol, 2008. **103**(6): p. 1443-50.
14. Ruemmele, F.M., *Role of Diet in Inflammatory Bowel Disease.* Ann Nutr Metab, 2016. **68 Suppl 1**: p. 33-41.
15. Ananthakrishnan, A.N., *Epidemiology and risk factors for IBD.* Nat Rev Gastroenterol Hepatol, 2015. **12**(4): p. 205-17.
16. Zhang, Y.Z. and Y.Y. Li, *Inflammatory bowel disease: pathogenesis.* World J Gastroenterol, 2014. **20**(1): p. 91-9.
17. Basson, A., et al., *Mucosal Interactions between Genetics, Diet, and Microbiome in Inflammatory Bowel Disease.* Front Immunol, 2016. **7**: p. 290.
18. Neuman, M.G., *Immune dysfunction in inflammatory bowel disease.* Transl Res, 2007. **149**(4): p. 173-86.

19. Strober, W., I.J. Fuss, and R.S. Blumberg, *The immunology of mucosal models of inflammation.* Annu Rev Immunol, 2002. **20**: p. 495-549.
20. Pithadia, A.B. and S. Jain, *Treatment of inflammatory bowel disease (IBD).* Pharmacol Rep, 2011. **63**(3): p. 629-42.
21. Nair, H., et al., *Global burden of respiratory infections due to seasonal influenza in young children: a systematic review and meta-analysis.* Lancet, 2011. **378**(9807): p. 1917-30.
22. Thompson, W.W., et al., *Estimates of US influenza-associated deaths made using four different methods.* Influenza Other Respir Viruses, 2009. **3**(1): p. 37-49.
23. Bouvier, N.M. and P. Palese, *The biology of influenza viruses.* Vaccine, 2008. **26 Suppl 4**: p. D49-53.
24. Taubenberger, J.K. and D.M. Morens, *The pathology of influenza virus infections.* Annu Rev Pathol, 2008. **3**: p. 499-522.
25. Debast, S.B., M.P. Bauer, and E.J. Kuijper, *European Society of Clinical Microbiology and Infectious Diseases: update of the treatment guidance document for Clostridium difficile infection.* Clin Microbiol Infect, 2014. **20 Suppl 2**: p. 1-26.
26. Surawicz, C.M., et al., *Guidelines for diagnosis, treatment, and prevention of Clostridium difficile infections.* Am J Gastroenterol, 2013. **108**(4): p. 478-98; quiz 499.
27. El Feghaly, R.E., et al., *Markers of intestinal inflammation, not bacterial burden, correlate with clinical outcomes in Clostridium difficile infection.* Clin Infect Dis, 2013. **56**(12): p. 1713-21.
28. Gerding, D.N., et al., *Administration of spores of nontoxigenic Clostridium difficile strain M3 for prevention of recurrent C. difficile infection: a randomized clinical trial.* JAMA, 2015. **313**(17): p. 1719-27.
29. Leav, B.A., et al., *Serum anti-toxin B antibody correlates with protection from recurrent Clostridium difficile infection (CDI).* Vaccine, 2010. **28**(4): p. 965-9.
30. Brown, D., et al., *Trauma in silico: Individual-specific mathematical models and virtual clinical populations.* Sci Transl Med, 2015. **7**(285): p. 285ra61.
31. Jeena, P.M., et al., *In silico children and the glass mouse model: clinical trial simulations to identify and individualize optimal isoniazid doses in children with tuberculosis.* Antimicrob Agents Chemother, 2011. **55**(2): p. 539-45.
32. Kovatchev, B.P., et al., *In silico preclinical trials: a proof of concept in closed-loop control of type 1 diabetes.* J Diabetes Sci Technol, 2009. **3**(1): p. 44-55.
33. Abedi, V., Lu, P., Hontecillas, R., Verma, M., Vess, G., Philipson, C., Carbo, A., Leber, A., Juni, N.T., Hoops, S., and Bassaganya-Riera, J., *Phase III Placebo-Controlled, Randomized Clinical Trial with Synthetic Crohn's disease Patients to Evaluate Treatment Response*, in *Emerging Trends in Applications and Infrastructure in Computational Biology, Bioinformatics and Systems Biology*, H.R.a.T. Arabnia, Q. N. , Editor. 2015, Elsevier: Cambridge, MA. p. 411-425.
34. Leber, A., et al., *Systems Modeling of Interactions between Mucosal Immunity and the Gut Microbiome during Clostridium difficile Infection.* PLoS One, 2015. **10**(7): p. e0134849.
35. Leu, H.B., et al., *Identification of new biosignatures for clinical outcomes in stable coronary artery disease - The study protocol and initial observations of a*

prospective follow-up study in Taiwan. BMC Cardiovasc Disord, 2017. **17**(1): p. 42.
36. Molins, C.R., et al., *Development of a metabolic biosignature for detection of early Lyme disease.* Clin Infect Dis, 2015. **60**(12): p. 1767-75.
37. Tsalik, E.L., et al., *Host gene expression classifiers diagnose acute respiratory illness etiology.* Sci Transl Med, 2016. **8**(322): p. 322ra11.
38. Zeevi, D., et al., *Personalized Nutrition by Prediction of Glycemic Responses.* Cell, 2015. **163**(5): p. 1079-94.
39. Lo Vecchio, A. and G.M. Zacur, *Clostridium difficile infection: an update on epidemiology, risk factors, and therapeutic options.* Curr Opin Gastroenterol, 2012. **28**(1): p. 1-9.
40. Lessa, F.C., et al., *Burden ofClostridium difficileInfection in the United States.* New England Journal of Medicine, 2015. **372**(9): p. 825-834.
41. Hall, A.J., et al., *The Roles of Clostridium difficile and Norovirus Among Gastroenteritis-Associated Deaths in the United States, 1999-2007.* Clinical Infectious Diseases, 2012. **55**(2): p. 216-223.
42. See, I., et al., *NAP1 strain type predicts outcomes from Clostridium difficile infection.* Clin Infect Dis, 2014. **58**(10): p. 1394-400.
43. Suwantarat, N. and D.A. Bobak, *Current Status of Nonantibiotic and Adjunct Therapies for Clostridium difficile Infection.* Current Infectious Disease Reports, 2010. **13**(1): p. 21-27.
44. Lowy, I., et al., *Treatment with monoclonal antibodies against Clostridium difficile toxins.* N Engl J Med, 2010. **362**(3): p. 197-205.
45. Gilmore, M.S., et al., *Targeted Restoration of the Intestinal Microbiota with a Simple, Defined Bacteriotherapy Resolves Relapsing Clostridium difficile Disease in Mice.* PLoS Pathogens, 2012. **8**(10): p. e1002995.
46. Holmes, E., et al., *Gut microbiota composition and activity in relation to host metabolic phenotype and disease risk.* Cell Metab, 2012. **16**(5): p. 559-64.
47. Buffie, C.G., et al., *Precision microbiome reconstitution restores bile acid mediated resistance to Clostridium difficile.* Nature, 2014. **517**(7533): p. 205-208.
48. Iapichino, G., et al., *Impact of antibiotics on the gut microbiota of critically ill patients.* J Med Microbiol, 2008. **57**(Pt 8): p. 1007-14.
49. Hecht, G., et al., *Clostridium difficile toxin A perturbs cytoskeletal structure and tight junction permeability of cultured human intestinal epithelial monolayers.* J Clin Invest, 1988. **82**(5): p. 1516-24.
50. Jafari, N.V., et al., *Clostridium difficile modulates host innate immunity via toxin-independent and dependent mechanism(s).* PLoS One, 2013. **8**(7): p. e69846.
51. Jarchum, I., et al., *Critical role for MyD88-mediated neutrophil recruitment during Clostridium difficile colitis.* Infect Immun, 2012. **80**(9): p. 2989-96.
52. Brazil, J.C., et al., *Neutrophil migration across intestinal epithelium: evidence for a role of CD44 in regulating detachment of migrating cells from the luminal surface.* J Immunol, 2010. **185**(11): p. 7026-36.
53. Ausiello, C.M., et al., *Surface layer proteins from Clostridium difficile induce inflammatory and regulatory cytokines in human monocytes and dendritic cells.* Microbes Infect, 2006. **8**(11): p. 2640-6.

54. Stagg, A.J., et al., *The dendritic cell: its role in intestinal inflammation and relationship with gut bacteria.* Gut, 2003. **52**(10): p. 1522-9.
55. Carbo, A., et al., *Systems Modeling of Molecular Mechanisms Controlling Cytokine-driven CD4+ T Cell Differentiation and Phenotype Plasticity.* PLoS Computational Biology, 2013. **9**(4): p. e1003027.
56. Barnes, M.J. and F. Powrie, *Regulatory T cells reinforce intestinal homeostasis.* Immunity, 2009. **31**(3): p. 401-11.
57. Miao, H., et al., *Quantifying the early immune response and adaptive immune response kinetics in mice infected with influenza A virus.* J Virol, 2010. **84**(13): p. 6687-98.
58. Carbo, A., et al., *Predictive computational modeling of the mucosal immune responses during Helicobacter pylori infection.* PLoS One, 2013. **8**(9): p. e73365.
59. Wendelsdorf, K., et al., *Model of colonic inflammation: Immune modulatory mechanisms in inflammatory bowel disease.* Journal of Theoretical Biology, 2010. **264**(4): p. 1225-1239.
60. Pflughoeft, K.J. and J. Versalovic, *Human microbiome in health and disease.* Annu Rev Pathol, 2012. **7**: p. 99-122.
61. Viladomiu, M., et al., *Modeling the Role of Peroxisome Proliferator-Activated Receptor gamma and MicroRNA-146 in Mucosal Immune Responses to Clostridium difficile.* PLoS One, 2012. **7**(10): p. e47525.
62. Blake, K.M., et al., *Neutrophils migrate across intestinal epithelium using beta2 integrin (CD11b/CD18)-independent mechanisms.* Clinical and Experimental Immunology, 2004. **136**(2): p. 262-268.
63. Mahida, Y.R., Makh, S., Hyde, S., Gray, T., and Borriello, S.P., *Effect of Clostridium difficile toxin A on human intestinal epithelial cells: induction of interleukin 8 production and apoptosis after cell detachment.* Gut, 1996. **38**: p. 337-347.
64. Riegler, M.S., R., Pothoulakis, C., Hamilton, G., Zacherl, J., Bischof, G., Cosentini, E., Feil, W., Schiessel, R., Lamont, J.T., and Wenzl, E., *Clostridium difficile Toxin B is more potent than Toxin A in damaging human colonic epithleium in vitro.* J. Clin. Invest., 1995. **95**: p. 2004-2011.
65. Hoops, S., et al., *COPASI--a COmplex PAthway SImulator.* Bioinformatics, 2006. **22**(24): p. 3067-74.
66. Terrier, M.C.Z., Simonet, M.L., Bichard, P. and Frossard, J.L., *Recurrent Clostridium difficile infections.* World J Gastroenterol, 2014. **20**(23): p. 7416-7423.
67. Hussack, G., et al., *Neutralization of Clostridium difficile Toxin A with Single-domain Antibodies Targeting the Cell Receptor Binding Domain.* Journal of Biological Chemistry, 2011. **286**(11): p. 8961-8976.
68. Foglia, G., et al., *Clostridium difficile: Development of a novel candidate vaccine.* Vaccine, 2012. **30**(29): p. 4307-4309.
69. McDermott, A.J., et al., *The role of Gr-1+cells and tumour necrosis factor-αsignalling duringClostridium difficilecolitis in mice.* Immunology, 2015. **144**(4): p. 704-716.
70. Pothoulakis, C. and J.T. Lamont, *Microbes and microbial toxins: paradigms for microbial-mucosal interactions II. The integrated response of the intestine to*

Clostridium difficile toxins. Am J Physiol Gastrointest Liver Physiol, 2001. **280**(2): p. G178-83.
71. Kasendra, M., et al., *Clostridium difficile toxins facilitate bacterial colonization by modulating the fence and gate function of colonic epithelium.* J Infect Dis, 2014. **209**(7): p. 1095-104.
72. McLoughlin, R.M. and K.H. Mills, *Influence of gastrointestinal commensal bacteria on the immune responses that mediate allergy and asthma.* J Allergy Clin Immunol, 2011. **127**(5): p. 1097-107; quiz 1108-9.
73. Longman, R.S., et al., *CX(3)CR1(+) mononuclear phagocytes support colitis-associated innate lymphoid cell production of IL-22.* J Exp Med, 2014. **211**(8): p. 1571-83.
74. Scott, K.P., et al., *Manipulating the gut microbiota to maintain health and treat disease.* Microbial Ecology in Health & Disease, 2015. **26**(0).
75. Marteau, P.R., de Vrese, M., Cellier, C.J., and Schrezenmeir, J., *Protection from gastrointestinal diseases with the use of probiotics.* Am J Clin Nutr, 2001. **73**(2): p. 430-436.
76. Sorg, J.A. and A.L. Sonenshein, *Bile Salts and Glycine as Cogerminants for Clostridium difficile Spores.* Journal of Bacteriology, 2008. **190**(7): p. 2505-2512.
77. Sorg, J.A. and A.L. Sonenshein, *Chenodeoxycholate Is an Inhibitor of Clostridium difficile Spore Germination.* Journal of Bacteriology, 2008. **191**(3): p. 1115-1117.
78. Weingarden, A.R., Chen C., Bobr, A., Yao, D. Lu, Y, Nelson, V.M., Sadowsky, M.J., and Khoruts, A., *Microbiota transplantation restores normal fecal bile acid composition in recurrent Clostridium difficile infection.* Am J Physiol Gastrointest Liver Physiol, 2014. **306**: p. G310-G319.
79. Prado-Montes de Oca, E., *Human β-defensin 1: A restless warrior against allergies, infections and cancer.* The International Journal of Biochemistry & Cell Biology, 2010. **42**(6): p. 800-804.
80. Pazgier, M., et al., *Human β-defensins.* Cellular and Molecular Life Sciences, 2006. **63**(11): p. 1294-1313.
81. Nacken, W., et al., *S100A9/S100A8: Myeloid representatives of the S100 protein family as prominent players in innate immunity.* Microscopy Research and Technique, 2003. **60**(6): p. 569-580.
82. Louie, T.J., et al., *Fidaxomicin versus vancomycin for Clostridium difficile infection.* N Engl J Med, 2011. **364**(5): p. 422-31.
83. Buffie, C.G., et al., *Profound alterations of intestinal microbiota following a single dose of clindamycin results in sustained susceptibility to Clostridium difficile-induced colitis.* Infect Immun, 2012. **80**(1): p. 62-73.
84. Ishida, Y., et al., *Essential Involvement of IFN- in Clostridium difficile Toxin A-Induced Enteritis.* The Journal of Immunology, 2004. **172**(5): p. 3018-3025.
85. Schlackow, I., et al., *Surveillance of infection severity: a registry study of laboratory diagnosed Clostridium difficile.* PLoS Med, 2012. **9**(7): p. e1001279.
86. Gasch, M., et al., *Generation of IL-8 and IL-9 Producing CD4+ T Cells Is Affected by Th17 Polarizing Conditions and AHR Ligands.* Mediators of Inflammation, 2014. **2014**: p. 1-14.
87. Rao, K., et al., *Procalcitonin levels associate with severity of Clostridium difficile infection.* PLoS One, 2013. **8**(3): p. e58265.

88. Rao, K., et al., *The systemic inflammatory response to Clostridium difficile infection.* PLoS One, 2014. **9**(3): p. e92578.
89. Swale, A., et al., *Calprotectin and lactoferrin faecal levels in patients with Clostridium difficile infection (CDI): a prospective cohort study.* PLoS One, 2014. **9**(8): p. e106118.
90. Mei, Y., et al., *Multiscale modeling of mucosal immune responses.* BMC Bioinformatics, 2015. **In press**.
91. Beard, D.A., et al., *An In-Silico Model of Lipoprotein Metabolism and Kinetics for the Evaluation of Targets and Biomarkers in the Reverse Cholesterol Transport Pathway.* PLoS Computational Biology, 2014. **10**(3): p. e1003509.
92. Mathew, S., et al., *Global sensitivity analysis of a mathematical model of acute inflammation identifies nonlinear dependence of cumulative tissue damage on host interleukin-6 responses.* Journal of Theoretical Biology, 2014. **358**: p. 132-148.
93. Shapira, Y., N. Agmon-Levin, and Y. Shoenfeld, *Defining and analyzing geoepidemiology and human autoimmunity.* J Autoimmun, 2010. **34**(3): p. J168-77.
94. Okada, H., et al., *The 'hygiene hypothesis' for autoimmune and allergic diseases: an update.* Clin Exp Immunol, 2010. **160**(1): p. 1-9.
95. Smyth, D.J., et al., *FUT2 nonsecretor status links type 1 diabetes susceptibility and resistance to infection.* Diabetes, 2011. **60**(11): p. 3081-4.
96. McGovern, D.P., et al., *Fucosyltransferase 2 (FUT2) non-secretor status is associated with Crohn's disease.* Hum Mol Genet, 2010. **19**(17): p. 3468-76.
97. Chen, X., et al., *A Mouse Model of Clostridium difficile–Associated Disease.* Gastroenterology, 2008. **135**(6): p. 1984-1992.
98. Rothberg, M.B., S.D. Haessler, and R.B. Brown, *Complications of viral influenza.* Am J Med, 2008. **121**(4): p. 258-64.
99. Dawood, F.S., et al., *Estimated global mortality associated with the first 12 months of 2009 pandemic influenza A H1N1 virus circulation: a modelling study.* Lancet Infect Dis, 2012. **12**(9): p. 687-95.
100. Kotalik, J., *Preparing for an influenza pandemic: ethical issues.* Bioethics, 2005. **19**(4): p. 422-31.
101. Bassaganya-Riera, J., et al., *PPAR-gamma activation as an anti-inflammatory therapy for respiratory virus infections.* Viral Immunol, 2010. **23**(4): p. 343-52.
102. Quigley, E., *Influenza therapies: vaccines and antiviral drugs.* Drug Discov Today, 2006. **11**(11-12): p. 478-80.
103. Hackett, C.J., *Innate immune activation as a broad-spectrum biodefense strategy: prospects and research challenges.* J Allergy Clin Immunol, 2003. **112**(4): p. 686-94.
104. de Jong, M.D., et al., *Fatal outcome of human influenza A (H5N1) is associated with high viral load and hypercytokinemia.* Nat Med, 2006. **12**(10): p. 1203-7.
105. Butler, D., *Cheaper approaches to flu divide researchers.* Nature, 2007. **448**(7157): p. 976-7.
106. Fedson, D.S., *Confronting the next influenza pandemic with anti-inflammatory and immunomodulatory agents: why they are needed and how they might work.* Influenza Other Respi Viruses, 2009. **3**(4): p. 129-42.

107. Fedson, D.S., *Confronting an influenza pandemic with inexpensive generic agents: can it be done?* Lancet Infect Dis, 2008. **8**(9): p. 571-6.
108. Bassaganya-Riera, J., et al., *Abscisic acid regulates inflammation via ligand-binding domain-independent activation of peroxisome proliferator-activated receptor gamma.* J Biol Chem, 2011. **286**(4): p. 2504-16.
109. Lu, P., et al., *Molecular modeling of lanthionine synthetase component C-like 2: a potential target for the discovery of novel type 2 diabetes prophylactics and therapeutics.* Journal of Molecular Modeling, 2011. **17**(3): p. 543-53.
110. Sturla, L., et al., *Binding of abscisic acid to human LANCL2.* Biochem Biophys Res Commun, 2011. **415**(2): p. 390-5.
111. Hontecillas, R., et al., *Dietary abscisic acid ameliorates influenza virus-associated disease and pulmonary immunopathology through a PPAR g-dependent mechanism.* Journal of Nutritional Biochemistry, 2012. **In Press**.
112. Lu, P., et al., *Lanthionine synthetase component C-like protein 2: a new drug target for inflammatory diseases and diabetes.* Curr Drug Targets, 2014. **15**(6): p. 565-72.
113. Chung, C.H., et al., *Identification of lanthionine synthase C-like protein-1 as a prominent glutathione binding protein expressed in the mammalian central nervous system.* Biochemistry, 2007. **46**(11): p. 3262-9.
114. Zhang, W., et al., *Structure of human lanthionine synthetase C-like protein 1 and its interaction with Eps8 and glutathione.* Genes Dev, 2009. **23**(12): p. 1387-92.
115. Lu, P., et al., *Molecular modeling of lanthionine synthetase component C-like protein 2: a potential target for the discovery of novel type 2 diabetes prophylactics and therapeutics.* J Mol Model, 2011. **17**(3): p. 543-53.
116. Lu, P., et al., *Computational modeling-based discovery of novel classes of anti-inflammatory drugs that target lanthionine synthetase C-like protein 2.* PLoS One, 2012. **7**(4): p. e34643.
117. Bissel P, B.K., Hinckley J., Jortner B., Magnin-Bissel G., Werre S., Ehrich M., Carbo A., Philipson C., Hontecillas R., Philipson N., Gandour R., Bassaganya-Riera J., *Exploratory Studies on Safety of BT-11: A proposed orally active therapeutic for Crohn's disease.* Int J Tox, 2015.
118. Carbo A., H.R., Cooper J., Gandour R., Ehrich M., Bassaganya-Riera J., *Lanthionine Synthetase C-like Receptor 2 (LANCL2): A Novel Therapeutic Target for Inflammatory Bowel Disease.* Gastroenterology, 2015. **148**(4): p. S686-S687.
119. Enrich M., B.P., Boes K, Honckley J, Jortner B, Magnin-Bissel G, Werre S, Carbo A, Hontecillas R, Philipson C, Gandour R, BAssaganya-Riera J., *Safety profile of BT-11: A novel LANCL2-based therapeutic for Crohn's disease.* Society of Toxicology 2015 Meeting, 2015.
120. Guri, A.J., R. Hontecillas, and J. Bassaganya-Riera, *Abscisic acid synergizes with rosiglitazone to improve glucose tolerance and down-modulate macrophage accumulation in adipose tissue: possible action of the cAMP/PKA/PPAR gamma axis.* Clin Nutr, 2010. **29**(5): p. 646-53.
121. Guri, A.J., et al., *T cell PPAR gamma is required for the anti-inflammatory efficacy of abscisic acid against experimental inflammatory bowel disease.* Journal of Nutritional Biochemistry, 2011. **22**(9): p. 812-9.
122. Fresia, C., et al., *G-protein coupling and nuclear translocation of the human abscisic acid receptor LANCL2.* Sci Rep, 2016. **6**: p. 26658.

123. Veckman, V., et al., *TNF-alpha and IFN-alpha enhance influenza-A-virus-induced chemokine gene expression in human A549 lung epithelial cells.* Virology, 2006. **345**(1): p. 96-104.
124. van Heel, D.A., et al., *Inflammatory bowel disease is associated with a TNF polymorphism that affects an interaction between the OCT1 and NF(-kappa)B transcription factors.* Hum Mol Genet, 2002. **11**(11): p. 1281-9.
125. Tate, M.D., et al., *Neutrophils ameliorate lung injury and the development of severe disease during influenza infection.* J Immunol, 2009. **183**(11): p. 7441-50.
126. Narasaraju, T., et al., *Excessive neutrophils and neutrophil extracellular traps contribute to acute lung injury of influenza pneumonitis.* Am J Pathol, 2011. **179**(1): p. 199-210.
127. Cox, G., *IL-10 enhances resolution of pulmonary inflammation in vivo by promoting apoptosis of neutrophils.* Am J Physiol, 1996. **271**(4 Pt 1): p. L566-71.
128. Sun, J., et al., *Effector T cells control lung inflammation during acute influenza virus infection by producing IL-10.* Nat Med, 2009. **15**(3): p. 277-84.
129. Ouyang, W., et al., *Regulation and functions of the IL-10 family of cytokines in inflammation and disease.* Annu Rev Immunol, 2011. **29**: p. 71-109.
130. Hofmann, P., et al., *Susceptibility of mononuclear phagocytes to influenza A virus infection and possible role in the antiviral response.* J Leukoc Biol, 1997. **61**(4): p. 408-14.
131. Harty, J.T., A.R. Tvinnereim, and D.W. White, *CD8+ T cell effector mechanisms in resistance to infection.* Annu Rev Immunol, 2000. **18**: p. 275-308.
132. Sanders, C.J., P.C. Doherty, and P.G. Thomas, *Respiratory epithelial cells in innate immunity to influenza virus infection.* Cell Tissue Res, 2011. **343**(1): p. 13-21.
133. Verhoeven, D. and S. Perry, *Differential Mucosal IL-10-induced immunoregulation of innate immune responses occurs in influenza infected infants/toddlers and adults.* Immunol Cell Biol, 2016.
134. Zhao, Y., et al., *IL-4 induces a suppressive IL-10-producing CD8+ T cell population via a Cdkn2a-dependent mechanism.* J Leukoc Biol, 2013. **94**(6): p. 1103-12.
135. Licona-Limon, P., et al., *TH2, allergy and group 2 innate lymphoid cells.* Nat Immunol, 2013. **14**(6): p. 536-42.
136. Maroof, A., et al., *Interleukin-4 can induce interleukin-4 production in dendritic cells.* Immunology, 2006. **117**(2): p. 271-9.
137. Monticelli, L.A., et al., *Innate lymphoid cells promote lung-tissue homeostasis after infection with influenza virus.* Nat Immunol, 2011. **12**(11): p. 1045-54.
138. Jain-Vora, S., et al., *Interleukin-4 alters epithelial cell differentiation and surfactant homeostasis in the postnatal mouse lung.* Am J Respir Cell Mol Biol, 1997. **17**(5): p. 541-51.
139. Levings, M.K. and J.W. Schrader, *IL-4 inhibits the production of TNF-alpha and IL-12 by STAT6-dependent and -independent mechanisms.* J Immunol, 1999. **162**(9): p. 5224-9.
140. Jamieson, A.M., et al., *Role of tissue protection in lethal respiratory viral-bacterial coinfection.* Science, 2013. **340**(6137): p. 1230-4.
141. Zaiss, D.M., et al., *Amphiregulin enhances regulatory T cell-suppressive function via the epidermal growth factor receptor.* Immunity, 2013. **38**(2): p. 275-84.

142. Ghoneim, H.E., P.G. Thomas, and J.A. McCullers, *Depletion of alveolar macrophages during influenza infection facilitates bacterial superinfections.* J Immunol, 2013. **191**(3): p. 1250-9.
143. Kim, H.M., et al., *Alveolar macrophages are indispensable for controlling influenza viruses in lungs of pigs.* J Virol, 2008. **82**(9): p. 4265-74.
144. Schneider, C., et al., *Alveolar macrophages are essential for protection from respiratory failure and associated morbidity following influenza virus infection.* PLoS Pathog, 2014. **10**(4): p. e1004053.
145. Bassaganya-Riera, J., et al., *Activation of PPAR gamma and delta by conjugated linoleic acid mediates protection from experimental inflammatory bowel disease.* Gastroenterology, 2004. **127**(3): p. 777-91.